B cell mediated immune response in chronic viral infection studied through immunoglobulin engineering

Inauguraldissertation

zur

Erlangung der Würde eines Doktors der Philosophie

vorgelegt der

Philosophisch-Naturwissenschaftlichen Fakultät der

Universität Basel

von

Marianna Florova

2021

Genehmigt von der Philosophisch-Naturwissenschaftlichen Fakultät
auf Antrag von Prof. Dr. med. Daniel D. Pinschewer, Prof. Dr. Jean Pieters, Prof. Dr. Hanspeter Pircher.

Basel, 25.5.2021

Prof. Dr. Marcel Mayor, Dekan

Table of Contents

List of Figures and Tables

Abbreviations

AAV	Adeno-associated virus
Ab	Antibody
AID	Activation-induced cytidine deaminase
ARM	Armstrong
ASC	Antibody secreting cell
BCR	B cell receptor
BHK-21	Baby Hamster Kidney 21 cells
BM	Bone marrow
bnAb	Broadly neutralizing Antibody
BSL-2	Biosafety level 2
CAR	Chimeric antigen receptor
CD	Cluster of differentiation
CDR	Complementarity-determining region
CD40L	CD40 ligand
CD40LB	Fibroblast cell line stably expressing CD40 ligand and B-cell activating factor
cDNA	complementary DNA
CH	Heavy chain constant region
Cl13	Clone-13
CMV	Cytomegalovirus
CRISPR	Clustered regularly interspaced short palindromic repeats
CTL	Cytotoxic T lymphocyte
DNA	Deoxyribonucleic acid
DSB	Double-stranded break
dsDNA	Double-stranded DNA
EBV	Epstein-Barr virus
ELISA	Enzyme-linked immunosorbent assay
eng	Engineered
EYFP	Eukaryotic yellow fluorescent protein
FACS	Fluorescence-activated cell sorting
Fcγ	Fc receptor gamma
FITC	Fluorescein isothiocyanate
FO	Follicular
FR	Framework region
GC	Germinal center
GFP	Green Fluorescent Protein
GP	Glycoprotein
GPC	Glycoprotein complex
GSG	Glycine-serine-glycine
gRNA	Guide ribonucleic acid
HA	Homology arm
HC	Heavy chain
HBV	Hepatitis B virus
HCV	Hepatitis C virus
HDR	Homology-directed repair
HEK-293	Human embryonic kidney 293 cells

HEL	Hen egg-white lysozyme
HIV	Human immunodeficiency virus
HPV	Human papilloma virus
HRP	Horse radish peroxidase
HSV	Herpes simplex virus
i.p.	Intraperitoneal
i.v.	Intravenous
IgH	Heavy chain immunoglobulin
IL	Interleukin
IRF-3	Interferon regulatory transcription factor-3
KI	Knock-in
KL25eng	KL25 engineered
KL25HC	KL25 heavy chain
Kl25tg	KL25 transgenic
LC	Light chain
LCMV	Lymphocytic choriomeningitis virus
LLPC	Long-lived plasma cell
MHC	Major histocompatibility complex
MOI	multiplicity of infection
mRNA	messenger RNA
MZ	Marginal zone
n	Number of biological replicates
N	Number of independent experiments
nAb	Neutralizing antibody
NC	Negative control
NP	Nucleoprotein
Nur77	Nuclear receptor 77
OD	Optic density
pA	Polyadenylation signal
PCR	Polymerase chain reaction
PD-1	Programmed cell death
PFU	Plaque forming unit
PNA	Peanut agglutinin
prom	Promoter
P2A	Porcine teschovirus-1 2A self-cleaving peptide
RAG	Recombination-activating gene
RNP	Ribo-nucleoprotein
RT	Room temperature
SD	Standard deviation
SEM	Standard error of mean
SHIV	Simian-human immunodeficiency virus
SPF	Specific pathogen free
SV40	Simian vacuolating virus 40
TCR	T-cell receptor
tg	Transgene/transgenic
T2A	Thosea asigna virus 2A self-cleaving peptide
VDJ	Variable, diversity, joining
VH	Variable heavy
VHF	Viral hemorrhagic fever
VSV	Vesicular stomatitis virus

VL	Variable light
WHO	World health organization
WT	Wild type
α-DG	α-dystroglycan

I. Introduction

Viral immune evasion

Each viral pandemic reminds the biomedical community of the need for a deeper understanding of mechanisms used by viruses to evade the organism`s immune defense. Multiple strategies by which a pathogen evades the host, such as viral epitope escape mutations [1-3], latency, and reservoir formation [4-6]; but also induced immunomodulatory mechanisms, such as cellular apoptosis dysregulation [7-9], viral tropism for immune cells [10, 11], natural killer (NK)-mediated cytotoxicity escape [12, 13], alteration of the macrophage function [14], blocking of viral antigens on major histocompatibility (MHC) class I molecules [13, 15], interference with the antibody and complement functions [16, 17] and inference with the glucose metabolism [18] and cytokines [19, 20] have been described.

The number of mechanisms outlined here is not complete and stems from an inseparable virus-host co-evolution. Some of the co-evolved viruses employ multiple mechanisms of evasion and host immune subversion to establish chronicity. Months or years can pass before the host-destructive pathogenicity of a virus is revealed in the form of a malignancy (EBV, HBV, HCV, HPV), encephalitis (HSV-1, HSV-2, measles), cirrhosis (HBV, HCV), or immunodeficiency syndrome (HIV) [21]. How can viruses replicate, form reservoirs and establish persistence with very little recognition from the host immune system? How can the immune response be modulated toward an efficient viral clearance?

Although our understanding of the viral immune evasion has improved over the years and has been extensively studied from the perspective of T cell-mediated immunity and MHC presentation, less is known about the mechanisms regulating B cell responses in chronic infections.

B cell responses in chronic viral infection

Acute viral infections, such as influenza in humans or vesicular stomatitis virus (VSV) in mice, are transient and rapidly eliminated by the host immune systems. Chronic viral infections, human immunodeficiency virus (HIV), hepatitis C virus (HCV), and hepatitis B virus (HBV), pose a protracted burden on the host immune system, and despite the extensive research in the respective fields, there is no cure for either HIV or HBV, or vaccination (HIV, HCV).

As a model, the advantage of the LCM virus is its ability to establish either acute or chronic viral infection, depending on the strain [22]. Here we concentrate on the chronic, LCMV Clone 13 infection model, which is characterized by a protracted viremia and viral antigen persistence in the organs of wild-type (WT) C57BL/6 mice for months [23, 24]. The T cell mediated immune response, in the form of cytotoxic T lymphocytes (CTLs) and $CD4^+$ T helper cells is exhausted later in the infection course [25, 26], and viral clearance depends on the B cell response [27].

Both, early induced immunoglobulin M (IgM) [28, 29] and IgG can reduce the viral load and mediate clearance of the chronic infection [30], the latter being a characteristic isotype of antibodies identified and studied for their ability to prevent entry of the virus into the target cells or in other words to neutralize the virus [31, 32]. However, neutralizing antibodies (nAb) against chronic pathogens arise late, if at all [33-37]. To date, virus neutralization is a correlate of protection for most vaccines in clinical use ([38], WHO). It is dependent on the formation of long-lasting antibody secreting cells. In addition, as manifested by the HBV vaccination, immunological memory can be a prerequisite for protection, after the initial high antibody titer subsides [39].

The development of a successful vaccine against HIV and HCV still requires more mechanistic insights into the immunology of neutralizing antibody formation. Thus far, several reasons for the insufficiency in the B cell response have been postulated; they are directly linked to the

recognition of the viral antigen by the B cell receptor (BCR). Viruses escape the neutralization by mutating their surface proteins [40, 41]. Immune evasion also results from conformational masking and glycosylation of the BCR-targeted viral epitopes [42-45].

B cell maturation towards neutralizing specificity is a continuous, multifaceted process throughout the course of a viral infection. Activation of a naïve B cell by an antigen can happen in a T cell-independent or dependent fashion, in the antigen contact zones such as the peritoneum, marginal zone (MZ) or B cell follicles (FO), respectively. Naïve circulating B cells are chemotactically attracted to the follicular zones in the lymph nodes and spleen. They interact with soluble antigens or antigens presented on macrophages and dendritic cells [46, 47]. The peptides, presented on the B cells` major histocompatibility complex II (MHC-II), are recognized by $CD4^+$ T cells, which increases the expression of CD40 ligand (CD40L) and IL-4, to further stimulate B cell proliferation [48-51]. The interaction between the B and T cells and the subsequent proliferation leads to a germinal center (GC) formation. Further B cell clones with the specificity for immunizing antigens can enter the GCs [52-55]. Thus, both starting affinity and frequency of naïve specific precursors may be limiting factors for GC reactions [56], where the BCR is modified by class switch recombination and affinity maturation [55]. High BCR affinity is a result of activation-induced cytidine deaminase (AID)-driven somatic hypermutation (SHM) of the antigen-binding variable regions of immunoglobulin (Ig) genes [57, 58] and shapes the B cells` fate upon germinal center exit [59]. Random non-productive SHM can potentially lead to the formation of autoreactive B cell clones [60, 61]. Self-antigen binding within the GC activates tolerance mechanisms, which includes but is not limited to Fas-regulated clonal deletion [62-64]. B cell clones binding to self-antigen to the same or lower extent than foreign immunogens are transiently or terminally positively selected [65-68]. Moreover, autoreactivity is not an uncommon feature in the pool of antibody producing B cells that can neutralize a broad spectrum of viruses within the host

[69-72]. How exactly these specificities are formed within the high GC clonal diversity remains an open question.

In addition to the affinity, the BCR isotype may play a role in the B cell fate and non-IgM classes bias towards plasma cell differentiation [73-75]. Long-lived plasma cells (LLPC) are a later result of the GC reaction when compared to memory B cells [76]. Both LLPC, residing within the bone marrow, and memory B cells confer effective responses following repeated viral exposures [77-79]. Additionally, a GC-independent subset of IgM memory B-cells and IgM LLPC have been recognized [80] [81]. Both IgG and IgM memory B cells can re-enter the GCs upon secondary recall [82, 83]

Most of the above-mentioned understanding of B cell responses is based on immunization studies, and we will discuss it further with our observations of B cell populations and antibody responses in the physiological infectious context.

B cell repertoire diversity

The naïve B cell repertoire is the starting material for the generation of antibody responses in chronic viral infection. In LCMV, we do not know the number of antigen-specific, non-experienced B cells with a binding ability for neutralizing epitopes. It has been recognized that precursor frequencies of B cells, specific for some viral proteins, and particularly neutralizing epitopes, are low [84-86]. Studies of HIV and influenza patients show that B cells with a correct neutralizing epitope specificity may be rare or have a very low affinity and thus are outcompeted in GC reactions [87-90].

The pre-immune B cell repertoire is formed in the bone marrow and adjusted by tolerance mechanisms. BCR diversity generation starts with the recombination activating gene (RAG)-

dependent functional rearrangement of the immunoglobulin heavy chain. The diversity (D_H) gene is first rearranged to the joining (J_H) gene before joining to the (V_H) region; this is followed by the immunoglobulin light chain rearrangement of V_L and J_L regions [91]. Combinatorial diversity of just functional rearrangement creates a repertoire capable of recognizing $5x10^{13}$ different antigens (for comparison, there are approximately 10^{14} cells in the human body, 10^{13} of those are human) [92].

BCR rearrangement depends on the formation of double-stranded breaks (DSB) and is guided by the recombinant signal sequences (RSS); conserved sequences with 12 and 23 base pair spacers, adjacent to the recombination site. Subsequent DNA repair via signal joint formation or non-homologous end joining (NHEJ) is imprecise, adding base pairs in the process and further contributing to the immunoglobulin variability through junctional diversity [93].

The antibody molecule interacts with an antigen at the complementarity-determining regions (CDRs), while framework regions (FRs) are a structural component of the antigen-binding antibody fragment (Fab). There are three CDRs with unique V_H/V_L combinations, contributing to the antibody diversity. CDR3 is often longer and contains hydrophobic residues in the antibodies, which can neutralize persistent viruses [94, 95].

BCR diversity of the naïve immunoglobulin molecules, therefore, comes from the number of V, D, J genes, combinatorial diversity of the V – (D)J joining of either the heavy or the light chain, junctional diversity of the recombination process, and further combinatorial diversity of the V_H and V_L pairing.

The B cell reactivity to foreign pathogens has to be achieved without generating potentially harmful autoreactivities; hence, the central-tolerance checkpoint plays a key role in reducing the frequency of autoreactive cells in the naive, pre-immune B cell repertoire.

The successfully rearranged BCR is expressed in an IgM membrane isoform and is tested for reactivity towards self-antigens at the immature B cell stage [96].

Non-self-reactive B cells egress from the bone marrow and initially, due to the alternative mRNA splicing, express IgM and IgD immunoglobulin isotypes on the surface. A later expression of other isotypes, such as IgG, is a result of the class-switch recombination and takes place outside of the bone marrow. IgD is mostly expressed on the cell surface in conjunction with IgM. The function of IgD is mostly unclear; however, differences in baseline signaling via IgD and IgM immunoglobulins were recently recognized. This suggests a role for IgD in B cell quiescence and differentiation restriction into autoantibody secreting cells [97].

Self-reactive B cells follow one of the four possible faiths depending on the degree of self-reactivity:

- Programmed cell death and clonal deletion [98]
- Receptor editing via RAG re-induction, replacing the self-reactive receptor before bone marrow egress [99, 100]
- Anergy; a functionally unresponsive state with downregulated IgM expression in the periphery [101]
- Antigenic ignorance while expressing both IgM and IgD isotypes on the surface [102]

Recent studies show that receptor editing, rather than clonal deletion, is the main repertoire-modulating mechanism of bone marrow B cell development [103, 104].

Clonal deletion and anergy are concepts established using transgenic mice expressing hen egg-white lysozyme (HEL)-specific BCR crossed to mouse lines expressing membrane-bound or soluble form of the HEL, respectively [105, 106]. Furthermore, other transgenic models, including those with knocked-in neutralizing antibody specificities, seem to follow similar regulatory principles [98, 107, 108].

Regulation of B cell responsiveness by autoantigen-binding IgM and IgD surface molecules have recently been shown using nuclear receptor 77 (Nur77) reporter mouse model and allow for further studies of the polyclonal pre-immune repertoire [109, 110].

Immunoglobulin engineering

In our studies, we use both, recombinant antibodies and specific B cells with an engineered immunoglobulin.

In the recombinant antibody technology, variable chains of the antibody are sequenced and cloned into expression vectors that encode also the constant region with an isotype of choice. For the light chain and for the heavy chain, two expression vectors are then typically transfected into a human embryonic kidney (HEK 293) or a Chinese hamster ovary (CHO) with derived cell lines for antibody production. Recombinant monoclonal antibody production has become a large category of biopharmaceuticals used in immunotherapy, included that of infectious diseases [111-114]. In basic research, the versatility of the technology allows for rapid sequence mutagenesis to generate, among other things, a high-probability unmutated common ancestor antibody for the study of its maturation pathways towards neutralization [115-117]. Antigenic exposure during LCMV infection, as opposed to soluble proteins, induces IgG2a antibody isotype in mice [118, 119]; however, recombinant antibody technology is not restrictive in this regard.

For germline B cell immunoglobulin engineering, pronuclear injection of a foreign DNA into the single-cell stage mouse embryo was developed in the 1970-ties [120]. B cell receptor expression in genetically modified mouse models first depended on the heavy and light chain as transgenes (tg), randomly integrated into the genome. The second approach of precise immunoglobulin knock-in, originating in the 1990s, involves embryonic stem cells transfected

with foreign DNA recombining via homology-directed repair (HDR). Multiple selection rounds proceed with identifying the HC or LC locus integrated clones before they are injected into blastocysts and implanted into a pseudo-pregnant foster mother [121, 122]. Mouse models generated by these ways were instrumental in elucidating tolerance mechanisms, such as central deletion [98, 123-125], LC editing [99, 100], HC replacement [126], peripheral anergy [105, 127] and B cell migration into peripheral niches [128, 129]. After 2009, immunoglobulin knock-in strategies created mouse models with broadly neutralizing antibodies (bnAb) against HIV, extending the knowledge of tolerance involvement in chronic viral infection [130-134]. Additionally, mouse models with knocked-in germline-reverted bnAbs laid ground for the understanding of BCR maturation in the context of sequential immunization [135-138]

The limitations of the conventional techniques lie in the unproductive (transgenesis) and time-consuming (ES cell knock-in) nature, compared to the novel technique using CRISPR/Cas9 genetic scissors. Cas9 is a Streptococcus pyogenes-derived enzyme capable of introducing double-stranded breaks precisely, in the desired genomic position, as navigated by the guide RNA (gRNA) coupled to the enzyme [139-141]. This, together with HDR, ensures precise immunoglobulin gene integration with a single pronuclear injection and a rapid generation of genetically modified mice expressing desired BCRs [142-144].

With the emergence of CRISPR/Cas9, primary B cell engineering became a new territory that we and others decided to explore. Gene editing of T cells and hematopoietic stem cells for immune therapy is being established in the clinics [145, 146], with further CRISPR/Cas9 optimizations of the editing techniques ongoing [147, 148]. The fragility of the primary mouse B cells precluded in vitro manipulation prior to the CRISPR/Cas9 era. Even then, the first BCR-engineering techniques were optimized on cell lines, hybridomas or Cas9-expressing transgenic mice [149-152]. Human primary BCR engineering protocols were more rapidly

established than those for mouse B cells [153-155]. Additionally, human B cells seem to be more permissive to genetic manipulation than mouse B cells [156, 157]; however, this is inconsistent and may depend on the way the cells are activated before transfection or infection with an antibody gene delivering virus [158]. Optimal in vitro activation protocols prevent B cell end-differentiation and isotype switch, which is an advantage for adoptive transfer studies of GC-dependent viral clearance [159]. During primary BCR rearrangements, immunoglobulin repair is mediated via NHEJ, whereas most of the CRISPR/Cas9 editing techniques rely on HDR. In other non-immune cells, the microhomology-mediated non-homologous repair is functional [160-164]. It is essential to optimize different B cell activation, transfection and infection protocols, gene templates and repair mechanisms in order to achieve primary BCR-engineering efficiencies and viability for mouse adoptive transfer experiments.

The lymphocytic choriomeningitis virus infection model

LCMV is an enveloped single-stranded RNA virus of the *Arenaviridae* family. There are 45 other viruses within the family that can infect mammals (*Mammarenaviridae*) [165].
Mammalian viruses are classified according to their regional origins into Old World viruses, including LCMV and Lassa virus, which are endemic in West Africa, and New World viruses found in South America [166-171]. Natural hosts of LCMV are rodents. In adult mice, transmission via blood, saliva, urine or feces, leads to a transient infection. A transplacental transmission of the virus causes a life-long asymptomatic persistence. LCMV has been found to be circulating among European rodent populations [172, 173]. Its seroprevalence in humans seems to be dependent on the potential of rodent contact and was reported worldwide [174-178]. Human LCMV infection can cause aseptic meningitis [179-182] in adults and, upon congenital infection, possibly fatal neural deficits [183-185]. Other viruses of the *Arenaviridae* family, such as the Lassa virus, can cause a lethal hemorrhagic fever [168, 186].

LCMV glycoprotein and neutralizing antibodies

LCMV has now been used for almost 100 years to study viral persistence, immunological tolerance, and immunopathogenesis [187, 188]. The viral genome consists of two single-stranded negative-strand RNA segments, encoding the nucleoprotein (NP) and the glycoprotein (GP) on the short segment (S) and the viral polymerase (L) and matrix protein (Z) on the large segment (L) [189-191]. The RNA-binding NP is required for polymerase activity, while the Z protein is essential for viral budding [192-194]. The GP mediates attachment of the virions to the cells through α-dystroglycan (α-DG) as a receptor and membrane fusion with endosomes [195-197].

More recently, many tools have been developed in the experimental model to study B cells and antibody responses. Reverse genetics techniques allow for an assembly of "design" viruses directly from cDNA [198, 199]. Recombinant acute (Armstrong) and chronic (Clone 13) viruses, expressing the GP of the WE strain, are ideal for the studies involving B cell-mediated neutralization. Hence, a recombinant virus, rCl13/WE GP, is persistent but can be neutralized by the monoclonal antibodies KL25, WEN 1, WEN2, WEN3. KL25 is the most studied LCMV neutralizing antibody and was isolated from a BALB/c mouse after a sequential LCMV-WE immunization [31]. Genetically engineered BCR-transgenic models were generated bearing this specificity. Historically, KL25 HC and LC transgeneses were successfully expressed [29, 30], but only the HC gene was targeted to the immunoglobulin locus [200]. Despite the limitations, adoptive transfers of KL25 specific B cells provide new means to study neutralizing B cell responses.

The neutralizing antibody KL25 binds to the only surface determinant of LCMV, the WE glycoprotein. Its complex (GPC) consists of a 44kDa GP1 globular head shielded by an array of glycans and a 35 kDa GP2 subunit, anchoring the GPC in the viral membrane via a hydrophobic transmembrane region [195, 196]. LCM virus-neutralizing antibodies bind the

GP1 subunit [201, 202]. A single amino acid change resulting from a “hot-spot” mutation in the GP1 subunit prevents epitope-binding and neutralization by the KL25 antibody in vitro [28]. The asparagine at position 119 of GP1 is particularly crucial in this regard. Several substitutions (N119S, N119K, N119D) can significantly decrease the binding of the KL25 antibody [28]. These mutations represent a viral escape, which is a consequence of applied selective pressure, when KL25 transgenic, cytotoxic T lymphocyte deficient mice are neonatally infected with the LCMV-WE virus [40, 203]. Analogously, we observe the same escapes forming upon an adoptive transfer of KL25 knock-in B cells into LCMV carriers. rCl13/WE GP carrying an N119S mutation can, therefore, be considered a low-affinity antigen for KL25 antibody or KL25 B cells.

1. Chronic viral infection promotes efficient germinal center B cell responses

Bénédict Fallet[1]†, Yi Hao[2,3]†, Marianna Florova[1]†, Karen Cornille[1], Alba Verge de los Aires[2], Giulia Girelli Zubani[2], Yusuf I. Ertuna[1], Victor Greiff[4,5], Ulrike Menzel[4], Karim Hammad[6], Doron Merkler[6], Sai Reddy[4], Jean-Claude Weill[2]‡, Claude-Agnès Reynaud[2]‡ and Daniel D. Pinschewer[1]‡*

[1] University of Basel, Division of Experimental Virology, Department of Biomedicine – Haus Petersplatz, 4009 Basel, Switzerland

[2] Team "Development of the Immune System," Institut Necker-Enfants Malades, Institut National de la Santé et de la Recherche Médicale U1151-Centre National de la Recherche Scientifique UMR 8253, Faculté de Médecine Paris Descartes, Université Paris Descartes, Sorbonne Paris Cité, Paris, France

[3] Department of Pathogen Biology, School of Basic Medicine, Tongji Medical College, Huazhong University of Science and Technology, Wuhan, China

[4] Department of Biosystems Science and Engineering, ETH Zürich, Basel, Switzerland

[5] Department of Immunology, University of Oslo, Oslo, Norway

[6] Department of Pathology and Immunology, University of Geneva, Geneva, Switzerland

† These authors contributed equally to the present work

‡ These authors contributed equally to the present work

* Corresponding author: Daniel.Pinschewer@unibas.ch

One Sentence Summary

In the context of chronic viral infection, germinal center B cells hypermutate efficiently, adapt to viral variants and yield higher antibody-secreting-cell output for longer periods of time than in acute infection, altogether enabling potent neutralizing antibody formation.

Abstract

Persistent viral infections subvert key elements of adaptive immunity but the impact on germinal center (GC) B cell responses remains ill-defined.

To compare GC B cell responses in chronic and acute lymphocytic choriomeningitis virus infection we exploited activation-induced deaminase (AID) fate-reporter mice and performed adoptive B cell transfer experiments. GC B cells of chronically infected mice were similarly hypermutated as those emerging from acute infection. Chronic infection yielded GC B cell responses of higher cellularity than acute infection, more memory B cell and antibody secreting cell output for longer periods of time and higher titers of protective neutralizing antibodies. These differences were supposedly driven by the persisting virus, warranting for an optimal representation of the late B cell repertoire in the serum immunoglobulin of chronically infected mice. Efficient mutational adaptation of B cells to viral escape variants attested to unimpaired GC functionality, and even in hypermutation-impaired AID-mutant mice chronic infection selected for GC B cells with hypermutated BCRs and neutralizing antibody formation.

This demonstrates that, unlike for $CD8^+$ T cells, chronic viral infection drives a functional, productive and protective GC B cell response. Protracted GC responses of high cellularity and productivity represent correlates of neutralizing antibody induction, which should be mimicked for B cell-based vaccination against persistent viral diseases.

Introduction

Persistent viral diseases such as HIV, hepatitis B virus (HBV) and hepatitis C virus (HCV) infection represent major global health challenges and affect several hundred million people worldwide [204-206]. A commonly held concept suggests that viral persistence requires subversion of the host's adaptive immune defense. CD8+ T cell exhaustion, caused by chronic antigenic stimulation, represents a paradigmatic example [26, 207, 208]. In contrast to T cells, the effects of chronic antigenic stimulation on B cell responses to persisting viruses remain less well defined. In chronic HBV and HIV infection, the B cell compartment is subject to phenotypic alterations, with an accumulation of atypical $CD21^{neg}CD27^{neg}$ memory B cells and plasmablasts in peripheral blood [209, 210]. In these patients, circulating antiviral B cells express a range of inhibitory receptors such as FcRL4 and PD-1 [210-212]. Moreover, HBV-specific B cells of chronically infected patients fail to differentiate into antibody-secreting cells (ASCs) upon in vitro re-stimulation and produce inadequate amounts of immunoglobulin, both of which can be partially restored by PD-1 blockade [210, 212]. Impaired antibody responses to vaccination with third-party antigens [213] and a shortened life-span of memory B cells [214] can be interpreted to reflect generalized suppression of the humoral immune system in HIV-infected individuals. Similarly, chronic LCMV infection in mice is associated with suppressed antibody responses to third-party antigens [23, 215]. Counterintuitively, however, significant LCMV nAb responses are typically elicited under conditions of chronic infection but only rarely when acute LCMV infection is efficiently cleared [33]. Analogously, broadly neutralizing antibody (bnAbs) responses to HIV itself are most commonly found in patients with long-term uncontrolled viremia [216]. These findings raised the possibility that, unlike for CD8 T cell responses, high levels of persisting viral antigen may result in an efficient antiviral GC B cell response. In line with this hypothesis, the spontaneous resolution of HBV infection is associated with the formation of protective anti-HBs antibodies [217], and evidence is

accumulating that spontaneous HCV clearance relies on the timely formation of bnAbs [218-221]. Of note in this context, the envelope proteins of HIV, HCV and LCMV represent challenging targets for antibody neutralization owing to structural immune evasion features such as prominent glycan shields [41, 44, 222]. Accordingly, these viral envelope proteins commonly fail to induce potent neutralizing antibody (nAb) responses when presented to the immune system in the context of vaccination [44, 223-225], but they do so in the context of chronic infection [2, 27, 33, 216, 218-221]. Taken together, these observations raised the possibility that the humoral immune system meets the challenge of glycan-shielded antigens preferentially under conditions of chronic viremic infection. Such a response pattern – weak in vaccination and acute infection but potent in chronic infection – would seem counter-intuitive in light of the opposite findings for CD8 T cells. Only limited information is, however, available with regard to the functional efficiency of antiviral GC B cell responses in the chronic viral infection context.

At the onset of LCMV infection antiviral B cells are largely deleted as a consequence of interferon-driven inflammation, a process also referred to as “decimation” [226-228]. In light of the finding that naïve B cells can readily be recruited into an ongoing antiviral response [229, 230], we and others have proposed that antiviral B cell responses in the chronic phase of infection rely on a repertoire replenishment by new bone marrow emigrants [226, 229, 231]. Pioneering studies on chronic bacterial and parasitic infections have revealed striking deviations from the “canonical” B cell response as it has been defined in protein – adjuvant immunizations. A dominance of very low-affinity B cell clones at the onset of the response and their subsequent extrafollicular affinity maturation was observed in chronic murine salmonellosis [232]. In similar violation of commonly held concepts, hypermutated IgM+ memory B cells were found to dominate the recall response to *Plasmodium* parasites [233],

altogether emphasizing the need to better understand how B cells respond to chronic microbial exposure.

Here we set out to investigate how viral persistence impacts on the functionality of the GC B cell response. We report that the neutralizing capacity of murine LCMV envelope specific antibodies, as generated in the chronic infection context, requires their mutational maturation, analogously to human HIV and HCV neutralizing antibodies [234-239]. Most importantly, we found that chronic viremic infection drives a long-lived germinal center reaction with potent selection of hypermutated clones. The resulting output of memory B cells and plasma cells exceeded the cellular yields upon acute infection. In conclusion, our observations characterize the GC B cell responses underlying potent nAb formation in persistent viral infection. These insights should help to better mimic chronic infection when designing B cell-based vaccination approaches against persistent viral diseases.

Results

LCMV nAbs arise preferentially in chronic infection and require somatic hypermutation

To compare B cell responses in acute and chronic infection we made use of two genetically engineered variants of LCMV, both carrying the identical LCMV-WE strain envelope glycoprotein (WE-GP) as sole target for nAbs. The two viruses are based on either the Armstrong (rARM) or Clone 13 backbone (rCl13) and differ in a single amino acid position of the polymerase gene, which is essential for rCl13 persistence [23]. High-dose i.v. infection with rCl13 results in protracted high-level viremia whereas rARM, administered intraperitoneally at lower doses, represents a prototypic model of acute aviremic infection (Fig. 1.1A) [26, 44, 240]). These two extremes of a spectrum, both in terms of antigen load and persistence, yet with identical antigenicity allowed us to study the impact of viral chronicity on antiviral B cell responses in general, and on the size and dynamics of the GC response in particular. When measuring antibodies against the highly glycosylated outer globular domain of WE-GP (GP-1) by ELISA, those developed continuously over a period of sixty days and reached significantly higher titers in rCl13- than in rARM-infected mice (Fig. 1.1B). Also, most rCl13-infected mice mounted nAbs by day 62, whereas rARM infection elicited detectable nAb responses in only a minority of animals and at lower titers (Fig. 1.1C). Altogether these findings confirmed earlier observations that protracted LCMV infection was a more potent driver of GP-1 binding and neutralizing Ab responses than acute infection [33]. For some acute viral infections such as influenza virus or vesicular stomatitis virus it has been shown that germline-encoded antibodies can potently neutralize and, accordingly, these responses can be mounted within a few days [241, 242]. Conversely, nAb responses to HIV or HCV typically take weeks to months before they arise [2, 243]. Isolated monoclonal nAbs are often substantially hypermutated and the ability of unmutated ancestor antibodies to bind and/or neutralize the respective virus can be limited or undetectable [234]. In light of the

finding that LCMV nAb responses arose only between day 40 and day 60 after infection, we hypothesized that neutralizing activity required antibody maturation by hypermutation. To test this we studied two LCMV-neutralizing antibodies (WEN-1, WEN-3), which we reverted to their respective putative unmutated ancestor sequence (UA, WEN-1^{UA}, WEN-3^{UA}). WEN-1 and WEN-3 display V(D)J sequence hallmarks previously reported for HIV bnAbs [244]: The WEN-1 heavy chain features an extraordinary 25 amino acid-long CDR3 but diverges from its UA by only 7 amino acid changes, whereas the V_H of WEN-3 stands out for its high mutational load (33 nt mutations, 16 amino acid divergence from its UA, Supplementary Fig. 1.1). Both WEN-1^{UA} and WEN-3^{UA} bound detectably to WE-GP but only did so at ~10-100-fold higher concentrations than their respective hypermutated wt antibody counterparts (Fig. 1.1D). In line with impaired binding, neither of the UA antibodies retained detectable virus neutralizing capacity (Fig. 1.1E). LCMV envelope-binding non-neutralizing antibodies may, however, still exert protective antiviral effects [28]. To test whether the UA antibodies may afford antiviral protection, we passively immunized rCl13-infected mice with either hypermutated or UA antibodies on day 3 after virus inoculation (Fig. 1.1F). When either one of the hypermutated antibodies was administered, viremia was effectively suppressed, resulting in clearance of rCl13 by day 15. In contrast, neither of the UA antibodies reduced viral loads to a detectable extent and all mice remained viremic throughout the observation period of 20 days. Taken together, these data indicated that hypermutation of LCMV glycoprotein-specific antibodies was required for potent binding, virus neutralization and antiviral protection.

AID reporter system identifies LCMV-specific B cells in a polyclonal response

To investigate the underlying cellular correlate of LCMV nAb formation we embarked on a comprehensive long-term study of the LCMV-specific GC B cell response in rCl13 and rARM infected mice. First, we set out to test whether our AID reporter mouse model (AID^{rep} [245]) was suitable for that purpose. AID^{rep} mice are hemizygous for an engineered *aicda* locus (naturally encoding for activation-induced deaminase, AID), which expresses a tamoxifen- (TAM-) inducible Cre recombinase (Cre-ERT2). Additionally, AID^{rep} mice carry a Cre-inducible EYFP reporter gene in the ROSA26 locus, such that TAM administration induces EYFP expression selectively in approximately 10-20% of (AID expressing) GC B cells [245]. Thereby, timed TAM administration allows for the fate mapping of the GC B cell compartment of a given time window including these cells' progeny. Within the population of EYFP-labelled cells we used GL7 and B220 staining to discriminate memory B cells ($GL7^{-}B220^{+}$), GC B cells ($GL7^{+}B220^{+}$) and plasma cells ($GL7^{-}B220^{-}$). In keeping with our earlier findings [246, 247] EYFP-reporting $GL7^{+}B220^{+}$ B cells in rARM- and rCl13-infected mice were $CD38^{-}$ and bound PNA, identifying them as GC B cells, while $GL7^{-}B220^{+}$ memory B cells exhibited an inverse staining pattern (Supplementary Fig. 1.2A,B). To test whether EYFP reporting identified virus-specific B cells, we infected AID^{rep} mice with rCl13, while control groups were given the antigenically unrelated vesicular stomatitis virus (VSV) or were left uninfected. TAM was administered to all mice on day 0, 5 and 10, with a resulting labeling window extending approximately from day 0 – day 15 after infection (Fig. 1.2A). When analyzed on day 50, ~20 % of EYFP-reporting B cells of rCl13- infected mice bound the LCMV nucleoprotein (NP) in flow cytometry (Fig. 1.2B,C, Supplementary Fig. 1.2), which was several-fold over background of VSV-infected or uninfected controls. Given that NP represents approximately 17% of the viral proteome, these numbers were compatible with a faithful labeling of LCMV-reactive B cells in AID^{rep} mice. To further assess whether EYFP-reporting B cells in AID^{rep}

mice were indeed mostly LCMV-reactive we performed adoptive B cell transfer experiments (Fig. 1.2D). We infected AID^{rep} mice with either rCl13 or with Vaccinia virus (Vacc) on day 0, followed by TAM treatment as above. On day 30 we isolated splenic B cells from these donor mice, containing a population of supposedly rCl13- or Vacc-specific EYFP-labeled B cells, respectively. These ($CD45.2^+$) B cells were adoptively transferred into syngeneic ($CD45.1^+$) recipients, which had been infected with either rCl13 or Vacc beforehand. The recipients were infected ahead of the transfer rather than thereafter to avoid the "decimation" of adoptively transferred B cells by interferon-driven inflammation [226-228]. When analyzed six days after transfer, sizeable populations of $EYFP^+$ $CD138^–$ B cells and $EYFP^+$ $CD138^+$ antibody-secreting cells (ASCs) were detected in rCl13-infected recipients but not Vacc-infected recipients of B cells from rCl13-infected donors and vice versa (Fig. 1.2E,F). This result confirmed that AID^{rep} mice identified mostly virus-specific B cells rather than non-specifically activated polyreactive B cells, validating the AID^{rep} mouse model for our ambitions to study LCMV-specific GC B cell responses.

Chronic infection triggers a sustained GC response with prolonged plasma cell and memory B cell output

To compare the generation and maintenance of B cell responses in chronic and acute viral infection, we inoculated groups of AID^{rep} mice with either rCl13 or rARM and treated them with TAM in a manner corresponding to labeling windows from day 0 – 10 (early), day 10 – 20 (intermediate) or day 30 – 40 (late), respectively (Fig. 1.3A). On day 60 after infection we enumerated $EYFP^+$ $GL7^+$ $B220^+$ GC B cells, which consistently co-expressed CD95, $EYFP^+$ $GL7^–$ $B220^+$ memory B cells (MemB cells) and $EYFP^+$ $GL7^–$ $B220^–$ ASCs (Fig. 1.3B, Supplementary Figure 1.3A, B). Thereby we assessed LCMV-specific B cells and plasma cells fulfilling two criteria: First, these cells or their precursors had expressed AID in the early,

intermediate and late labeling windows, respectively. Secondly, they were still present at the d60 time point of analysis as either GC B cells, MemB cells or ASCs. This experimental approach did not, however, inform about the clonal relationship between cells labeled in different time windows. We found that EYFP+ GC B cells were approximately 3-fold more numerous in rCl13- than in rARM-infected mice, irrespectively of the TAM labeling window (Fig. 1.3C). Conversely, the total number of GC B cells in rARM- and rCl13-infected animals was not significantly different (Supplementary Figure 1.3C). This indicated that antiviral GC responses were maintained at lower levels in acute as compared to chronic infection, with a proportional reduction in cells that had expressed AID during the early, intermediate and late labeling windows ("early-labeled", "intermediate-labeled" and "late-labeled" cells). For the intermediate and late labeling windows, reduced virus-specific GC B cell responses in rARM- as compared to rCl13-infected mice were also reflected in a lower proportional representation of AID-reporting cells amongst total GC B cells (Supplementary Figure 1.3D). In contrast, early-labeled MemB cell (Fig. 1.3D) and early-labeled ASC (Fig. 1.3E) pools were of comparable size in rCl13 and rARM infected animals, suggesting that in the early phase after virus inoculation, the MemB cell and ASCs output of acute and chronic infection was comparable. With transition from the early to intermediate and late labeling windows, however, the MemB cell and ASC output of rARM-infected mice declined progressively, which contrasted with sustained levels in rCl13 infection. These observations found independent support in immunohistochemical analyses from spleens of early-labeled mice, showing that EYFP+ cells inside splenic GCs were more numerous in rCl13 than in rARM infection (Fig. 1.3F). Taken together these observations indicated that GC responses in chronic infection were sustained at higher levels over time and in the long-term drove higher MemB cell and ASC output than acute infection.

Chronic infection is a potent long-term driver of B cell responses

We aimed to corroborate the hypothesis that at intermediate to late time points after virus inoculation chronic infection was a more potent driver of B cell responses than acute infection. For this we performed adoptive transfer experiments with Cell Trace Violet- (CTV-) labeled B cells of AID^{rep} mice, which express the monoclonal LCMV envelope-specific B cell receptor KL25 from a heavy chain knock-in and a light chain transgene (KL25HL-AID^{rep} mice, CD45.1; Fig. 1.4A). Twenty days prior to transfer, the syngeneic (CD45.2) recipients were infected with genetically engineered rCl13 or rARM variants (rCl13*, rARM*) carrying the N121K point mutation in their WE-GP envelope protein (WE-GP*). This envelope variant is only poorly neutralized by the KL25 antibody owing to only intermediate affinity binding as opposed to high-affinity interaction with WE-GP [28]. Intermediate affinity B cell receptor interactions were chosen for these experiments with KL25HL-AID^{rep} B cells in order to facilitate affinity maturation and render the experimental conditions more physiological. For induction of the AID-driven Cre reporter the recipients were given TAM on the day of B cell transfer and again three days later (d20, d23). Within five days after adoptive transfer (d25), virtually all KL25HL-AID^{rep} B cells had diluted CTV in both, chronically and acutely infected mice (Supplementary Fig. 1.4), indicating antigen-driven proliferation [230]. The proportion of KL25HL-AID^{rep} cells, which had activated AID (EYFP+) and/or expressed the GC marker GL7, increased from d25 to d35 both in rCl13*- and rARM*-infected recipients (Fig. 1.4B, Supplementary Fig. 1.4). Also, the EYFP/GL7 subset distribution, i.e. the proportion of KL25HL-AID^{rep} B cells activating AID and participating in GC reactions, was similar in acutely and chronically infected mice. Importantly, however, the number of KL25HL-AID^{rep} B cell progeny recovered from chronically rCl13*-infected mice exceeded those emerging from rARM* infection by ~5-fold (Fig. 1.4C). These numeric differences manifested in the AID-reporting (EYFP^{+}) and non-reporting (EYFP^{-}) compartments and were similarly

prominent for GC B cells ($GL7^+$) as they were for MemB cells ($GL7^-$). Accordingly, KL25HL-AID^{rep} B cells produced substantially higher antibody titers when transferred into chronically infected mice than upon transfer into acutely infected animals (Fig. 1.4D). This suggested that B cell clones recruited into the ongoing response or generated by hypermutation at later time points after infection were better represented in the serum immunoglobulin pool of chronically than acutely infected mice. Differential expansion of the adoptively transferred KL25HL-AID^{rep} B cell population was also evident at the histological level with markedly more EYFP+ KL25HL-AID^{rep} B cells inside GCs as well as outside GCs (Fig. 1.4E). In summary, these experiments established that in the time window from d20 – d35 after infection, virus-specific B cells expanded more vigorously in chronically than in acutely infected mice. They produced more antibody and yielded approximately five-fold more AID-reporting GC B cell and MemB cell progeny.

Comparable VH and JH intron mutation frequencies in B cells of acutely and chronically infected mice

Next we investigated whether chronic and acute infection settings differed in their ability to drive B cell hypermutation. We performed adoptive transfer experiments with KL25HL-AID^{rep} B cells on d20 after infection and sorted GL7+ GC B cell progeny on day 35 as outlined in Fig. 1.4A. We determined both, intronic sequences downstream of J_H as a readout of overall AID activity in the transferred KL25HL-AID^{rep} B cells and also KL25 V_H sequences as an indicator of affinity maturation. Neither of these target sequences provided clear evidence for a differential rate of hypermutation in acute as compared to chronic infection (Fig. 1.5A,B). This conclusion found independent support when we compared J_H intronic sequences of polyclonal isotype-switched GC B cells ($GL7^+$ IgM^- IgD^- $B220^+$) on day 60 after rCl13 and rARM infection (Supplementary Fig. 1.5A,B). Hence we performed a detailed analysis of coding

mutations in the KL25 V_H region of KL25HL-AID^{rep} B cells emerging from acute and chronic infection. We found evidence for an enrichment of recurrent mutations both in complementarity determining regions (CDRs) and framework regions (FRs) of the BCR (Fig. 5C). When systematically analyzing these sequences for evidence of affinity maturation we noted three CDRH3 mutations (W104L, F106L, Y108S), which were found in at least four out of eight individual mice infected with either rARM* or rCl13* (bold red residues in Fig. 1.5C). With the exception of F106L, these recurrent CDRH3 mutations were found in KL25HL-AID^{rep} B cells recovered from chronically as well as from acutely infected animals. We recombinantly expressed the three KL25 point mutant antibodies with amino acid changes in CDRH3 (W104L, F106L and Y108S) and assessed their ability to bind WE-GP* and to neutralize the corresponding WE-GP*-expressing virus rCl13*. KL25-W104L was the most prevalent mutant antibody (7 out of 8 mice studied) and it bound considerably better to WE-GP* than to the parental KL25 antibody, while the latter was a better binder on WE-GP (Fig. 1.5D). Most importantly, KL25-W104L neutralized rCl13* more potently than KL25wt, altogether indicating that the W104L mutation was acquired as a result of affinity maturation on the WE-GP* envelope protein of the infecting rCl13* virus (Fig. 1.5E). Improved WE-GP* binding and rCl13* neutralization by KL25-W104L was acquired at the expense of a relative reduction in the antibody's capacity to bind and neutralize rCl13. Similar trends were also noted for the other two CDRH3 KL25 mutants (KL25-F106L, KL25-Y108S; Supplementary Fig. 5C-F). Taken together, these data suggested that KL25HL-AID^{rep} B cells underwent affinity maturation upon adoptive transfer into either rCl13* or rARM* infected mice, and that this process was at least equally efficient in chronic infection as it was in acute infection.

Potent selection of hypermutated B cells in chronically infected mice

We report here that the generation of LCMV nAbs depends on hypermutation (Fig. 1.1D-F), and that nAbs are preferentially mounted in chronic as opposed to acute infection (Fig. 1.1C, [33]). Moreover, we have previously shown that the formation of nAbs and also the control of chronic LCMV infection fail in *aicda*$^{-/-}$ mice lacking class switch recombination and affinity maturation [27]. Hence we aimed to test whether AID-driven hypermutation, which apparently functions efficiently in chronically infected mice (Fig. 1.5), is rate-limiting for nAb generation and virus control. As a model of hypermutation-impaired B cells we made use of gene-targeted mice, which carry one deleted and one G23S-mutated allele of *aicda* (AID$^{G23S/-}$ mice, [248]). The AID-G23S mutation allows for class switch recombination while causing a substantial reduction in hypermutation rates [248]. We infected AID$^{G23S/-}$ and wt control mice with rCl13 to follow viremia and nAb kinetics. To our surprise, rCl13 control in AID$^{G23S/-}$ was only very modestly delayed, if at all (Fig. 1.6A). Also nAb responses followed similar kinetics as in wt mice, and reached comparable titers (Fig. 1.6B). Hence we sorted polyclonal GL7+ GC B cells on day 60 after infection for Ig$_H$ locus sequencing. The analysis of J$_H$ intronic sequences as a readout of overall AID activity confirmed our expectations [248] of approximately 10-fold reduced mutation frequencies in AID$^{G23S/-}$ mice (Fig. 1.6C). This difference between AID$^{G23S/-}$ and wt mice persisted when excluding non-mutated sequences from the analysis ("mutated introns" in Fig. 1.6C) and was also reflected in a paucity of highly mutated clones (Fig. 1.6D). To understand how AID$^{G23S/-}$ mice generated LCMV nAbs despite substantially reduced hypermutation frequencies, we determine the mutational burden in polyclonal V$_H$ sequences by unbiased high-throughput RNAseq. In marked contrast to the intronic sequences, a very modest 1.3-fold reduction in the number of V$_H$ mutations was observed in AID$^{G23S/-}$ mice (Fig. 1.6E), with a fair representation of highly mutated clones (Fig. 1.6F). It therefore appeared that the efficient selection of mutated clones enabled the formation of nAbs and the control of rCl13

infection even in hypermutation-impaired $AID^{G23S/-}$ mice. Taken together, these findings indicated that chronic infection provides a formidable selection machinery, which even under conditions of substantially reduced AID-driven mutation rates yields GC B cells with highly mutated V_H sequences.

Discussion

Our study establishes that the humoral immune system and GC B cell responses in particular are very effective at coping with chronic viral antigen exposure. Long-lived GC B cell responses, efficient selection of hypermutated clones and high MemB cell and ASC output altogether argue against humoral immune subversion, a conclusion which finds independent support in the accompanying paper. Intriguingly, this response pattern reflects the opposite of CD8 T cell exhaustion, yet from an evolutionary standpoint seems logical and beneficial for the host. Exhaustion is commonly thought of as nature's strategy to avoid fatal immunopathological consequences of inflammatory cytokine release and overshooting T cell cytotoxicity [249]. nAb-mediated virus clearance, on the contrary, is an innocuous and virtually non-inflammatory process. Immune complex disease, the only known side-effect of humoral immune defense in chronic viral infection, is rare and may selectively occur in a subset of patients with genetic predispositions [250].

It therefore appears that with progression to the chronic phase of viral infection, the relative efficacy of humoral immune defense increases while CD8 T cell responses undergo exhaustion. Interestingly, the CD4 differentiation profiles that predominate under these respective conditions is predicted to support a shift from cellular to humoral immune defense: With progression to chronicity Th1 responses become exhausted [251-253], similarly to CD8+ T cells, while Tfh cells start to dominate the CD4 T cell response [254-256]. Chronic infection also favors the emergence of Tfh cells with distinct functional profiles such as the ability to co-produce IL-10 and IL-21 [257]. Accordingly, potent Tfh responses represent an essential component of efficient GC reactions in the chronic infection context [257-259]. Equally importantly, sustained high-level antigen supply for continuous B cell receptor signaling fosters potent GC B cell responses and likely is accountable for more sustained ASC output in rCl13-infected animals.

Our observations help understand why nAbs to LCMV in mice, analogously to HIV and HCV in humans, are more readily elicited in chronic infection than upon acute infection or vaccination [33, 44, 216, 218-221, 223-225]. One widely held concept relates to the longer evolutionary trajectory of B cell receptors, which result from prolonged antigenic stimulation and continuous affinity maturation [260]. Our findings of comparable BCR hypermutation rates in chronically and acutely infected mice, although not contradictory to the above, suggest that additional mechanisms may be at work. (i) We propose that the continuously high ASC output even at late time points after the onset of chronic infection warrants for a better representation of the hypermutated GC B cell repertoire in the circulating serum antibody pool. Conversely, the hypermutated B cell pool emerging from acute infection would merely be available for accelerated nAb formation upon re-infection [230, 261]. The observation that not only rCl13- but also a few rARM-infected mice mounted nAb responses (Fig. 1.1C, right panel), supports this concept. It demonstrates that B clones of neutralizing capacity can be generated in acute infection, too. (ii) A second independent element that we assume is favoring nAb formation in chronic infection consists in the elevated cellularity of the GC B cell response. Studies in HIV-infected children as well as the search for minimally mutated HIV-bnAbs suggest that neutralizing B cell clones may be the product of a few serendipitous yet improbable mutations rather than of accumulated mutational load [235-238]. Similarly, HCV-bnAbs can apparently be generated with a limited number of critical somatic mutations [239]. A large pool of randomly mutated and efficiently selected B cell clones is therefore most likely to readily yield a few potently neutralizing ones. In line with this mechanism the accompanying paper describes that chronic infection results in higher intra-clonal diversification of responding B cells than acute infection. (iii) Last but not least, the combination of multiple weakly neutralizing antibodies can synergistically create substantial neutralizing activity [262-264]. Based on higher cellularity of the GC response and higher diversification (see above and

accompanying paper), we expect chronic infection to yield a broader spectrum of virus-specific serum antibodies and therefore more synergy-based neutralizing activity than acute infection.

A limitation of our study consists in its focus on B cells, without a concomitant analysis of CD4 T cell responses. Over the past years, however, a series of elegant studies have investigated the key contribution of Tfh cells to GC B cell responses in chronic LCMV infection, documenting also their impact on virus control [257-259]. Further, we acknowledge that our study focuses on late stages of infection, i.e. from three weeks after infection onwards. This choice was based on the late appearance of nAbs in rCl13-infected mice, with an intention to better understand the B cell correlate thereof. Accordingly, the present study complements previous reports from our lab and others, which have investigated B cell responses at the onset of LCMV infection [226-228]. Finally, LCMV infection in mice represents a versatile model to investigate the impact of chronic antigen load on immune responses, whereas other features of human infections such as the progressive loss of CD4+ T cells in human HIV infection are not recreated in the LCMV model but may also impact B cell responses.

In summary, our findings and those in the accompanying paper characterize GC B cell responses as an imperturbable element of antiviral defense, which operates effectively and even excels when continuously faced with high amounts of viral antigen. Thereby our study portrays the natural context in which GC B cell responses yield potent nAbs or even bnAbs against persisting viruses, depicting also the challenges yet to be met when attempting to safely mimic these processes for prophylactic vaccination.

Methods

Mice and Ethics statement

C57BL/6J wildtype mice were purchased from Charles River, France, CD45.1-congenic C57BL/6J have been obtained from the Swiss Immunological Mouse Repository, (SwImMR). AID-Cre-EYFP (AID^{rep}) mice carrying a targeted tamoxifen- (TAM-) inducible Cre recombinase (Cre-ERT2) in the *aicda* locus in combination with a Cre-inducible EYFP reporter gene in the ROSA26 locus have been described [245]. KL25HL mice, which express the monoclonal LCMV envelope-specific B cell receptor KL25 from a heavy chain knock-in and a light chain transgene, and KL25L mice, which express the light chain of the monoclonal LCMV envelope-specific B cell receptor KL25 as a transgene have been described [226]. KL25HL-AID^{rep} mice have been obtained by crossing AID-Cre-EYFP mice with KL25HL mice. AID^{G23S} mice (carrying a targeted G23S mutation on the *aicda* locus) were generously provided by Dr. T. Honjo [248]). F1 offspring resulting from the intercross of homozygous AID^{G23S} and homozygous AID-Cre-EYFP mice were used as hypermutation-impaired $AID^{G23S/-}$ mice for experiments. All mice were on a C57BL/6 background and were bred at the Laboratory Animal Science Center (LASC) of the University of Zurich, Switzerland, under specific pathogen-free (SPF) conditions. Experiments were performed at the University of Basel and at the University of Geneva, in accordance with the Swiss law for animal protection and with authorizations from the Veterinäramt Basel-Stadt and from the Direction Générale de la Santé, Domaine de l'Expérimentation Animale of the Canton of Geneva, respectively. Assignment to experimental groups was based on sex- and age-matching. Adult animals of both genders were used to reduce the number of animals bred for research purposes. Study sample sizes in mouse experiments were chosen based on experience in our labs with respect to group sizes readily revealing biologically significant differences in the experimental models

used. The groups were neither randomized nor were experiments conducted in a blinded fashion.

Viruses and Cell Lines

The recombinant LCMV strain Cl13 (rCl13) and Armstrong (rARM) expressing the surface glycoprotein of the LCMV strain WE (WE-GP) and the WE-GP N121K variants (rCl13*, rARM*) have been described [44] and were engineered by standard procedures [198]. Recombinant Vaccinia virus expressing VSVG and vesicular stomatitis virus serotype Indiana (VSV) have been described [265]. For virus production and titration BHK-21 cells (Clone 13, ECAAC), BSC40 cells (ATCC) and NIH 3T3 cells (ATCC) were used and were confirmed to be mycoplasma-negative. Owing to their origin from renowned international repositories they were not authenticated.

Flow cytometry and cell sorting

Single cell suspensions were obtained from spleens by mechanical or enzymatic digestion. Spleens were harvested in PBS containing 5% FCS and for mechanical digestion spleens pushed through a metal mesh in a petri dish and homogenized by pipetting. For enzymatic digestion spleens where cut into small pieces and incubated with collagenase D (Roche) and DNaseI (Calbiochem) at 37° C for one hour on magnetic rotators and then washed with PBS. Dead cells were excluded using the Zombie UV™ or Zombie Yellow™ Fixable Viability Kits (BioLegend), then washed with PBS. The following fluorophore-conjugated antibodies were used for staining: αB220 (Biolegend or BD Biosciences), αCD138 (BioLegend), GL-7 (eBioscience or Biolegend), αCD95 (BD Biosciences), αCD38 (BioLegend), biotinylated PNA (Vector Laboratories) and fluorophore-conjugated streptavidin (BioLegend). Anti-CD16/32 antibody and polyclonal rat IgG were added to the staining mixture to block Fc receptors. When

adoptive cell transfers were performed, donor and recipient cells were distinguished using αCD45.1- and αCD45.2 - fluorophore-conjugated antibodies (Biolegend). Cells were co-stained for 15 minutes at 4°C with combinations of the fluorophore- and biotin-conjugated antibodies and with fluorophore-conjugated streptavidin, then washed with FACS-Buffer. Subsequently, the cells were fixed using PBS containing 4% PFA. NP-binding cells were detected using a bacterially expressed, Alexa647-labelled recombinant NP [226, 230]. All media were adapted to mouse osmolarity. Labeled $EYFP^+$ (AID- reporting) cells (see section "mice") were detected using an LSRFortessa flow cytometer (Becton Dickinson). Data were analyzed using FlowJo software (Tree Star). Absolute splenocyte counts of ARM-infected and Cl13-infected mice were indistinguishable when compared at either five or eight weeks after infection.

For sorting of KL25HL-AID^{rep} B cell progeny, splenocytes were positively enriched for $CD45.1^+$ cells by magnetic-activated cell sorting (MACS) using biotin-coupled αCD45.1 antibody (BioLegend) and anti-Biotin MicroBeads (Miltenyi Biotec) following the provider's instructions. The cells were then stained with the following antibodies: αCD45.1 (Biolegend), αCD45.2 (Biolegend), αB220 (Biolegend) and GL-7 (Biolegend). $CD45.2^–$ $CD45.1^+B220^+GL7^+$ cells were sorted into PBS containing 5% FCS (1'000 to 10'000 cells). Dried pellets were frozen in liquid nitrogen and DNA was prepared by cell lysis [266].

For sorting of $AID^{G23S/-}$ GC B cells, 5'000 $B220^+GL7^+$ splenocytes from each mouse were sorted directly into TRI Reagent LS (Sigma-Aldrich). RNA was extracted as described below (see section "high throughput sequencing"). DNA was extracted using chloroform phase separation according to manufacturer's procedures (Sigma-Aldrich), yeast tRNA (Sigma-Aldrich) was added as a carrier.

Cell sorting was performed using a FACSAria II cell sorter (Becton Dickinson).

Adoptive B cell transfer, Tamoxifen and passive antibody administration

For adoptive transfer of CD45.1$^+$ KL25HL-AID^{rep} B cells, CellTrace Violet (Invitrogen) - labeled bulk splenocytes (2 x 10^6 cells per recipient) or purified B cells (2 x 10^5 cells per recipient) were injected intravenously in balance salt solution. B cells were purified by magnetic activated cell sorting using the Pan B Cell Isolation Kit for untouched B cells (Miltenyi Biotec). Syngenic (CD45.2$^+$) C57BL/6J mice served as recipients for short-term transfers. Transfers of KL25HL cells for analysis >1 week later were performed in KL25L recipients to avoid rejection by anti-idiotypic responses [226].

For adoptive transfer of Vaccinia virus- or LCMV-experienced EYFP$^+$ B cells we infected AID^{rep} mice on day 0 with the respective viruses, followed by tamoxifen treatment on day 0, 5 and 10. On day 30 splenic B cells were MACS-purified (Miltenyi Biotec Pan B Cell Isolation Kit for untouched B cells) and labeled with CTV. 2x10^6 – 8x10^6 B cells (purity > 95%) containing between 10^5 – 1.5x10^5 EYFP$^+$ B cells were transferred into Vaccinia virus- or LCMV-infected CD45.1$^+$-congenic C57BL/6J recipients.

Tamoxifen (2.5 mg Novadex (AstraZeneca) in 20% Clinoleic (Baxter) was administered by gavage.

Passive antibody administration was performed three days after infection by an intravenous bolus injection of 300 µg purified antibody in PBS.

Immunohistochemistry and image analysis

For the histological sections shown in Fig. 1.3, tissues were fixed in PBS containing 4% paraformaldehyde (Merck) for at least 4 hours at 4°C, then washed with PBS and cryoprotected with PBS-30% sucrose (Sigma-Aldrich) for at least 2 hours at 4°C. Tissues were then embedded in Tissue-freezing-medium (Leica Microsystems) and frozen on dry ice. For the microsections shown on Fig 1.4, tissues were fixed in PBS containing 4% paraformaldehyde

(Merck) for at least 4 hours at 4°C, then washed with PBS and embedded in paraffin. Immunostaining was performed on 3 µm-thick sections using antibodies against GFP (ICL lab), Alexa Fluor 647-directly labeled B220 (eBiosicence) and Lectin PNA Alexa Fluor™ 488 Conjugate (LThermoFisher). Immunostained slides were incubated with the Vector® TrueVIEW™ Autofluorescence Quenching Kit to remove autofluorescence signal (Vector Laboratories). Stained sections were scanned using a Panoramic Digital Slide Scanner 250 FLASH II (3DHISTECH) at 200 x magnification. Contrast was adapted using the "levels", "curves", "brightness" and "contrast" tools in Photoshop CS6.

Viruses, virus production, titration and infection

For LCMV batch production, BHK-21 cells (ATCC) were infected with the respective viruses at MOI = 0.01 and virus-containing supernatant was harvested 48 hours later.

Recombinant Vaccinia virus expressing VSVG was produced on BSC-40 cells and vesicular stomatitis virus serotype Indiana (VSV) was grown on BHK-21 cells (MOI = 0.01 for 24 hours) [265].

LCMV infectivity in blood was determined by immunofocus assay [267]. In brief, blood was collected into BSS supplemented with 1 IE/ml heparin (Na-heparin, Braun). Ten-fold serial dilutions were performed and were mixed 96-well plates and with NIH 3T3 cells (ATCC) in 24-well plates, followed by 3 hours of incubation at at 37°C. Then, overlay (1% methylcellulose in DMEM) was added and the cultures were incubated for two days. On the third day, supernatant was removed, the cells were fixed with 4% paraformaldehyde and permeabilized (1% TritonX100 in PBS). After blocking (5% FCS), infectious foci were visualized using VL4 rat-anti-LCMV-NP antibody and secondary HRP-conjugated goat-anti-rat-IgG (Jackson Immunoresearch), followed by a color reaction (DAB).

rARM and rARM* infections were performed by intraperitoneal (i.p.) injection of 200 plaque-forming units (PFU). rCl13 and rCl13* were administered intravenously (i.v.) at a dose of $2x10^6$ – $4x10^6$ PFU. Vaccinia virus and VSV were administrated i.v. at doses of $2x10^6$ and $2x10^7$ PFU, respectively.

Determination of neutralizing antibody titers

Neutralizing antibodies were measured in standard immunofocus assay-based [267] plaque reduction neutralization tests. Serial two-fold dilutions of antibody-containing sera and of purified monoclonal antibodies were conducted in MEM 2% FCS in a 96-well format. Approximately 50 PFU of virus was added to each well, followed by 90 minutes of incubation at 37°C. NIH 3T3 fibroblasts were added and incubated with the virus – antibody mixture at 37°C for 90 minutes, allowing the cells to adhere. Thereafter, overlay (1% methylcellulose in DMEM) was added. Two days later, infectious foci were identified as described for the LCMV immunofocus assay. Neutralizing titers in mouse sera were determined as the highest serum dilution yielding at least 50% focus formation reduction. For monoclonal antibodies, the number of infectious foci at a given antibody concentration was expressed as a percentage of the number of foci in control wells without antibody added.

Analysis of somatic mutations at the IgH locus

The J_H4 intronic sequence flanking rearranged V_H gene segments was amplified by PCR from DNA of sorted B cell subsets, from 10,000 to 1,000 cells. The PCR primers used are: in 5', a mixture of five FR3 primers amplifying most V_H gene families (V_H1, : GAGGACTCTGCRGTCTATTWC, V_H3: GAGGACACACCCACATATTAC, V_H5: GAGGACACRGCCATGTATTAC, V_H6: GAAGACACTGGAATTTATTAC, V_H7: GAGGACAGTGCCACTTATTAC, V_H9: ATGAGGACATGGCTACATATTTC, in a

6:1:3:1:1 ratio); in 3', a J_H4 intronic primer ($J_H4$rev: CACCAGACCTCTCTAGACAGC), with a nested amplification performed in cases of low cell numbers (using J_H4-nested: TGAGACCGAGGCTAGATGCC and the same V_H primer set) (2 min at 98°C and 50 cycles of 15 s at 98°C, 30 s at 64°C and 30 s at 72°C, with Phusion® DNA polymerase (New England Biolabs); or 30 cycles plus 25 additional cycles in cases of nested PCR). Mutations were determined within 448 base pairs of the J_H4 intron.

For the KL25 VDJ knock-in allele, two different PCR were performed: one encompassing the V_HDJ_H2 (V1-53) coding sequence, and the other one based on the flanking intronic sequence, consisting in a fused J_H2-J_H4 segment present in the knock-in construct, using the following conditions. V_HDJ_H2: 5' primer, CTCTCCGCAGGTGTCCACTCC; 3' primer, AGAAAGAGGTTGTAAGGACTCAC; J_H2-J_H4 segment: 5' primer, CTAGGCACCACTCTCACAGTC; 3' primer, CACCAGACCTCTCTAGACAGC (2 min at 98°C and 40 cycles of 15 s at 98°C, 30 s at 64°C and 30 s at 72°C). Mutations were determined for the 324 bp sequence of the V_H gene (including CDR3), and for 570 bp of the intronic sequence, immediately downstream of J_H2.

PCR products were cloned with the TOPO-TA cloning kit (Invitrogen) and sequences were determined with an ABI Prism 3130xl Genetic Analyzer. Mutations were analyzed with the help of the CodonCode Aligner software. Between 16 to 91 sequences per sample were determined for mutation frequency determination.

High throughput sequencing

Preparation of antibody libraries from rCl13-infected wt and $AID^{G23S/-}$ mice: Library preparation by RT-PCR was performed similar to the protocol described in Menzel et al. [268]. Total RNA was extracted (25 µL elution volume) using the TRIzol Plus RNA Purification Kit (Life Technologies) according to the manufacturer's protocol. First-strand cDNA was

synthesized with AccuScript High-Fidelity Reverse Transcriptase (Agilent Technologies) using total RNA and Oligo(dT) primers (Thermo Scientific) following the manufacturer's instructions. PCR- amplification was performed with Q5 Hot Start High-Fidelity DNA polymerase (NEB) in 50 µL reaction volumes with adjusted cycle numbers. For the eight germinal center samples an IgG-specific reverse primer was used. PCR1 products were purified using SPRI select beads (Beckman Coulter) at a ratio of 0.8X (elution in 30 µL water). Purified PCR1 products were submitted to PCR2-amplification, which adds full-length Illumina adapters to the library. Final products were gel-purified from 1% agarose gels. All amplicon libraries were quantified by qPCR using the KAPA Library Quantification Kit (KAPA Biosystems). Based on qPCR results, samples were diluted to 7 nM concentrations and a pool was prepared with equal amounts of library. Last, the pool was checked on a Fragment Analyzer (DNF-486 High Sensitivity NGS Fragment Analysis Kit, Advanced Analytical), the exact concentration determined (Qubit 2.0 Fluorometer) and diluted to a final concentration of 4 nM.

Illumina sequencing and data preprocessing: Illumina MiSeq sequencing was performed using 2x300 bp reads. Forward and reverse reads were paired using PANDAseq (Version 2.7, [2]) with parameter -0 300. Full length VDJ region annotation and somatic mutation enumeration of successfully paired sequences was performed using ImMunoGeneTics (IMGT)/HighV-QUEST [3, 4]. For downstream analyses, sequences were pre-processed and reads only retained based on the following criteria: (i) the IMGT-indicated "Functionality" of the sequencing was "productive"; (ii) CDR3s were of minimal length of 4 amino acids; (iii) CDR3 were present with a minimum abundance of 2. Nucleotide mutation numbers were based on IMGT. Number of reads in analyses shown ranged between 1.3 and $1.5x10^6$ per individual across both C57BL/6 and $AID^{G23S/-}$ mice.

Enzyme-linked immunosorbent assay (ELISA), recombinant proteins and monoclonal antibodies

GP-1-binding antibodies in mouse serum were determined using recombinant HEK293 cell-derived GP-1-Fc fusion protein as a substrate [33]. Binding of KL25 and the affinity-matured mutants KL25-W104L, KL25-F106L and KL25-Y108S to WE-GP and WE-GP* was determined using a synthetic HEK293 cell-derived fusion protein consisting of the extracellular WE-GP and WE-GP* domains, respectively, fused to human Fc (WE-GP-Fc, WE-GP*-Fc, [28]). For the aforementioned ELISA assay formats, 96-well high binding plates (Greiner Bio-One) were coated with 0.7 µg/ml goat anti-human IgG Fcγ antibody (Jackson, 109-005-098) in coating buffer (Na_2CO_3 15mM, $NaHCO_3$ 35mM, pH9.6) at 4°C overnight. Then, the plates were blocked for 2 hours at room temperature with PBS / 0.05% Tween / 5% milk (also used as buffer in the subsequent steps). Subsequently, GP-1-Fc, WE-GP-Fc or WE-GP*-Fc was added and incubated for 1h, followed by three wash steps with PBS / 0.05% Tween (PBS-T). Serum samples or monoclonal antibodies were added in a serially diluted manner and were incubated for 1h at RT. Following three more PBS-T wash steps, goat anti-mouse IgG-HRP conjugate antibody (1:750, Jackson) was added. Excess secondary antibody was washed away and HRP activity was detected using ABTS as a chromogen (Pierce). OD_{405} was determined in an ELISA reader.

The GP-binding capacity of WEN-1, WEN-1UA, WEN-3 and WEN-3UA was determined using as an ELISA substrate a HEK293-derived extracellular WE-GP domain with a C-terminal StreptagII sequence (GP-Streptag [44]). The ELISA assay was performed analogously to the above, except that GP-Streptag was captured by coating ELISA plates with 0.5ug/ml of Strep-TactinXT (Iba), and that the plates were blocked with 0.2% BSA in PBS.

Monoclonal antibodies

The unmutated ancestor sequences (WEN-1^{UA}, WEN-3^{UA}) of the rCl13-neutralizing monoclonal antibodies WEN-1 and WEN-3 (Supplementary Fig. 1.1 [32, 33]) were identified by IgBlast (IgBlast) sequence analysis. All mutations deviating from the closest germline V(D)J heavy (HC) and light chain (LC) sequences were reverted. The corresponding cDNAs were synthesized (Genscript) and introduced into HC and LC expression cassettes for recombinant expression in a mouse IgG1 format (provided by Dr. Shozo Izui, University of Geneva). The antibodies were produced by transient co-transfection of the HC and LC expression plasmids in CHO cells (Protein Expression Core Facility, PECF, of the Swiss Federal Technical Highschool, EPFL, Lausanne, Switzerland). The antibodies were purified on an ÄKTAprime plus purification system using Protein G columns (GE healthcare). After 24 hours of PBS dialysis, the purified antibodies were quantified by IgG ELISA. MOPC-21 (BioXcell) served as isotype control antibody. The KL25-W104L, KL25-F106L and KL25-Y108S antibodies as well as a matching KL25 wildtype control antibody were obtained by analogous procedures, except that a mouse IgG2a expression format was used for these experiments.

Statistical Analysis

The GraphPad Prism software version 7 (GraphPad Software) was used for all statistical analyses. Unpaired two-tailed Student's *t* tests were performed to compare one parameter between two groups. For comparison of one parameter between multiple groups one-way analysis of variance (ANOVA) was performed and for comparison of multiple parameters between two or more groups two-way ANOVA was used, both followed by Bonferroni's post-test for multiple comparison. For statistical analysis of absolute cell counts, values were log-

converted to obtain a near-normal distribution. *P* values ≥ 0.05 were regarded as not statistically significant (ns), *p* values < 0.05 as significant (*, #) and $p < 0.01$ as highly significant (**, ##). The number of experimental animals "*n*" per group, number of experimental repeats "N", the type of error bar displayed and the tests performed for statistical analysis are indicated in each figure legend.

ELISA quantification and curve fitting

For titer determination in mouse serum based on standard curve fit, GEN5 software (BioTek Instruments) was used. Binding and neutralization curves of monoclonal antibodies were fitted using GraphPad Prism software 7 (GraphPad Prism).

Figures

Figure 1

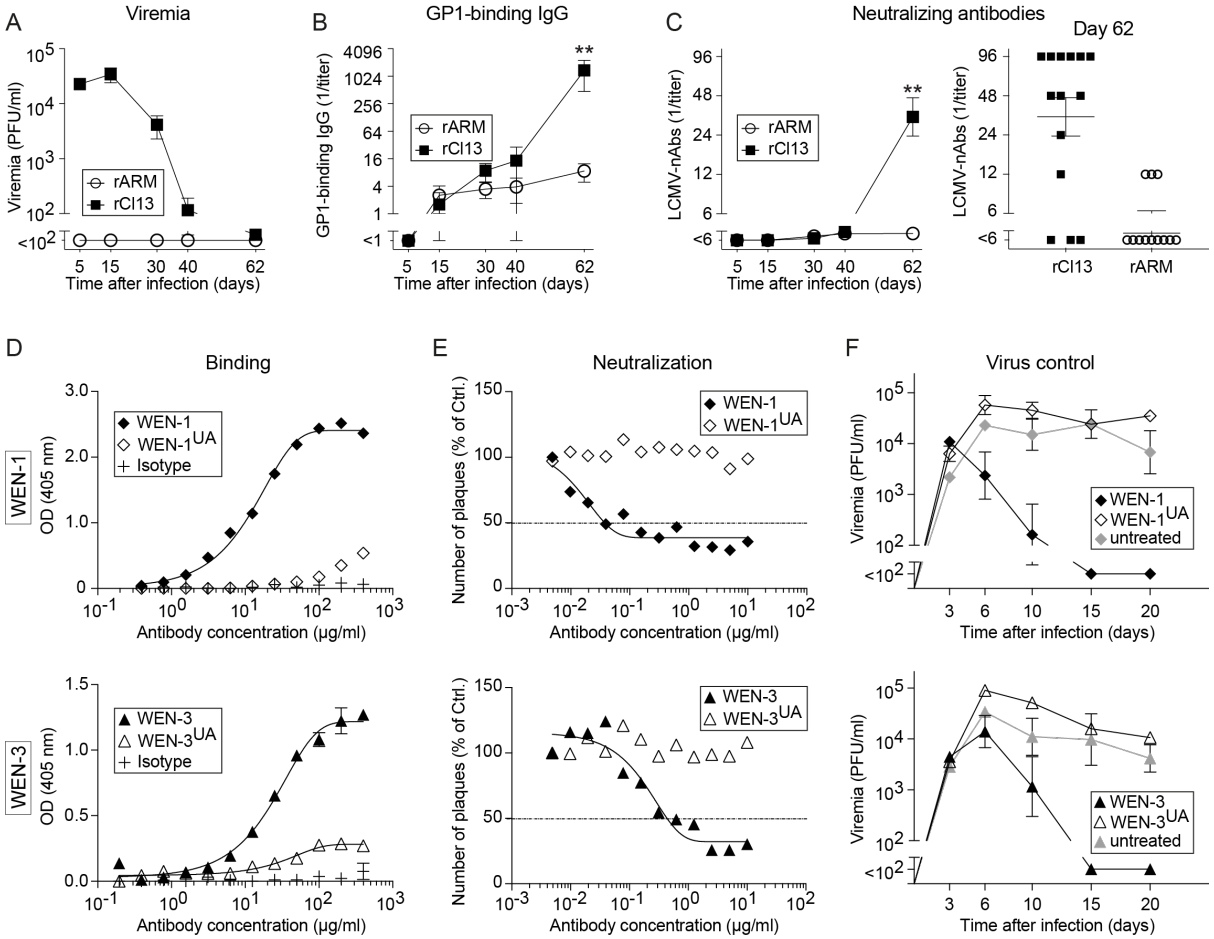

Figure 1. 1: LCMV nAbs arise preferentially in chronic infection and require somatic hypermutation

A-C: We infected mice with rCl13 or rARM and measured viremia (A), GP1-binding IgG titers (B) and rCl13-neutralizing antibodies (C) from blood on the indicated days. Symbols and bars represent means +/- SEM (A,B,C left panel). The right panel in (C) shows nAb titers of individual animals on day 62. n= 3 to 15 (A), n= 5 (B), n= 12 to 15 (C). N= 3. Two-way ANOVA with Bonferroni's post-test for multiple comparisons. **: $p < 0.01$.

D-E: Binding of the rCl13-neutralizing antibodies WEN-1 and WEN-3, of their respective

unmutated ancestors WEN-1^{UA} and WEN-3^{UA} and of an irrelevant isotype control antibody to WE-GP (D). Ability of the indicated antibodies to neutralize rCl13 (E). Symbols show the mean of 2 technical replicates. N = 2.

F: We infected mice with rCl13 on d0, followed by passive immunization with the indicated antibodies on d3. Viremia was monitored. Symbols represent the mean +/- SEM of 3 to 4 mice (WEN-1, one representative experiment) and of 4 to 6 mice (WEN-3, two combined experiments), respectively. N = 2.

Figure 2

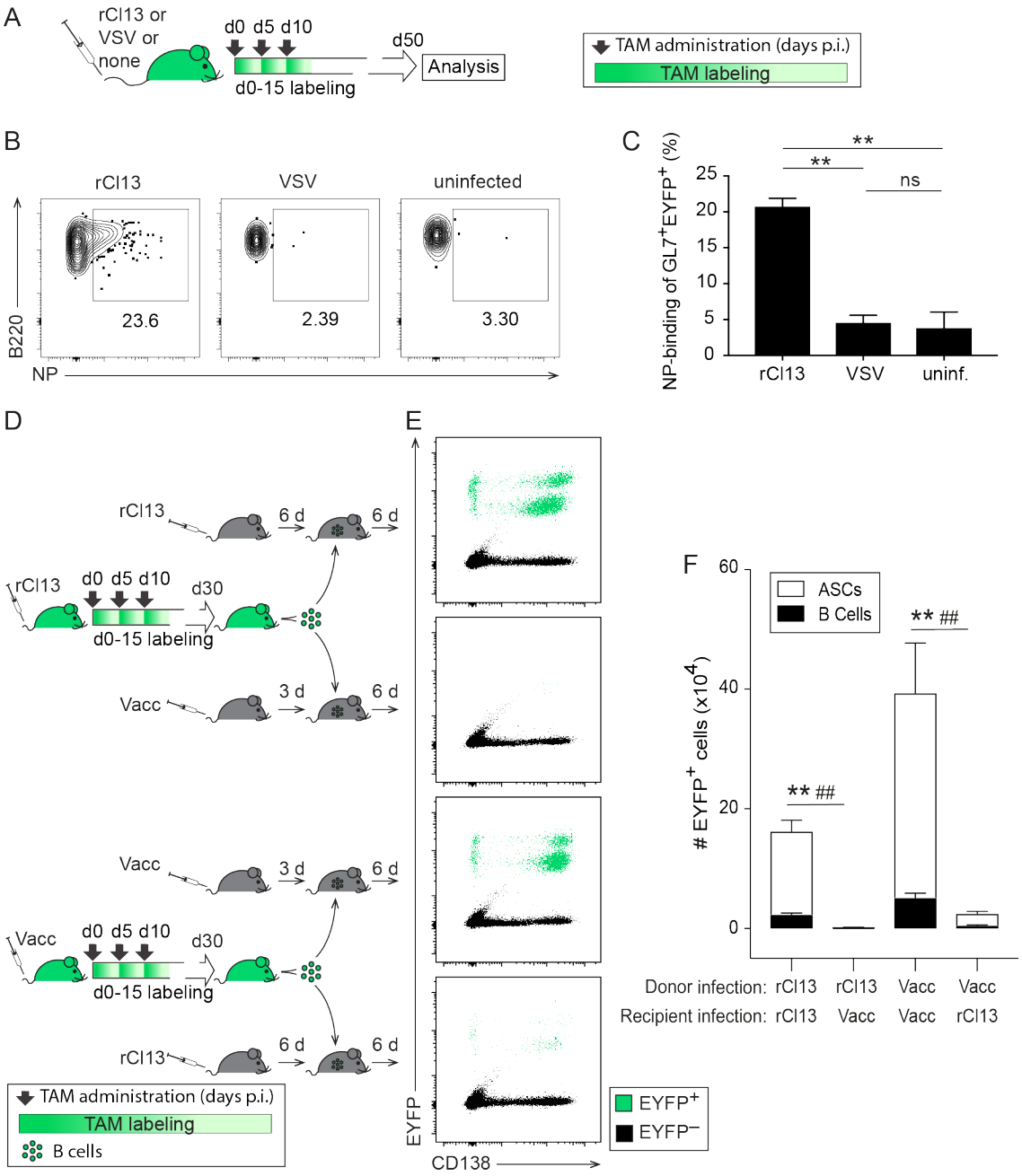

Figure 1. 2: AID reporter system identifies LCMV-specific B cells in a polyclonal response

A-C: We infected AID^{rep} mice with rCl13 or VSV on day 0 or left them uninfected. TAM was administered on day 0, 5 and 10. LCMV-NP-binding by splenic EYFP^{+} GL7^{+} B cells was analyzed on day 50 (for gating strategy see Supplementary Fig. 1.2).

D-F: We infected AID^{rep} mice with rCl13 or Vacc on day 0 and treated them with tamoxifen on day 0, 5 and 10. On day 30 we purified B cells from spleen by magnetic cell separation and transferred them into syngeneic C57BL/6 recipients, which had been infected with rCl13 six days before (d24) or with Vacc three days earlier (d27). Six days after transfer (d36) we measured the expansion and plasma cell differentiation of proliferated (CTV^{lo}) adoptively transferred EYFP-reporting B cells in the spleen. Two distinct $EYFP^+$ ASC populations correspond to different stages of maturation. Representative FACS plots are gated on $EYFP^+$ $B220^+$ $CD138^-$ $GL7^+$ B cells (B) and on recipient ($CD45.2^+$) lymphocytes in black with $EYFP^+$ CTV^{lo} donor cells overlaid in green (E), respectively (see Supplementary Fig. 1.2). Numbers in FACS plots represent percentages of gated cells amongst $EYFP^+$ $B220^+$ $CD138^-$ $GL7^+$ B cells. Bars represent means +/- SEM. n = 3 to 4 (C) and n = 4 (F). N = 2. One-way ANOVA with Bonferroni's post-test for multiple comparisons (C). Two-way ANOVA with Bonferroni's post-test for multiple comparisons (F). **, ##: $p < 0.01$. ** comparing B cells; ## comparing ASCs, respectively.

Figure 3

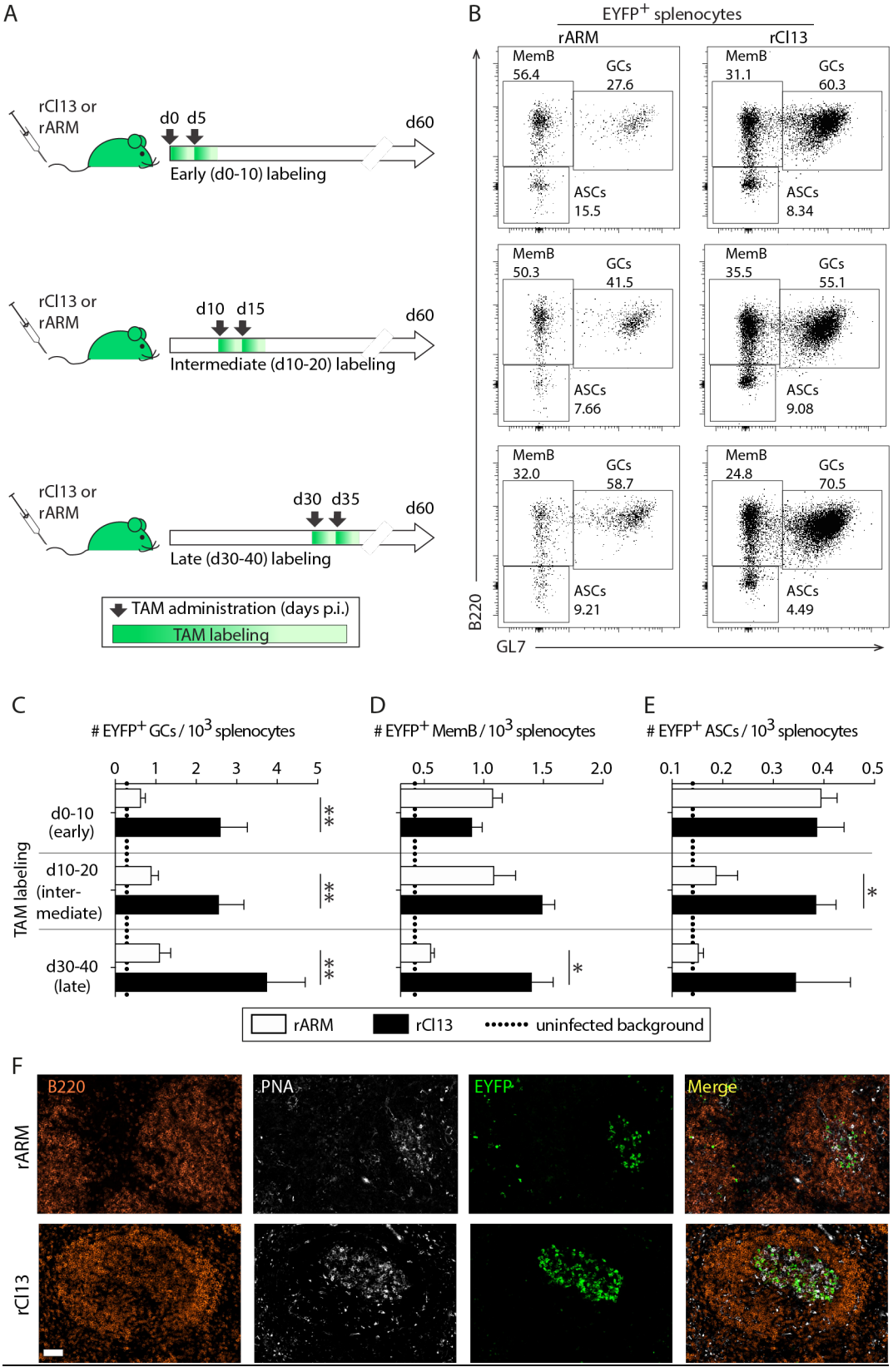
A
rCl13 or rARM
d0 d5
d60
Early (d0-10) labeling
rCl13 or rARM
d10 d15
d60
Intermediate (d10-20) labeling
rCl13 or rARM
d30 d35
d60
Late (d30-40) labeling
TAM administration (days p.i.)
TAM labeling
B
EYFP+ splenocytes
rARM
rCl13
MemB 56.4
GCs 27.6
ASCs 15.5
MemB 31.1
GCs 60.3
ASCs 8.34
MemB 50.3
GCs 41.5
ASCs 7.66
MemB 35.5
GCs 55.1
ASCs 9.08
MemB 32.0
GCs 58.7
ASCs 9.21
MemB 24.8
GCs 70.5
ASCs 4.49
B220
GL7
C
EYFP+ GCs / 10^3 splenocytes
0 1 2 3 4 5
TAM labeling
d0-10 (early)
d10-20 (inter-mediate)
d30-40 (late)
**
**
**
D
EYFP+ MemB / 10^3 splenocytes
0.5 1.0 1.5 2.0
*
E
EYFP+ ASCs / 10^3 splenocytes
0.1 0.2 0.3 0.4 0.5
*
rARM
rCl13
uninfected background
F
B220
PNA
EYFP
Merge
rARM
rCl13

Figure 1. 3: Chronic infection triggers a sustained GC response with prolonged plasma cell and memory B cell output

A: We infected AID^{rep} mice with rARM or rCl13 on d0, followed by TAM administration on d0 and d5 (early), d10 and d15 (intermediate) or d30 and d35 (late), respectively. B: EYFP-expressing cells were analyzed two months after infection. Representative FACS plots are gated on $EYFP^+$ cells (see Supplementary Fig. 1.3). Numbers in FACS plots indicate percentages of gated cells amongst $EYFP^+$ cells. C-E: EYFP-expressing GC B cells, MemB cells and ASCs in the spleen were enumerated. Doted lines indicate background levels of EYFP-expressing cells in uninfected control mice. F: Representative histological spleen sections from rCl13- and ARM-infected mice in the early-labeled group. Magnification bar: 50 μm. Bars represent mean +/- SEM. n = 4 to 5 (C-E) and n = 6 from three data sets (F). N = 2. Two-way ANOVA with Bonferroni's post-test for multiple comparisons. *: $p < 0.05$; **: $p < 0.01$.

Figure 4

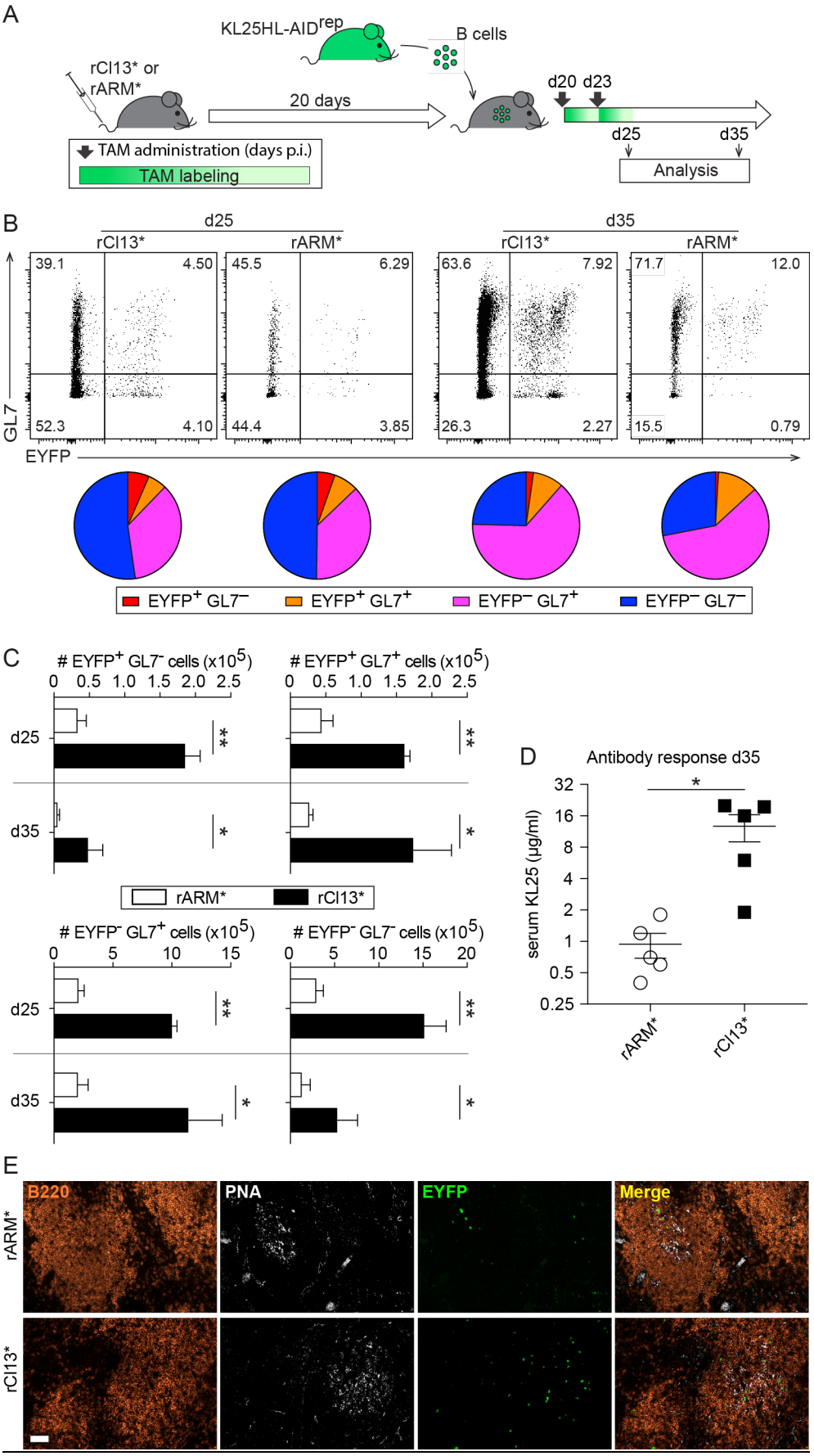
A
KL25HL-AID rep
B cells
rCl13* or
rARM*
20 days
d20 d23
d25
d35
TAM administration (days p.i.)
TAM labeling
Analysis
B
d25
d35
rCl13*
rARM*
39.1
4.50
52.3
4.10
45.5
6.29
44.4
3.85
63.6
7.92
26.3
2.27
71.7
12.0
15.5
0.79
GL7
EYFP
EYFP+ GL7−
EYFP+ GL7+
EYFP− GL7+
EYFP− GL7−
C
EYFP+ GL7- cells (x10^5)
EYFP+ GL7+ cells (x10^5)
EYFP- GL7+ cells (x10^5)
EYFP- GL7- cells (x10^5)
d25
d35
rARM*
rCl13*
D
Antibody response d35
serum KL25 (µg/ml)
rARM*
rCl13*
E
B220
PNA
EYFP
Merge
rARM*
rCl13*

Figure 1. 4: Chronic infection is a potent long-term driver of B cell responses

A: We infected syngeneic recipient mice with rARM* or rCl13* on d0, and 20 days later we adoptively transferred CTV-labeled KL25HL-AID^{rep} B cells. TAM was administered on the day of transfer (d20) and on d23.
B,C: Five and 15 days after adoptive transfer (d25, d35) we analyzed KL25HL-AID^{rep} B cells by flow cytometry for AID reporting (EYFP^{+}) and GC differentiation (GL7 expression). Representative FACS plots in (B) are gated on adoptively transferred proliferated B cells (CD45.1^{+} CD45.2^{-} CTV^{lo} B220^{+} CD138^{-} cells, gating strategy in Supplementary Fig. 1.4). The average proportional representation of EYFP^{+}GL7$^{–}$ (red), EYFP^{+}GL7^{+} (orange), EYFP$^{–}$GL7^{+} (magenta) and EYFP$^{–}$GL7$^{–}$ (blue) subsets is displayed in pie charts. Absolute numbers of these same cell populations are shown in (C). Bars represent means +/- SEM. n = 3 to 5.
D: The concentration of KL25 IgG in the serum of KL25HL-AID^{rep} B cell recipients was determined by GP-1 ELISA. Background GP-1-specific IgG levels in control mice without KL25HL-AID^{rep} B cell transfer were at least 4-fold lower than in the respective groups of recipients. Symbols show individual mice.
E: Histological sections from spleens of rCl13* and rARM* infected mice on d25. Scale bar: 50 μm. n=3, N ≥ 2. Two-way ANOVA with Bonferroni's post-test for multiple comparisons (C), unpaired two-tailed Student's t test (D). *: $p < 0.05$; **: $p < 0.01$.

Figure 5

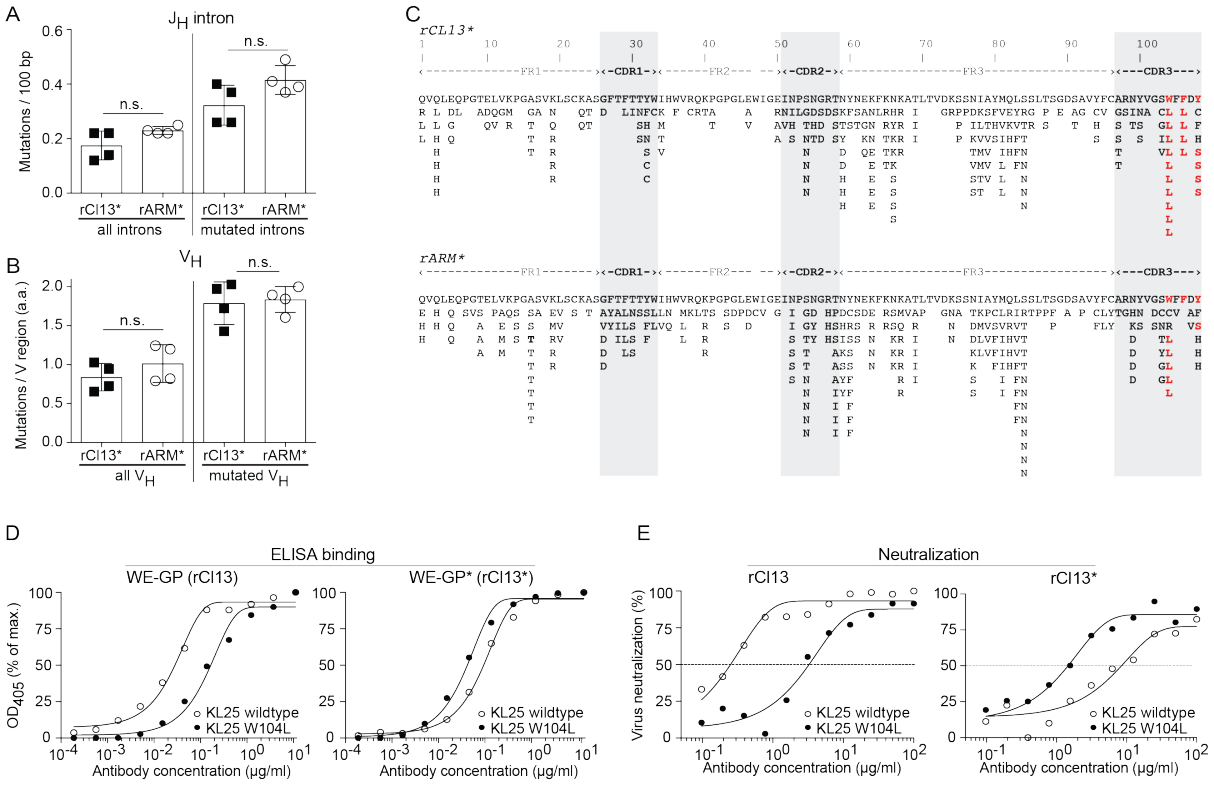

Figure 1. 5: Comparable VH and JH intron mutation frequencies in B cells of acutely and chronically infected mice

A-C: We performed adoptive transfer experiment as in Fig. 4 and on d36 we sorted isotype-switched adoptively transferred KL25HL-AID^{rep} GC B cells (CD45.1$^+$ CD45.2$^-$IgM$^-$IgD$^-$ GL7$^+$B220$^+$) by FACS for IgH locus sequencing. (A) Mutation frequencies in the J_H intron as base pair (bp) changes are shown for all sequences obtained (left) as well as for mutated introns only (right). (B) Mutations in the KL25 V_H gene as total amino acid changes per V sequence, for all sequences (left) or sequences with amino acid changes (right), taking only functional sequences into account. (C) All amino acid mutations collected from four rARM*- and four rCl13*-infected mice (708 sequences total, 85-91 sequences per mouse) are represented along the KL25 V_H protein sequence (rCl13* infection, top; rARM* infection, bottom). Mutations

are shown in bold red letters when present in at least 4 individual mice (out of 8). CDR positions are shaded in gray. Bars show means +/- SD, symbols represent individual mice. n = 4, N = 1 (A-C). Unpaired two-tailed Student's *t* test (A, B). ns: $p \geq 0.05$. D: Binding of KL25 wildtype and KL25-W104L to WE-GP and WE-GP*. E: Neutralization of rCl13 and rCl13* by KL25 wildtype and KL25-W104L. Symbols in (D,E) show the mean of 2 technical replicates. N = 3 (D,E).

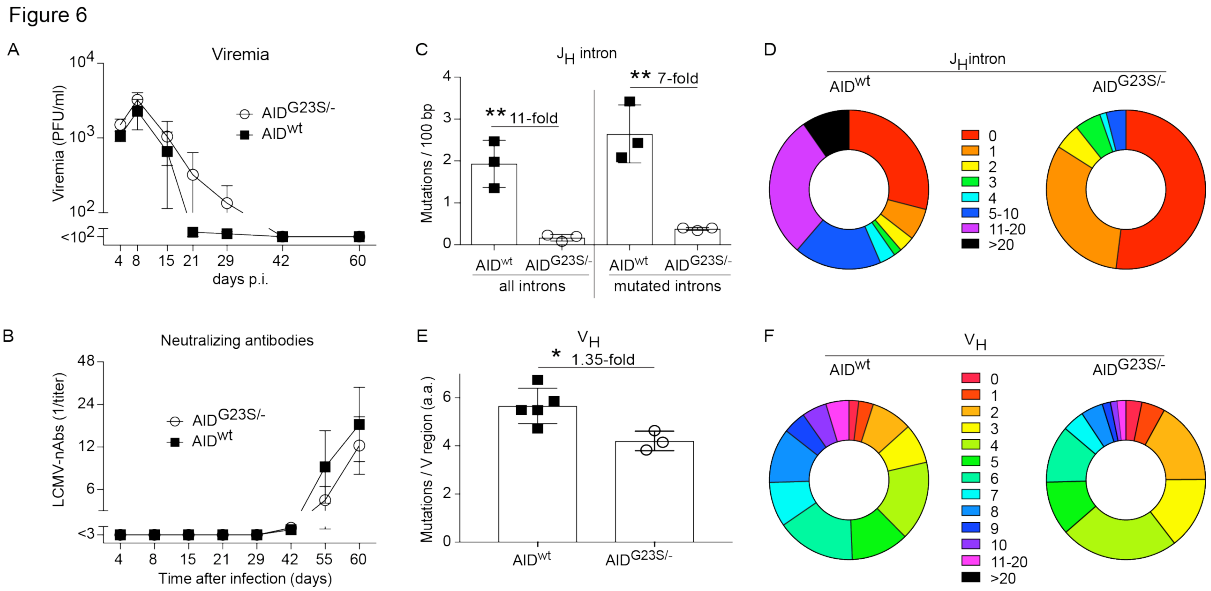

Figure 1. 6: Potent selection of hypermutated B cells in chronically infected mice

A,B: We infected $AID^{G23S/-}$ and wt control mice with rCl13 and measured viremia (A) and rCl13-neutralizing antibodies (B) over time.

C,D: Sixty days after infection we sorted GC B cells ($GL7^{+}B220^{+}$) from the spleen for IgH locus sequencing. Number of nucleotide mutations in all J_H introns (left) and in mutated J_H introns (right, C). Distribution of J_H intron mutation numbers (mutations per individual sequence) in $AID^{G23S/-}$ and wt control mice (D). Results represent 74 and 62 sequences, respectively, from 3 mice per group.

E: Number of amino acid mutations per sequenced V_H region. Distribution of V_H mutation

numbers in $AID^{G23S/-}$ and wt control (F). $1.3x10^6$ – $1.5x10^6$ sequences per mouse from 3-5 mice per group were analyzed. Symbols in (A,B) represent means +/- SEM. Bars in (C,E) represent means +/- SD, with symbols showing individual mice. Donut plots represent the distribution of sequences with the indicated mutation numbers. n = 7 to 8 (A, B), n = 3 (C, D). N = 2 (A, B, E, F), N = 1 (C, D). *: $p < 0.05$, **: $p < 0.01$ by unpaired two-tailed Student's *t* test. The fold difference between groups is indicated (C,E).

Supplementary figure 1

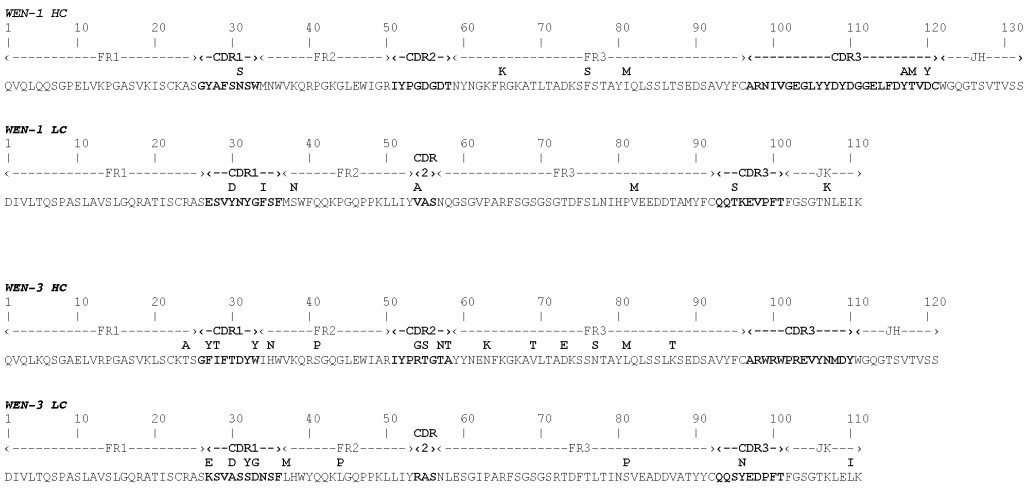

Supplementary figure 1. 1: V(D)J amino acid sequences of the LCMV-neutralizing monoclonal antibodies WEN-1 and WEN-3 in comparison to their respective unmutated ancestors

Heavy and light chain (HC, LC) sequences are represented, with changes from their V_H/J_H and V_K/J_K germline counterparts indicated above the sequence. CDR regions (IMGT nomenclature) are indicated in bold. The WEN-1 HC (IGHV1-82/D2-4/JH4) displays 8

nucleotide (and 7 amino acid) changes from germline with an unusual 25 amino acid-long CDR3; the WEN-3 HC (IGHV1-76/D2-3/JH4) has 33 nucleotide exchanges and 16 amino acid mutations. The WEN-1 LC (IGKV3-2/IGKJ4) harbors 12 nucleotide and 7 amino acid changes, and the WEN-3 LC (IGKV3-5/IGKJ4) comprises 13 nucleotide and 9 amino acid changes.

Supplementary figure 2

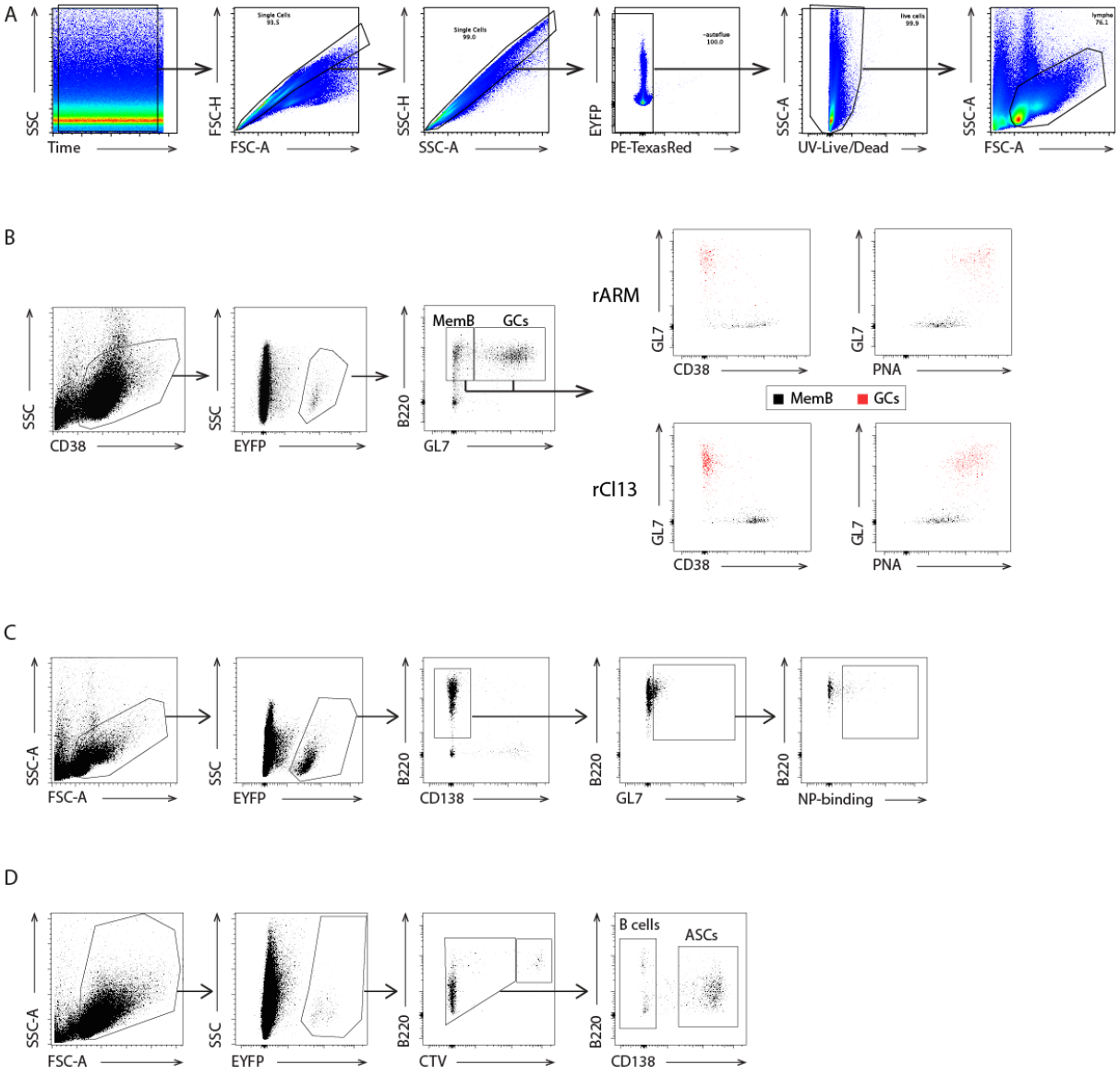

Supplementary figure 1. 2: General gating strategy for viable lymphocytes, characterization of EYFP-labeled GL7+B220+ GC B cells and GL7–B220+ memory B cells, and gating strategy for the FACS analyses described in Figure 2

A. For all experiments in this manuscript lymphocytes were gated as described here: The first and last few events were gated out in a Time vs SSC gate. Doublets were then excluded based on FSC-A vs FSC-H and SSC-A vs SSC-H profiles. The PE-TexasRed channel was kept free and was used to exclude autofluorescent cells. Dead cells were stained as described in Methods and were gated out as shown. Lymphocytes were then gated based on forward- and side-scatter. All gating strategies in subsequent Supplementary figures and panels are based upon the analogous pre-gating strategy.

B: We infected AID^{rep} mice either rARM or rCl13 on day 0 and treated them with tamoxifen on day 0 and day 5. On day 35 we characterized PNA and CD38 profiles of EYFP-expressing $B220^{+}GL7^{+}$ GC B cells and of $EYFP^{+}$ $B220^{+}GL7^{-}$ memB cells. Representative FACS plots from one out of four mice are shown except for GL7/CD38 and GL7/PNA plots, which display the combined events from two representative out of four mice.

C. We infected AID^{rep} mice with rCl13 or VSV on day 0 or left them untreated. Tamoxifen was administered on day 0, 5 and 10 as described for Fig. 2A. The gating strategy as shown was applied to quantify NP-binding cells.

D. We transferred Vacc-experienced or rCl13-experienced B cells into syngeneic C57BL/6 recipients, which had been infected with rCl13 six days before or with Vacc three days before, respectively, as described in Fig. 2D. The gating strategy as shown was used to enumerate proliferated CTV^{lo} $EYFP^{+}$ B cells and ASCs. Representative FACS plots are shown.

Supplementary figure 3

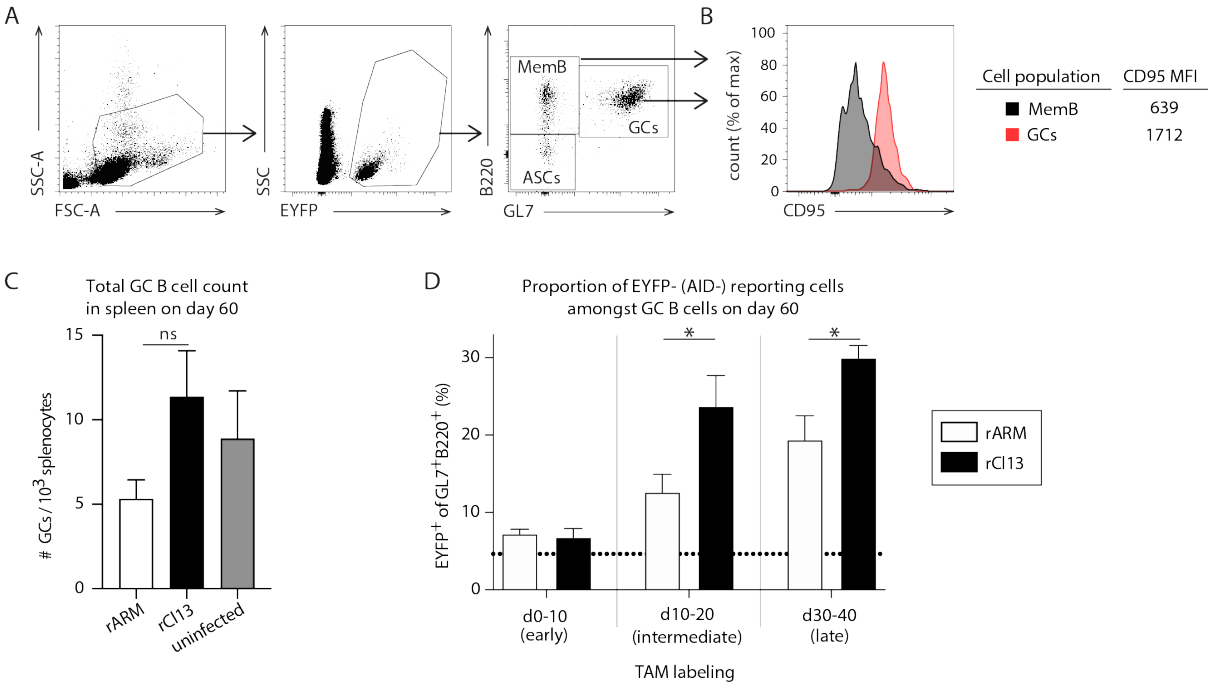

Supplementary figure 1. 3: Gating strategy for the FACS analyses shown in Figure 3, total GC B cell counts and representation of EYFP-reporting GC B cells in spleens of rARM- and rCl13-infected mice on day 60.

A,B: We infected AID^{rep} mice with rARM or rCl13, followed by tamoxifen labeling on day 0 and 5 (early), 10 and 15 (intermediate) or 30 and 35 (late) after infection as described in Fig 3A. The gating strategy as displayed in (A) was used to quantify EYFP$^+$ GC B cells, MemB cells and ASCs on day 60 after infection. The CD95 expression profile of EYFP-expressing B220$^+$GL7$^+$ cells in comparison to EYFP$^+$ B220$^+$GL7$^-$ memB cells was analyzed in (B). Representative FACS plots are shown.

C: We infected mice with rCl13 or rARM and left controls uninfected. Total GL7$^+$B220$^+$ GC B cells were enumerated in spleen 60 days later. One-way ANOVA with Bonferroni's post-test for multiple comparisons. ns: $p > 0.05$.

D: EYFP^{+} (AID-reporting) GL7^{+}B220^{+} GC B cells from Fig. 3C are displayed as a proportion of the total GL7^{+}B220^{+} GC B cell compartment. Bars in (C,D) represent means +/- SEM. The dotted line indicates background EYFP reporting cells in uninfected control mice. n = 4 to 5, N = 2. Two-way ANOVA with Bonferroni's post-test for multiple comparisons. *: $p < 0.05$.

Supplementary figure 4

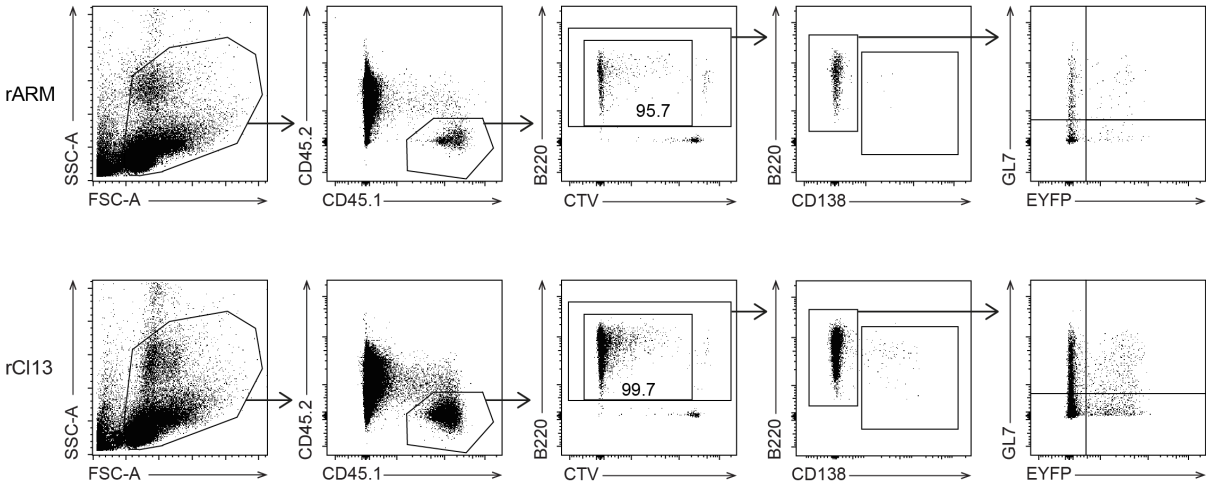

Supplementary figure 1. 4: Gating strategy for the FACS analyses shown in Figure 4

We infected wt recipient mice with rARM* or rCl13*. On day 20 after infection these animals were given KL25HL-AID^{rep} B cells by adoptive transfer and were administered TAM on day 20 and 23 as shown in Fig 4A. The gating strategy as displayed was used to determine EYFP and GL7 expression by the transferred KL25HL-AID^{rep} B cells. Numbers in FACS plots indicate the percentage of CTV^{lo} cells amongst transferred B220^{+} cells. Representative FACS plots are shown.

Supplementary figure 5

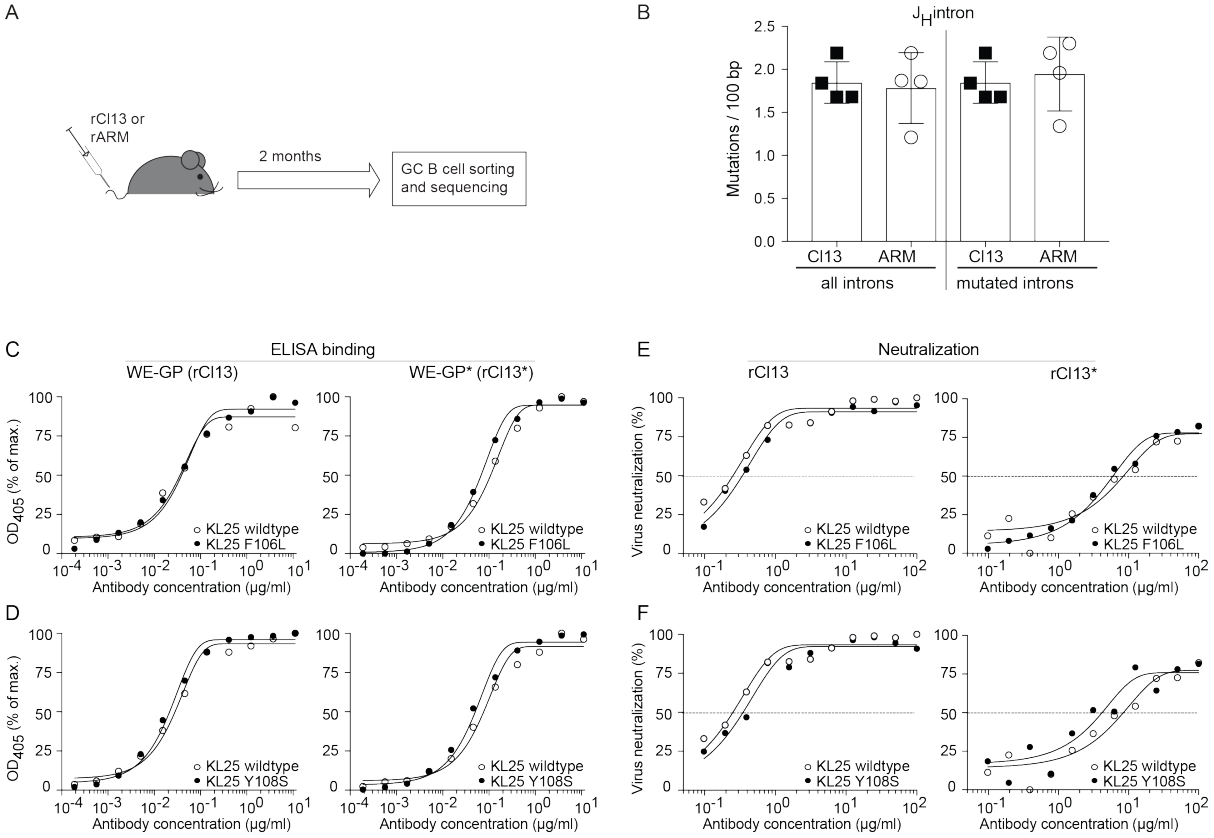

Supplementary figure 1. 5: Comparable mutational load in VH introns of GC B cells from rARM- and rCl13-infected mice and characterization of KL25 variants selected in rCl13* infection

A,B: We infected wt mice with rCl13 or rARM. Two month later we sorted $CD3^-$ IgD^- IgM^- $GL7^+$ $B220^+$ B cells from the spleen for IgH intron sequencing as described in Methods. Schematic of the experimental design (A). Mutations frequencies in the J_H intron are shown as nucleotide changes per 100 bp as calculated for all sequences (left) or for mutated sequences only (right), (B). Bars represent mean +/- SD. Symbols represent individual mice. n = 4, N = 1.

C,D: Binding of KL25 wildtype, KL25-Y108S and KL25-F106L to WE-GP and WE-GP*. E,F: Neutralization of rCl13 and rCl13* by KL25 wildtype, KL25-Y108S and KL25-F106L. Symbols in (C-F) show the mean of 2 technical replicates. N = 2 (D,E).

Acknowledgments

We wish to thank Kerstin Narr for helpful discussions and long-standing collaboration, Bénédicte Afonso for excellent technical assistance, Tatiana Fadeev for help with analysis of KL25 mutations, Karsten Stauffer for animal husbandry and the DBM flow cytometry core facility for FACS sorting.

Author contributions

B.F., Y.H, M.F., Y.I.E., V.G, U.M., D.M., S.R., J.C.W., C.A.R and D.D.P. contributed to experimental conception and design; B.F., Y.H., M.F., K.C., A.V.d.l.A., G.G.Z., Y.I.E., V.G., U.M., K.H., D.M., S.R., J.C.W., C.A.R. and D.D.P., acquired, analyzed and/or interpreted the data; B.F., Y.H., M.F., J.C.W., C.A.R and D.D.P. drafted or critically revised the article for important intellectual content.

Funding

This work was supported by the European Research Council (ERC grants No. 310962 to D.D.P. and No. 693267 to C.A.R.) and by the Swiss National Science Foundation (project grant No. 310030_173132 to D.D.P and project No. 323630_151472 to B.F.).

2. Protective antibodies against chronic systemic viral infection emerge from an IgM^{low} B cell population pruned by RAG2 expression

Marianna Florova[1], Guido Paesen[2], Mehmet Sahin[1], Anna Sophia Beethschen[1], Kerstin Narr, Thomas A Bowden[2], Daniel D Pinschewer [1]

Affilitiations

[1] Department of Biomedicine – Haus Petersplatz, Division of Experimental Virology, University of Basel, 4009 Basel, Switzerland.

[2] Nuffield Department of Clinical Medicine, Division of Structural Biology,

University of Oxford, OX3 7BN Oxford, United Kingdom

Corresponding author:

Daniel D. Pinschewer,

Department of Biomedicine – Haus Petersplatz, Division of Experimental Virology, University of Basel,

4009 Basel, Switzerland.

Daniel.Pinschewer@unibas.ch

One sentence summary

IgM^{low}, IgD^{+} phenotype and restricted peripheral egress of virus specific B cells is a direct consequence of their ability to bind the viral glycoprotein.

Abstract

Protective neutralizing antibodies against chronic viral pathogens arise late after the onset of the infection and are not trivial to elicit with immunization. Both in the polyclonal B cell repertoire and upon characterizing the newly generated neutralizing antibody, KL25 heavy and light chain knock-in mice, expressing B cells with high affinity to the lymphocytic choriomeningitis virus (LCMV) glycoprotein (GP), we observed an IgM molecule downregulation on the surface of the naïve B cells that was indirectly proportional to the LCMV GP binding. IgM^{low} IgD^{+} phenotype did not negatively affect the activation potential, adaptation and antibody production upon germinal center entry of the GP-binding B cells in chronic viral infection; however, RAG2-dependent negative selection during light-chain receptor editing renders glycoprotein binding specificity a rare phenomenon in the peripheral B cell repertoire.

Introduction

Multiple chronic viral infections in humans, such as HIV and HCV, and an experimental mouse lymphocytic choriomeningitis virus (LCMV) have a common denominator in a delayed neutralizing antibody formation [269], [33, 243]. In addition, can depend on a very limited starting B cell repertoire [270, 271] One of the hypotheses that provide explanations for both low viral antigen immunogenicity and low precursor frequency is viral host antigen mimicry, whereby structural similarity between the viral and endogenous host antigens leads to an immune response dysregulation. In this context, a limited interaction with heavily glycosylated viral epitopes of the envelope glycoproteins [41, 44] [272] as well as immune tolerance as a barrier in neutralizing antibody development [108] have been recognized. However, only B-cell receptor (BCR) engineered mouse models expressing virus neutralizing specificities can address the relevant functional and regulatory context of the host immune response.

The penetrance of a specific virus-neutralizing BCR in BCR knock-in animals into the pool of the peripheral B cells can vary depending on a mouse model and ranges from complete abrogation of specific B cells by the central check-point deletion [130] to a largely physiological B cell development [273]. Additionally, virus specific B cells have a spectrum of functionality or can remain anergic [110].

Immunoglobulin gene knock-in strategy from the physiological loci, minimizes aberrant gene expression and ensures physiological germinal centre affinity maturation. It relies on the employment of homology-directed repair, with the respective rearranged V(D)J cassettes, replacing J segments of immunoglobulin heavy or kappa loci [121]. More recently, the use CRISPR/Cas 9 genetic scissors allows for performing analogous targeting strategies rapidly.[142] [144]

In the model of chronic LCMV infection, antibodies elicited later, rather than early, in the infection course are neutralizing [33, 34]. In particular KL25 specificity, induced as a result of

a sequential immunization, was pivotal for the recent studies of B cell response subversion in the context of chronic LCMV infection and adoptive B cell transfers [30].

Here we report a rare phonotype of LCMV GP1 binding B cells, using a newly generated HkiL mouse and their functionality in chronic LCMV infection.

Results

Generation of LCMV neutralizing antibody knock-in mouse model

KL25 neutralizing antibody heavy chain (HC) knock-in was previously generated via homologous recombination to replace the DQ52 and J_H segments of the endogenous immunoglobulin locus on chromosome 6 of the wild type (WT) C457BL/6 mouse [200]. We crossed these mice to C57BL/6 RAG2 knock-out mice, resulting in the TgH-RAG2 strain, which served as a background strain for further genetic manipulation, creating a condition where no B cells are present in the periphery, unless the light chain (LC) gene is inserted into the genome for BCR expression.

In the closest possible proximity to the homology arms, we designed two guide RNAs navigating the double-stranded break induced by CRISPR/Cas 9 ribonucleoprotein, deleting the IgK J segments of chromosome 12. The guide RNAs were tested for cutting efficiency in vitro. The homology-directed repair ensured an insertion of the KL25 LC cassette consisting of the antibody VJ region with its native promoter (Fig. 2.1A).

Fertilized oocytes were injected with the Cas9 RNPs and a plasmid template and implanted for a surrogate pregnancy, yielding 4 out of 11 founder animals with the KL25 LC knock-in. As measured by flow cytometry, the presence of B cells in blood serves as a simple detection method for identifying the founders (Fig. 2.1B). In addition, to confirm the precise integration, we performed a long-range PCR with primers inside the cassette and outside in the genomic region (Fig 2.1A,C). To confirm the specificity of the knocked-in BCR we developed a flow cytometric co-staining with two different recombinant LCMV glycoprotein, one consisting of the trimeric GP complex (GPC), and GP1 subunit only, we could confirm the strict monoclonality of the peripheral B cells of the founder animal bind the LCMV GP1 subunit in isolation and not only in the GP1-GP2 heterodimeric context (Fig 1D). We named this newly created KL25 expressing mouse line HkiL-Rag and crossed it to WT C57BL/6 Ly5.1 mice to

restore RAG 2 expression in the HkiL mouse line. Analogously to the above, we used the KL25 antibody heavy chain to develop a molecular strategy for immunoglobulin heavy chain (HC) knock-in targeting by CRISPR/Cas9 and flow cytometry-based identification of founder animals using the aforementioned GP staining (Appendix 1).

IgM downregulation is characteristic of the phenotype of GP1 binding B cells in blood and lymphoid organs

Previous mouse lines generated to express KL25 BCR relied on LC being expressed from a randomly integrated transgene. Examples are the TgHL [30] and BasL36 lines (Narr K., et al. unpublished). We set out to compare the peripheral B cell repertoire of these several mouse models expressing a monoclonal repertoire of KL25 expressing B cells (Table 1). Both HkiL-Rag and BasL36 mice exhibited high levels of KL25 BCR expression in and strictly monoclonal population of peripheral B cells (Fig. 2.2A), with more than 99% of the splenic B cells being specific TgHL mice with LC transgene has a lower KL25 expression of approximately 60% (Fig. 2.2B). In HKiL mice, The RAG2 sufficiency had no detectable effect on the monoclonality of the B cells in the periphery (Fig. 2.2C). As compared to C57BL/6 WT mice, the number of B cells in the spleen and periphery was slightly reduced for all of the transgenic animals, with up to 2.5-fold reduction in HkiL mice (Fig. 2.2D, Sup. Fig. 2.1B). A reduction in the peripheral B cell compartment of BCR-transgenic mouse models can be accounted for by autoreactive specificities. Hence, we further analyzed the B lymphocytes for their levels of surface IgM expression. We observed that GP1 binding B cells of monoclonal Basl36 and HkiL-Rag mice exhibited a strong downregulation of surface IgM, both in blood (Fig. 2.2 E,F) and spleen (Sup. Fig 2.1C, D). Additionally, the B cell compartments commonly characterized by IgM expression, were depleted. This affected germinal center B cells ($B220^{+}$, $CD23^{-}$, $CD21^{+}$) (Fig. 2.2G, Sup. fig. 2.1E) with only 5% of the splenic B cells of HkiL mice

expressing the CD21 marker (Fig.2H). Due to their anatomic location, marginal zone B cells are considered the first T-independent line of defense against bloodborne pathogens, while follicular B cells are associated with secondary high-affinity antigen interactions [274]. Analogously, IgM expression is characteristic of the B1 B cell population in the peritoneal cavity. We found that HkiL B cells do not differentiate into B1($B220^{+}$, $CD11b^{+}$) B cells (Fig. 2.2H, I). The contribution of BCR signaling to these HkiL differentiation pathways remains to be investigated. Taken together, the peripheral B cells of BasL36 and HkiL mice expressing neutralizing specificity have IgMlow, IgD^{+} phenotype and fail to differentiate into compartments, where antibody production is rapid and independent of T cell help.

IgM downregulation rather than secondary V(D)J rearrangement characterize the bone marrow development of HkiL B cells

Since the monoclonal B cells in the periphery were found to be of a strict IgM^{low} IgD^{+} phenotype, flow cytometry was used to examine the bone marrow (BM) development of the KL25 specific B cells (BasL36, HkiL), to investigate a potential contribution of central tolerance mechanisms on this phenotype. IgM expression is crucial for central tolerance check-point and secondary V(D)J rearrangement, or receptor editing, occurs in the IgM-expressing stage of immature B cells in the bone marrow[275]. Therefore, we specifically looked at the E (immature B cell) and F (mature B cell) fractions of the bone marrow (BM) B cells [276], which have been defined based on B220 and IgM expression.

We observed no difference in the size of the total late mature BM B cell population ($B220^{high}$, $CD43^{-}$) of RAG2-sufficient KL25 B cells when compared to WT mice. In contrast, the immature B cell subpopulation ($B220^{int}$, $CD43^{-}$) was significantly reduced in KL25 expressing B cells (Fig. 2.3A). Additionally, the IgM expression of this sub-population, undergoing tolerance check-point, was lower than that of WT mice, with subsequent further

downregulation at the pre-egressing mature B cell population (Fig. 2.3B). Hence, we identified that the IgM downregulation was imprinted early at the To investigate whether other BCR transgenic models available to us, namely vesicular stomatitis virus-specific (VI10) and hen-egg lysozyme specific (MD4) B cells, exhibit similar alterations in their B cell development, namely premature IgM downregulation, we stained splenocytes of MD4 and VI10 mice for IgM/IgD expression and LCMV GP binding (Fig. 3C). Both IgM and IgD, were expressed on the surface of the splenic B cells (Fig. 2.3C), and these B cells did not bind LCMV GP, as expected (Fig.D). Additionally, the bone marrow development in these models included a $B220^{int}$, IgM^{high} stage, before IgD was upregulated on the surface of pre-egressing B cells ($B220^{high}$, $CD43^{-}$)(Fig. 3E, F).

These findings suggested that LCMV GP1 specific B cells follow an unusual bone marrow development, characterized by very transient or almost absent IgM expression as previously found for certain autoreactive BCR specificities (REFS). In contrast to the findings reported from these BCR transgenic / knock-in models with known autoreactivity, however, RAG-competent HkiL B cells did not undergo BCR rearrangement that would have measurably altered their specificity.

IgM downregulation correlates with LCMV GP1 binding and is restored upon B cell activation

Inhomogeneous levels of GP1 binding by TgHL B cells revealed an inverse correlation between LCMV GP1 binding and IgM expression (Fig. 2.4A blue). HkiL B cells represented an extreme of this spectrum in terms of GP1 binding and IgM downregulation (Fig. 4A, red). IgM^{low}, IgD^{+} B cells have previously been described as anergic or were found to respond only when stimulated with high-affinity antigen. Therefore, we set out to investigate whether HkiL B cells can are responsive to stimulation. We co-cultured HkiL B cells with fibroblasts stably

expressing CD40L and Baff [159], which in conjunction with added soluble IL-4 simulate antigen independent T cell help and stimulate B cell proliferation and memory formation (REF). Both IgM and IgD were upregulated on the surface of HkiL B cells after 4 days of co-culture (Fig. 2.4B), alongside elevated levels of the activation markers CD86 and Fas (Fig.2. 4C).

To determine whether the lack of IgM expression on B cells of HkiL mice was due to the animals' monoclonal B cell repertoire, and to test these cells' survival in polyclonal WT recipients, we transferred 1 million HkiL or WT B cells, expressing the CD45.1 congenic marker, into naïve CD45.2 recipients. During the observation period of seven days, there was no change in the IgD/IgM profile (Fig. 4D) of the transferred HkiL cells, and they homed to the spleen and survived comparably to WT cells, as evident in equal numbers of HkiL and WT B-cells recovered on day 7 (Fig. 2.4E)

When we modified the transfer settings, and the HkiL B cells were transferred into chronically LCMV-infected recipients, we observed almost immediate IgM upregulation on day 1, followed by loss of both, IgM and IgD by day 7, supposedly as a result of isotype class switch (Fig. 2.4F). Taken together, KL25 BCR-transgenic and -knock-in B cells downregulate IgM as a function of GP1-binding but re-express IgM upon activation in vivo and in vitro by antigen-independent and -dependent stimulation, respectively.

KL25-expressing IgMlow B cells enter germinal centers and produce antibody in chronic viral infection

To assess the functionality of KL25 B cells in chronic LCMV infection, we inoculated CD45.2^{+} recipients with rCl13/WE-GP and six days later transferred 5x10e3 CD45.1^{+} KL25 B cells (Fig. 2.5A), which results in approximately 250 cells engrafted in spleen. HkiL, BasL36 and TgHL B cells were used in parallel for this assessment. The experimental setting was

chosen to ensure high-affinity BCR interaction and allowed KL25 to neutralize the virus. Within 7 days after adoptive transfer, all types of transferred $B220^{+}$ B cells had measurably expanded in spleen (Fig. 2.5B). However, the expansion capacity was different, depending on the donor mouse type. The expansion and the long term maintenance was significantly lower for the previously published TgHL mice (Fig. 2.5C, E), with differences obvious already on d7, when TgHL B cells accounted for only ~0.2% of splenic B cells, as opposed to HkiL-Rag and BasL36 cells amounting to ~0.9% and ~1.8%, respectively (Fig. 5D). All types of KL25 B cells participate in the germinal center reaction, as evident in up to 80% and ~97% of the transfered B cells exhibiting a GL-7+ CD38+ phenotype on day 7 and day 54, respectively (Fig. 2.5F). While there was no obvious difference in the capacity of the various donor cell types to undergo isotype class switch (Fig. 5G), KL25 antibody production (determined as anti-GP1 titers by ELISA) differed substantially between them. They were highest in recipients of HkiL-Rag B cells, supposedly as a result of immunoglobulin expression from the natural IgH and IgK loci, followed by BasL36 and TgHL (Fig. 2.5H). To assess whether KL25 B cells can be triggered by low affinity antigen, we used rCl13 WE virus with a mutation in the GP, N119S, which arises from the selective pressure of GP binding B cells in viral escapes [28]. We confirmed the minimal binding of the mutated N119S GP to the KL25 antibody (Fig. 2.5I) and designed an experiment, where animals were infected with the rCl13 WE N119S virus and transferred KL25 specific B cells 6 days later (Fig. 5J). To prevent a possible adaptation disadvantage of the donor HkiL or BasL36 B cells, we also restricted the number of KL25 HC genes to one, as opposed to the bi-allelic expression in HkiL-Rag, creating a physiological immunoglobulin in HkiL-Rag het mice. Prior to transfer, HkiL Rag B cells bound both WE and WE N119S GP, albeit to a lower extend for the later (Fig. 2.5K). The ability of the B cells to adapt to the lower-affinity virus escape variant was unique for the mouse models with the LC targeted in the immunoglobulin locus, HkiL-Rag, HkiL Rag Het, as measured by the serum

antibodies binding N119S GP in Elisa (Fig. 2.5L). Correct LC gene regulation withing the IgK locus is essential for the formation of the neutralizing antibodies, since only HkiL-Rag and HkiL-Rag het, but not BasL36 were able to mount a neutralizing antibody response. Moreover, the time and extend of it is dependent on the singular expression of the immunoglobulin genes, as HkiL-Rag Het donor cells produce higher neutralizing titer, sooner, on day 24 post transfer (Fig. 2.5M). Taken together, our findings demonstrate the importance of precise knock-in strategies for the correct expression and regulation of the antibody genes in the viral infection studies and adaptability of LC knock-in but not LC transgenic B cells to the low-affinity virus.

Rare GP1 binding B-cells in oligoclonal and polyclonal repertoires downregulate IgM and report elevated levels of baseline BCR signaling

The KL25 BCR has undergone substantial affinity maturation from ist unmutated common ancestor. Hence, we investigated whether a GP1-binding B cells in the naïve polyclonal B cell repertoire exhibit an analogous phenotype. In the polyclonal B cell population of wild type, GP1 binding cells ($GPC^{+}/GP1^{+}$) were undetectable (Fig. 2.6A, B). A restriction of B cell specificities by bi-allelic knock-in of the KL25 heavy but not light chain (TgH mice) leads to the enrichment of both GPC ($GPC^{+}/GP1^{-}$) and GP1 ($GPC^{+}/GP1^{+}$) binding cells (Fig. 2.6C). GPC-only binding cells ($GP1^{-}$) exhibited very high surface IgM, indicating it was not the KL25 heavy chain per se that dictated surface IgM levels but the antigenic specificity, which depended on endogenous light chain re-arrangement (Fig. 2.6D). Intriguingly, RAG2 haploinsufficiency of TgH mice (TgH $RAG2^{+/-}$) resulted in a 10-fold enrichment of GP1-binding B cells as compared to TgH $RAG2^{+/+}$ mice (Fig. 2.6E). Therefore, RAG2 availability, which supposedly represents a rate-limiting factor for BCR editing, limited the egress of an thereby the availability of GP1- binding B cells in the peripheral BCR repertoire of TgH mice (Fig. 2.6C, E). Analogous to GP1-binding B cells of WT mice, GP1-binding B cells of TgH

RAG2$^{+/+}$ and TgH RAG2$^{+/-}$ mice exhibited an IgM^{low} surface phenotype (Fig. 2.6D, F). This phenotype was most pronounced in HkiL mice expressing high levels of both KL25 HC and LC (Fig. 2.6G, H).

Low surface IgM levels are only one hallmark of phenotype. The orphan nuclear receptor Nur77 is activated by tonic BCR signaling and was found to be upregulated on self-antigen specific B cells [109]. Hence, we crossed TgH mice to Nur77-GFP BAC-transgenic reporter mice [277], where eGFP under control of the Nur77 regulatory context, serves as a surrogate for self-reactivity. Flow cytometric analysis demonstrated elevated GFP reporting in naive GP1-binding cells as compared to GPC^{+}/GP^{-} and GPC^{-}GP1^{-} B cells in the same animals, indicating that the BCR of naive GP1^{+} cells provide elevated tonic stimulation (Fig. 2.6I).

We set out to characterize endogenous light chains the pair with the knocked-in KL25 heavy chain of TgH RAG2$^{+/+}$ mice to result in GP1 binding (GPC-/GP1+) cells (Fig. 6I). We identified 5 different variable-joining region (VJ) rearrangements, which included the unmutated common ancestor LC of KL25. When recombinantly expressed, the antibodies consisting of the KL25 HC and these endogenously paired LCs bound GPC as well as GP1, as expected (Fig. 2.6J, K). The highest-affinity antibody amongst them, based on the IGKV14-111 LC V element, even modestly reduced viral infection in the in vitro plaque reduction assay (Fig. 2.6L, M) and in vivo upon passive antibody therapy (Fig. 2.6N). We demonstrate that multiple BCR rearrangements binding to GP1 lead to the downregulation of IgM and the upregulation of Nur77 receptor.

GP1-binding IgM^{low} B cells but not GPC-only-binding IgM^{high} B cells control chronic LCMV infection

With HkiL B cells being efficient in clearing chronic infection, we tested the relative antiviral efficiency of GPC^{+}/GP1^{-} B cells (IgM^{high}, IgD^{low} phenotype) and of GPC^{-}/GP1^{+} B cells

(IgM$^{int/low}$, IgD^{+}). For this, we sorted three groups of TgH B cells according to their GP-binding capacity (GPC^{-}/GP1^{-}, GPC^{+}/GP1^{-}, GPC^{+}/GP1^{+}; Fig. 2.7A) and transferred 10 000 of either cell subsets into Cl13 WE infected animals. HkiL B cells (IgM^{lo}w/ IgD^{+}) served as positive control, negative control mice were left without adoptive cell transfer (Fig. 2.7B). In the first 14 days after adoptive transfer GP1-binding antibody responses were only detectable in recipients of GPC^{+}/GP1^{+} TgH B cells or of HkiL B cells, confirming that the sorting according to surface antigen binding corresponded to the specificity of antibodies produced by the B cells (Fig. 2.7C). HkiL B cells were most effective at clearing chronic LCMV infection upon transfer. Additionally, the transfer of GPC^{+}/GP1^{+} binding cells but not of GPC+/GP1- binding B cells resulted in the premature clearance of LCMV from blood (Fig. 2.7D).

As judged based on the cloned BCRs, GPC^{-}/ GP1^{+} TgH B cells commonly have a lower GP1 binding affinity than HkiL B cells, yet, which may be due to longer-term antigen exposure of the former, they expand to a higher extend on day 31. (Fig. 2.7E). In case of the former this may be due to rapid elimination of the cells' cognate antigen, while the latter cells' expansion likely was hampered by poor antigen recognition.

All donor cell types enter germinal centres, and we noted a trend for the proportion of cells in GCs on day 31 binding and affinity (Fig. 2.7F). On day 25 post-transfer, a higher proportion of high-affinity, IgMlow HkiL B cells had differentiated into isotype switched memory B cells than of any of the TgH cell subset. In contrast, HkiL B cell progeny contained the lowest proportion of CD138^{+} antibody secreting cells in spleen (Fig. 2.7G, H), and also low-affinity GPC^{+}/GP1^{+} TgH B cells exhibited significantly lower proportions of CD138^{+} B cells progeny than GPC^{-}/GP1^{-} B cells (Fig. 2.7H). Taken together, these results demonstrated efficient LCMV control by GP1- binding IgM^{low} B cells

Discussion

We report a particular phenotypic signature of LCMV GP1 binding B cells, characterized by the IgM downregulation, present already in the immature B cell stage in the bone marrow. In addition to this, we observe a RAG2 dependent reduction of the GP1 binding B cell repertoire in both monoclonal HkiL, and the TgH mice when pairing endogenous light chains. Given that virtually 100% of B cells in heterozygous HkiL and BasL36 mice bind GP1 and there is no substantial reduction of peripheral B lymphocyte counts in the BasL36 mouse model with the LC as a transgene, the decrease in B cell number is unlikely a result of incomplete allelic exclusion or aberrant heavy chain rearrangement. The receptor editing, on the other hand, is thought to happen at the immature/mature stage of the B cell development and be largely dependant on the LC secondary rearrangement [278]. Upon monoallelic deletion of the RAG 2 gene, decreased receptor editing leads to an enrichment in GP1 binding population. The nature of the LC knock-in in HkiL mice, deleting all J elements and thus prohibiting VJ rearrangement, results in a peripheral B cell reduction, since editing-induced specificity changes are not possible. Since the KL25 light chain employs the IgK J1 element, it would be of interest to investigate, whether targeted replacement of only this element with a KL25 VJ knock-in cassette would lead to a different, more polyclonal B cell repertoire in HkiL mice, which might emerge based on receptor editing. It has previously been suggested that there was a "hole" in the virus-specific BCR repertoire [271]. Thus far, the rarity of the virus-neutralizing specificities among naïve B cells have not been manifested in such a manner, that identifies light chain mediated BCR revision as a main causative element.

Despite the IgMlow, IgD+ phenotype and higher expression of Nur-77 in LCMV GP-1 binding B cells, we have not detected the activation of additional tolerance mechanisms such as anergy or deletion employed in the periphery influencing the B cell functionality

Extensively studied model of self-tolerance in B cell, based on hen egg lysozyme specificity placed grounds for behavioral concepts of self-reactive B cells, with anergy being a hallmark of IgMlow B cell phenotype in the periphery [279, 280]. In the context of chronic viral infection, several HIV mouse models with the knocked-in neutralizing-autoreactive BCR specificity, such as 2F5, 4E10, lead to clonal deletion of the B cells. Only small populations of specific B cells can egress the bone marrow are shown to be functionally silenced. [130, 281, 282]

However, we do not observe anergy of the IgMlow IgD+ B cells, nor functional disadvantage in the infectious settings with high and low-affinity antigens. On the contrary, upon adoptive transfer IgMlow, IgD+ B cells are more effective at viral clearance than IgMhigh B cells binding other glycoprotein epitopes.

Similarly, one of the most potent HIV broadly neutralizing specificity antibody to date, isolated from an elite virus controller, does not upon knock-in lead to obvious tolerance hinders [273], although being found to be engaging with the self-antigens [70].

In addition, a possibility of a "sweet spot" has been described, where mild self-reactivity primes the B cells for optimal functional potential with respect to foreign antigen [110]. Together, with the possibility of B-cell "redemtion" [65, 66, 283] we observe a paradigm shift in the importance of self-reactive foreign antigen-specific B cells in the repertoire and self-reactive B cells having a functional spectrum.

Given the dual potently neutralizing – tolerant nature of KL25 B cells, it would be of crucial importance to elucidate how the process of affinity maturation contributed to this phenotype and how this differs from the B cells carrying KL25 unmutated germline ancestor specificity, especially given our observation of largely reduced affinity and neutralizing potency of such antibodies.

B cell binding for LCMV GP1 correlates directly with IgM downregulation, depicting foreign antigen affinity as a sole activator of B cell tolerance mechanisms and repertoire restriction. Consequence of this is implicit in the difficulty to elicit protective antibody immunity in HIV infection, unless tolerance mechanisms are taken into account. HkiL mouse model provides a platform to study the viral antigen immunogenicity, in the context of affinity maturation of hard-to-elicit neutralizing antibodies for pathogens evading host tolerance mechanisms.

Methods

Genotyping, PCR reactions

Long range PCR used to confirm the correct integration of KL25 VJ gene was performed using Phusion polymerase (NEB) and primer pairs targeting the gene and region outside of the homology arms with respect to both 5 and 3 prime (5HA fwd: GCA AAT GTC TGA TGA GTG CTT GTC A, 5HA rev: GGC TTC TGC TGG TAC CAG ATC ATG TA, 3HA fwd: GCT TCC TGC TAA TCA GTG CCT CAG GTA A, 3HA rev: TTG AGC TCT GGA AGG CAG AAT AGT AGA AGG C). The following cycling conditions were used: 98°C for 1 min; 35× (98°C for 10 s, 69°C for 30 s, and 72°C for 2 min); 72°C for 10 min. For each reaction 50ng of the genomic DNA purified using Qiagen DNA purification kit was used.

PCR reaction to generate genomic DNA fragments flanking the IgL J region for gRNA testing was set up using Phusion polymerase (NEB) and specific primers (appendix table) using the following conditions: 98°C for 1 min; 35× (98°C for 10 s, 57°C for 30 s, and 72°C for 30 s); 72°C for 10 min. PCR products were purified using the Qiagen PCR purification kit and diluted to a 50 ng/ul concentration.

Guide RNA identification

sgRNAs were identified using CrispRGold (https://crisprgold.mdc-berlin.de/), given that they fulfill the condition of flanking the $J_{\kappa}1$-$J_{\kappa}5$ exons in the intronic region and are not included in the homology arms. Two such sgRNAs for each 5 and 3 prime (crRNA51: AAGCATGCGTGGAAGCGCTT, crRNA52: CAAGCATGCGTGGAAGCGCT, crRNA31: GGGTCTGACTGCAGGTAGCG, crRNA32: TGAGATCTGGGTCTGACTGC)

with the closest proximity to the homology arm were chosen, synthesized (IDT) and tested in vitro for cutting efficiency (unpublished). Subsequently, crRNA52 and crRNA32 were used for the pronuclear injections.

In vitro sgRNA testing for cutting efficiency

Equimolar ratios of crRNA and tracrRNA (IDT) were mixed for a final concentration of 100uM and heated at 95°C for 5 minutes, and cooled down to room temperature. RNP complexes were created by mixing 1ul (100 pmol) of sgRNA and 1.6ul (100 pmol) of S.Pyogenes Cas9 protein (IDT) in IDT buffer. The coupling reaction was allowed to proceed for 30 min at RT. Subsequently, 400ng (8ul) of DNA substrate was added per reaction and filled up with IDT buffer to total volume of 50ul. Such Cas9 digestion reaction was incubated for 60 minutes at 37°C. Analogous reactions without Cas9 protein were prepared as controls.

For analysis, the samples were stained using Ethidium bromide and separated through 1% agarose gel.

Pronuclear injection

Pronuclear injections and breeding of founder animals were performed by the Institute of Laboratory animal services center (LACS) at the university of Zurich. Further breeding was performed under specific pathogen-free (SPF) in LACS Zurich. Experiments were performed at the University of Basel in accordance with the Swiss law for animal protection and with authorizations from the Veterinäramt Basel-Stadt and from the Veterinäramt of the Canton of Zurich, respectively.

For pronuclear injection mix, first 10 pmol of S. pyogenes Cas9 protein (IDT), 18.4 pmol of each crRNA and tracrRNA (IDT) were mixed together in 5ul of 10x injection buffer (100mM Tris-HCL, 1mM EDTA (pH8.0)) and incubated at 37°C for 10 minutes. After that 1ug of plasmid DNA was add and the reaction was filled up to 50ul with double destiled H_20. 200

fertilized oocytes were injected and after a brief incubation implanted into the pseudo pregnant foster mothers.

Mice

WT C57BL/6 mice were purchased from Charles River laboratories. TgHL and Basl36 mice carry an immunoglobulin heavy chain (HC) knock-in (KI) derived from the neutralizing KL25 specificity [200] and a light chain (LC) in a form of a transgene, with and without Thy1.1 ectodomain respectively ([284], Narr K., unpublished). HkiL Rag mice were intercrossed with a C57BL/6 on a CD45.1 congenic background to restore the RAG 2 expression (HkiL). For adoptive transfer experiment either HkiL Rag mice or HkiL Rag het mice with the monoallelic LC knock-in and biallelic HC or monoallelic HC knock-in, respectively, were used. MD4 mice, transgenic for HC and LC of the anti-hen egg lysozyme were generously provided by C. Goodnow [279], and VI10 mice, carrying an VSV glycoprotein specific immunoglobulin HC as a knock-in [200] and a LC transgene (Narr K., unpublished), were used in the phenotyping experiments. TgL mice transgenic for KL25 light chain used as recipients in the transfer experiments were generated in our laboratory [30]. All mice were kept under specific-pathogen-free conditions for colony maintenance and experiments. They were bred at the Institute of Laboratory animal sciences at the University of Zurich or ETH Phenomics Center Zurich. Experiments were performed at the University of Basel, Petersplatz in accordance with the Swiss law and cantonal animal protection authorities (License BS-32652/2654 and BS-31800/2653)

Recombinant protein and antibody production

LCMV GP proteins for flow cytometric staining:

An LCMV WE GP1 gene fragment (encoding residues 81 to 241) was cloned into the pHLsec vector for transient expression as a secreted, hexahistidine-tagged protein in HEK236T cells, according to Aricescu et al. (2006). Five days post-transfection, the expression medium was collected, supplemented with NaCl (to a final concentration of 0.75M) and Tris pH 8.0 (15mM), clarified (10,000 x g, 20 min, 4˚C), and brought over a 5-ml HisTrap excel column (Cytiva). Protein was eluted using a 15-750 mM imidazole gradient in 10 mM Tris pH 8.0, 200 mM NaCl, and further purified by size-exclusion chromatography over a superdex 200 increase 10/300 GL column (Cytiva) using 15 mM Hepes pH 7.4, 150 mM NaCl as running buffer. Labelling with Alexa Fluor™ 647 was carried out according to the manufacturer's instructions (Thermo Fisher Scientific).

An LCMV GPC gene fragment (encoding residues 1- 431) with or without N119S mutation in mammalian expression vector, containing a CMV promoter and a Twin-Strep-tag fused to the C-terminal of the glycoprotein, was used for transient transfection of CHO cells (3mg of vector/litre of culture) at Protein Expression Core Facility, PECF, of the Swiss Federal Technical Highschool, EPFL, Lausanne, Switzerland. Supernatant was collected 7 days later and titrated for the use in flow cytometric staining.

Flow cytometry analysis

All organs were collected and cell suspensions kept on ice in B cell medium (DMEM, 10% FCS, HEPES, Sodium Pyruvate, NEAA). Spleens were pushed through a metal mesh in a Petri dish and homogenized by pipetting. Bone marrow was flushed with a syringe and needle and homogenized by pipetting. Peritoneal cavity was lavaged with 5ml medium, using syringe-needle system.

Dead cells were excluded from the analysis using Zombie UV Viability kit (Biolegend).

For founder identification, following antibodies were used for staining: αCD3-PE, αCD19-FITC, αB220-PE-Cy7.

Specificity staining was performed using GP1 and/or GPC recombinant proteins. Cells were incubated at 37ºC for 30 minutes while shaking in 200ul GPC-StreptagII supernatant, 5ug of Fcg blocking antibody (Jackson Immunoresearch) and 0.3 ug of GP1-AF647. Samples were subsequently washed and resuspended in 50ul FACS buffer and labelling antibody mixture: 0.2ul Streptactin-PE (IBA) and 0.5ul of B220-BV421(BioLegend), IgM-PerCP-eFluor710 (eBioscience), IgD-APC-Cy7 (BioLegend).

HkiL lymphocyte population was characterized from blood, spleen, bone marrow and peritoneal cavity. The following antibody panel in 50ul FACS buffer was used for the staining: 5ug Fcg blocking antibody (Jackson Immunoresearch), 0.5ul each of CD3-BV421 (BD) or FITC (BD), B220-BV605 (BioLegend) or BV421 (BioLegend) CD21-PerCP-Cy5.5 (BioLegend), CD23 -PE (BD), CD24 – FITC (BD), IgM -APC (BioLegend) or PerCP-eFluor710 (eBioscience), IgD -APC-Cy7 (BioLegend), CD19-PE (BioLegend), CD11b-APC-Cy7 (BioLegend), CD5-PE (BD), CD19- APC (BioLegend). The mixture was incubated for 15 minutes at room temperature before washing and acquisition.

For adoptive transfer experiments, spleens were collected at the final time point and homogenized. One tenth of the spleen was used for staining. Splenocytes were incubated with GPC-Streptag II protein and 5ug of Fcg blocking antibody at 37°C for 30 minutes, shaking. Afterwards washed cell suspensions were stained 50ul of FACS buffer supplemented with following antibodies: 0.2 ul of Streptactin-APC (IBA), 0.5ul each of CD45.2-BV605 (BioLegend), CD45.1-BV421 (BioLegend), B220-AF700 (BioLegend), IgM-PerCP-eFluor710 (eBioscience), GL-7-AF488 (BioLegend), CD38-PE-Cy7 (BioLegend), CD138-PE (BD). Samples were aquired with LSRFortessa flow cytometer (Becton Dickinson) and data

analyzed using FlowJo software (Tree Star). Absolute spelnocyte counts were performed using fluorescent labeling (CTL labeling kit) and visualization via CTL counter (CTL).

Viruses and cells lines

The infections and subsequent focus forming assays were performed using the recombinant LCMV strain Clone 13 virus (rCl13) expressing the WE glycoprotein (WE-GP). Alternatively, for the experiments investigating the B cell adaptation, a virus variant of rCl13 with a N119S mutation in the WE-GP (WE GP N119S) was used [44, 198].

The cell lines used for virus propagation and titration were BHK21 (ECAAC) and NIH 3T3 (ATCC) respectively. Stably transfected fibroblasts, expressing BAFF and CD40L were used for B cell activation in vitro [159]

Virus production, Titration and Infection

The virus stocks for the experiments were propagated on BHK-21 cells (ATCC), which were infected at MOI 0.01 for two hours, after which the supernatant was replaced and collected 48 or 72h post infection.

LCMV infectivity from the virus stocks or blood of infected animals was determined via Immunofocus forming assay in 96-well plate format [285]. A drop of blood was collected in 950ul of BSS supplemented with 1IE/ml Heparin (Braun). For the assay three-fold serial dilutions were made and subsequently incubated with NIH 3T3 cells (ATCC) for 2 hours, before a viscous overlay (DMEM 1% methylcellulose) was applied. 48 hours later, the medium was discarded and the cell layer fixed with 4% paraformaldehyde for 30 minutes and permeabilzed (BSS 1% Triton X-100). After blocking (PBS 5% FCS), a staining for infectious foci was performed with VL4 rat-anti-LCMV-NP antibody, followed by a secondary HRP-

cojugated goat-anti-rat IgG (Jackson Immunoresearch), each for one hour. The DAB colour reaction was applied subsequently.

Experimental animals were infected with the viruses, rCl13 or rCl13*, intravenously with the high dose of 2-6x106 PFU

Neutralizing antibody titer measurement

The neutralizing antibody titer from the serum of experimental animals was measured using immunofocus reduction neutralization test. 5ul of the serum was prediluted 1:18 and further serially diluted 1:2 in MEM 2% FCS in 96-well plate. Diluted antibody containing sera were incubated with 60 PFU of rCl13/WE GP or rCl13/WE GP N119Sü virus for 90 minutes at 37°C. Subsequently, NIH 3T3 fibroblasts were added and mixture further incubated for two hours until the cells adhere. DMEM 1% Methylcelulose was added as a last step before a 48 hour incubation at 37°C. After two days a staining procedure was performed (see above) and number of foci counted using an immunospot analyzer (CTL). Neutralizing titer from the sera was determined from the highest dilution yielding at least 50% reduction in foci number.

TgH light chain sequencing

TgH B cell subset binding LCMV GPC and GP1 was sorted and genomic DNA extracted (Qiagen DNeasy blood and tissue kit). Rearranged light chain immunoglobulins were amplified using multiple PCRs with forward primer binding to variable domain coding regions and reverse primer to the light chain kappa or lambda constant region. Second round of PCR included analogous primer sets extended by restriction sides allowing for later cloning of amplified fragments into expression vectors (Mouse IgG Library primer set, Progen). Briefly, the PCR reaction was carried out with 5U of Phusion HF Polymerase (NEB), 50ng of DNA

template, 10uM of each primer (Microsynth) and 2.5mM dNTP (NEB), completed with ddH20 in 40ul reaction volume. The following cycling conditions were used: 98°C for 1 min; 30× (98°C for 10 s, 55°C for 30 s, and 72°C for 2 min); 72°C for 10 min. Second PCR reaction was caried out analogously, using 5ul from the first reaction as a template. Purified PCR fragments (Qiagen PCR purification kit) were cloned into vectors using MluI (5`) and NotI (3`) restriction sides and resulting colonies sequenced with Sanger sequencing. Functional VJ sequences were identified using IgBlast, synthesized (Genescript) and introduced into HC and LC expression cassettes for recombinant expression in a mouse IgG2a format (provided by Dr. Shozo Izui, University of Geneva).

Statistical Analysis

The GraphPad Prism software version 9 (GraphPad Software) was used for all statistical analyses. For comparison of one parameter between multiple groups one-way analysis of variance (ANOVA) was performed and for comparison of multiple parameters between two or more groups two-way ANOVA was used, both followed by Turkey's post-test for multiple comparison. For statistical analysis of absolute cell counts and percentage values were log-converted to obtain a near-normal distribution. P values ≥ 0.0021 were regarded as not statistically significant. Statistical analysis was performed in Figure 5.

The number of experimental animals "*n*" per group, number of experimental repeats "N", the type of error bar displayed and the tests performed for statistical analysis are indicated in each figure legend.

For titer determination in mouse serum based on standard curve fit, GEN5 software (BioTek Instruments) was used. Antibody titers were log-converted to obtain a near normal distribution. Binding and neutralization curves of monoclonal antibodies were fitted using GraphPad Prism software 7 (GraphPad Prism).

Tables

Mouse line	**Tgh**	**TgHL**	**Basl36**	**HkiL**
Heavy chain	ki/ki	ki/ki	ki/ki	ki/ki
Light chain	-	tg	tg	ki/wt
Reference	Hangartner et al., 2003	Fallet et al., 2016	Narr et al., unpublished	This manuscript

Table 2. 1: KL25-BCR expressing mouse models

Genetic description of KL25 transgenic models indicating the form of genetic modification introducing the heavy and the light chain gene into the WT genome. (ki) stands for a monoallelic knock-in in the respective heavy or the light chain immunoglobulin; (tg) stands for a transgene randomly integrated in the genome; (wt) stands for a wild type allele

Figures

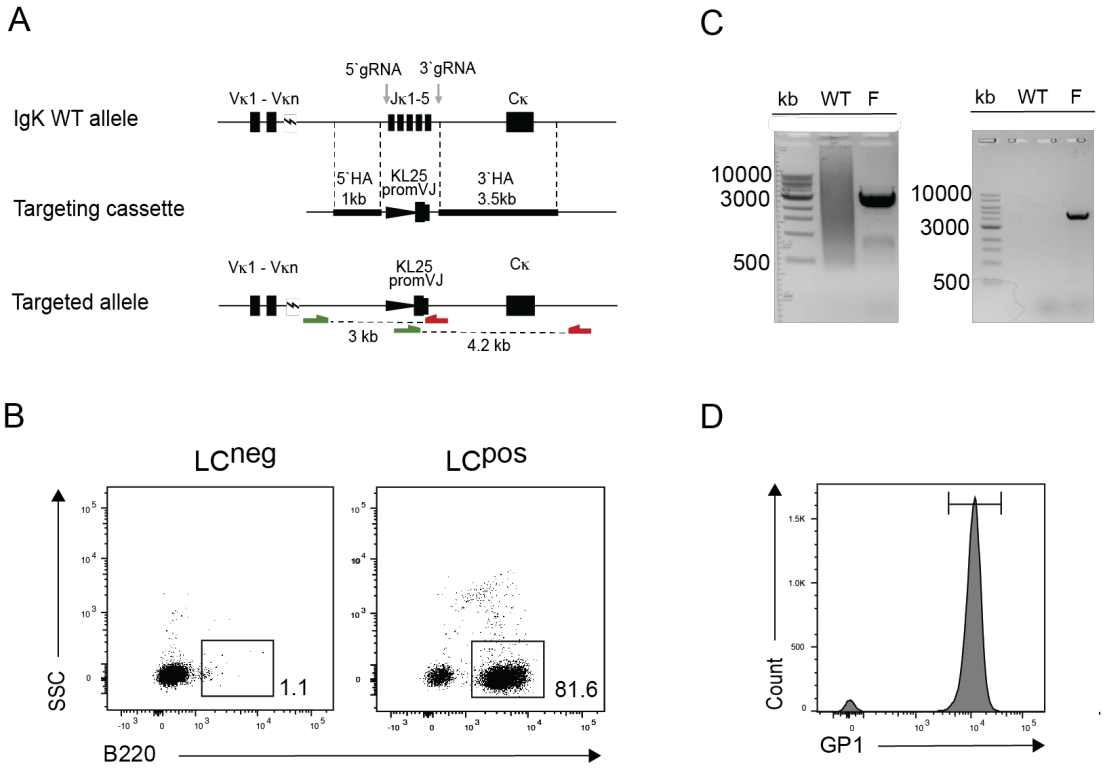

Figure 2. 1: CRISPR/Cas9 B cell editing optimization using a GFP reporter insert

(A) Targeting strategy schematic for immunoglobulin kappa locus (IgK) for mouse chromosome 6. The targeting cassette comprising of homology arms and promoter originating from pVKR2neo vector, variable-diversity (VJ) segment and splice donor of KL25 antibody. Genotyping strategy for long range PCR with forward (green) and reverse (red) primers is depicted on the schematic of the targeted allele (B) Representative FACS plots from blood analysis of founder animals, LC^{neg} plot showing profile of TgH RAG2 mouse without LC integration, LC^{pos} with it. Numbers in FACS plots indicate percentages of gated B cells ($B220^{+}$) among lymphocytes. (C) Long range PCR genotyping for KL25 LC integration in founder mouse, following the PCR strategy illustrated in (A).

(D) Representative FACS plot of LCMV GP1 binding of the lymphocytes in the blood of the founder mouse with LC integration.

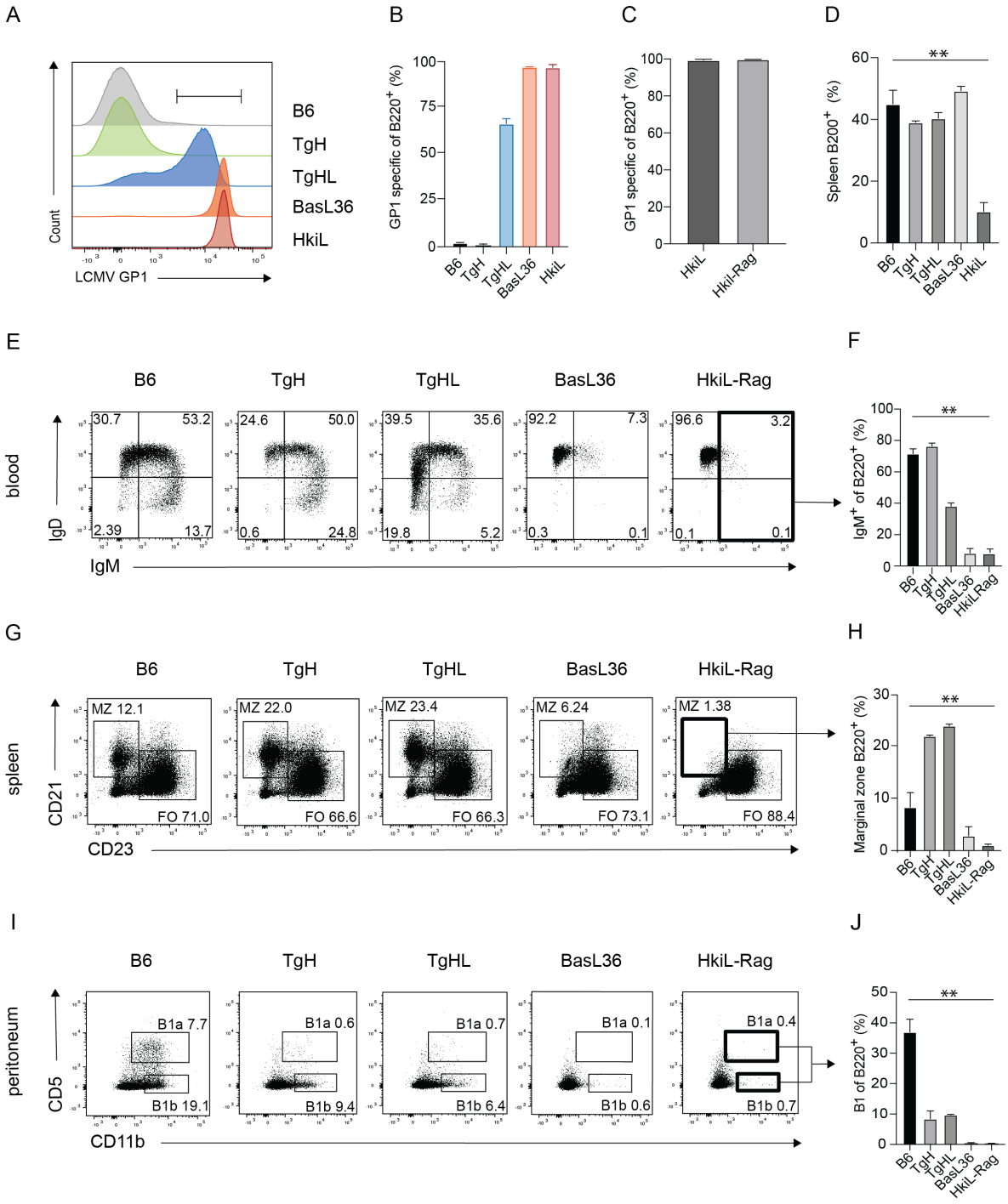

Figure 2. 2: IgM downregulation is characteristic of the phenotype of GP1 binding B cells in blood and lymphoid organs

(A-B) Representative histogram FACS plots of LCMV GP1 binding B cells from the spleen of KL25 transgenic animals (gated on $B220^+$, as in Sup. Fig. 2.1A) with a graphical gate setting

for the percentual representation of GP1 binding cells in (B). (C) Percentage of $B220^+$ GP1 binding B cells in the spleen of HkiL and Hkil-Rag mice. (D) Graph of B cell percentage ($B220^+$) among splenocytes of KL25 transgenic animals as compared to B6. (B-D) Bars show the means and SD. Number of biological replicates (n) = 2-4. (E) Flow cytometric analysis of $B220^+$ B cells from the blood of KL25 mouse models showing IgM/IgD profile (pre-gated as in Sup. Fig. 2.1A). (F) Graph of percentage of IgM^+ B cells (right upper and lower quadrant of (E)) in the blood. (G) Flow cytometric analysis of $B220^+$ solenocytes with marginal zone B cells (MZ) gated as $CD23^{low}$ $CD21^{high}$ and follicular B cells (FO) as $CD23^{high}$, $CD21^{low}$. Numbers represent percentage of B cells in the gates. (H) Percentual quantification of MZ B cells gated as shown in (G). (I) Flow cytometric analysis of $B220^+$ peritoneal B cells with depicted gates and percentages for B1a ($CD11b^+CD5^+$) and B1b ($CD11^+CD5^-$) B cells. (J) Percentage of B1 ($CD11b^+$) B cells shown in (I). (F,H,J) n=2-6, symbols represent means ± SD. Pre-gating see Sup. Fig. 2.1A

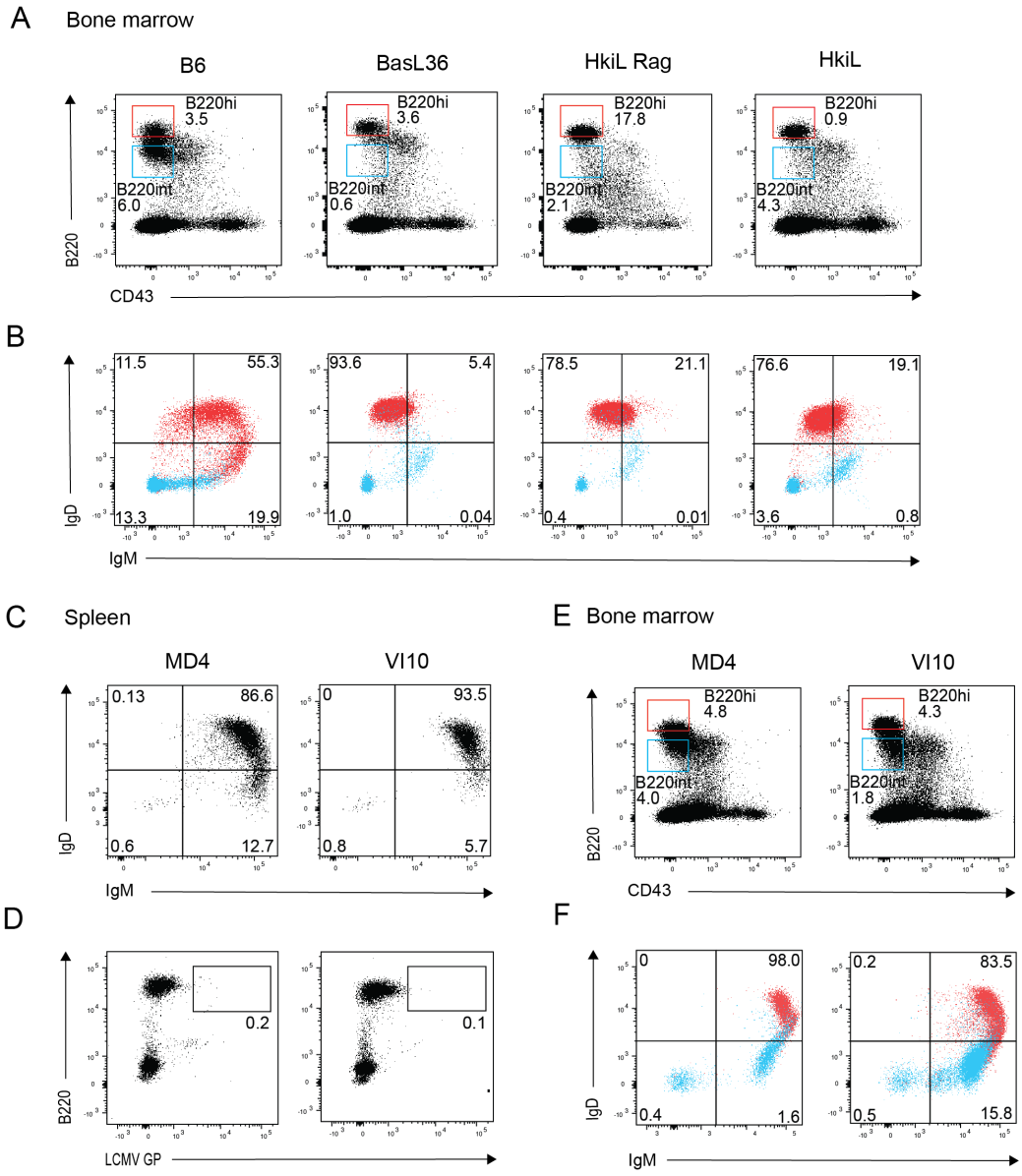

Figure 2. 3: IgM downregulation rather than secondary V(D)J rearrangement characterize the bone marrow development of HkiL B cells

(A-B) Representative FACS plots comparing bone marrow cells of KL25 transgenic models (BasL36, HkiL, Hkil-Rag) to WT C57BL/6 mice. (A) Representative FACS plots identifying $CD43^{-}B220^{+}$ B cells from the bulk bone marrow lymphocyte population. Gates and numbers indicate percentage of cells with intermediate and high B220 expression, $B220^{int}$ and $B220^{hi}$ respectively. (B) IgM/IgD expression profile of bone marrow B cells when gated as in (A),

$B220^{hi}$ cells are color coded red and $B220^{int}$ cells color coded blue. (C-F) Representative FACS plots comparing MD4, VI10 transgenic mouse models. (C) Representative FACS plots showing IgM/IgD expression profile of $B220^{+}$ splenocytes. Numbers represent percentages in the gated quadrants. (D) LCMV GP1 binding of $B220^{+}$ splenocytes as measured by flow cytometry and depicted by gates and percentages. (E) Representative FACS plots identifying $CD43^{-}B220^{+}$ B cells from the bulk bone marrow lymphocyte population of MD4 and VI10 mice. Numbers and gates indicate percentage of cells with intermediate and high B220 expression. (F) IgM/IgD expression profile of bone marrow B cells when gated as in (E), $B220^{hi}$ cells color coded red and $B220^{int}$ cells color coded blue. (A-F) n=4

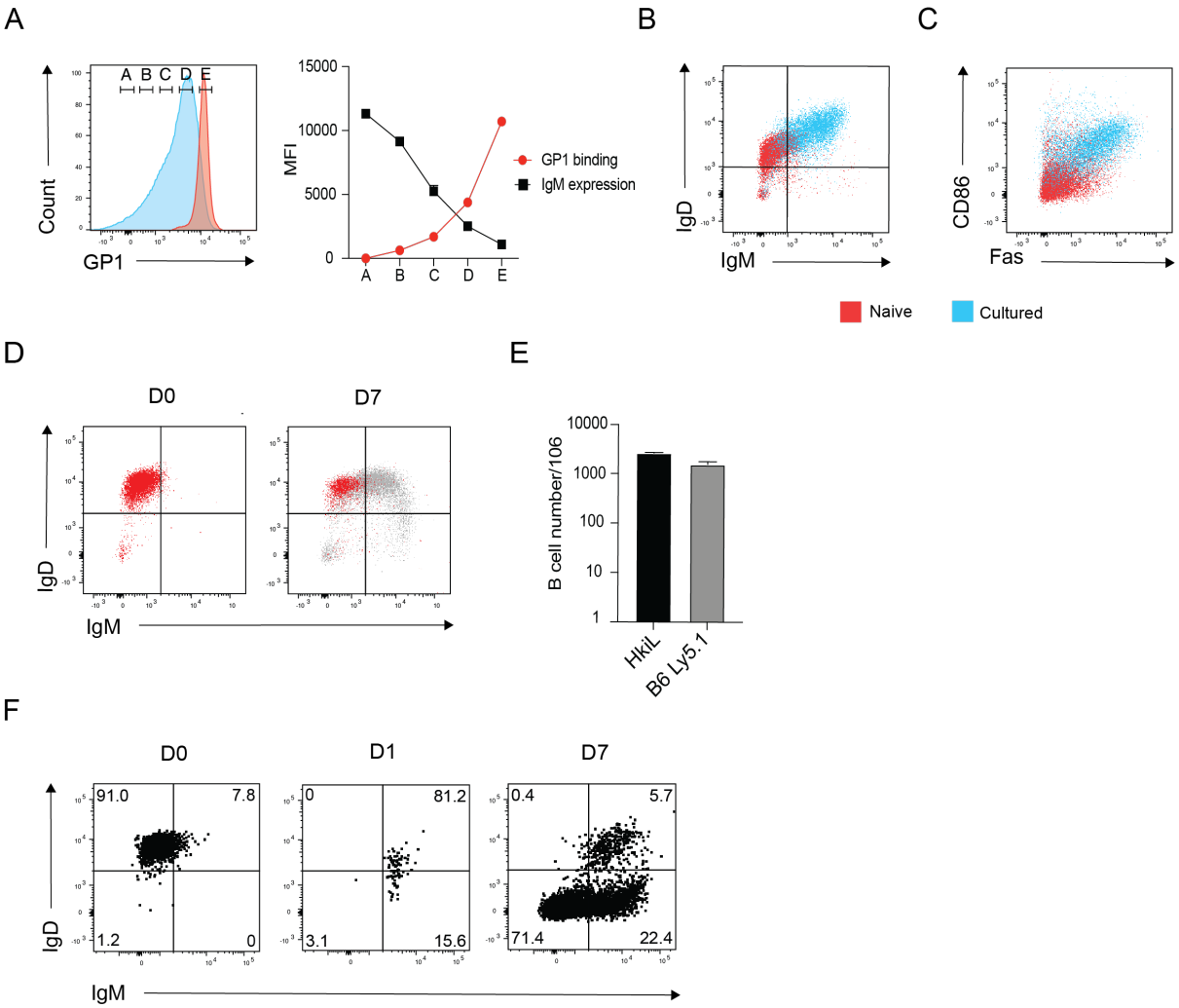

Figure 2. 4: IgM downregulation correlates with LCMV GP1 binding and is restored upon B-cell activation

(A) Flow cytometry histogram of GP1 binding of B220^{+} TgHL (blue) and HkiL (red) B cells. An alphabetical gating strategy was applied to measure the GP1 and IgM MFI, which was subsequently plotted on the right. Each point represents the MFI of either IgM or GP1 binding of B220^{+} cells for a given gates. n=4 (B-C) Two million of purified HkiL B cells were co-cultured for 4 days with irradiated 3T3 fibroblasts stably expressing CD40L and BAFF (CD40LB) in the presence of soluble IL-4. (B) Representative FACS plot of IgM/ IgD expression profile of HkiL cells (B220^{+} pre-gated) before (red) and after 4 days of culture

(blue). (C) Activation profile of HkiL cells ($B220^+$) before (red) and after 4 days of culture (blue). (D-E) One million of HkiL or C57BL/6 Ly5.1 B cells ($B220^+$, $CD45.1^+$) were transferred into naïve C57BL/6 recipients ($CD45.2^+$) and IgM and IgD expression of the donor cells was measured on day 3 and day 7 post transfer. (D) FACS plots of IgM/IgD profile of HkiL B cells (red) prior to transfer (D0) and seven days post transfer (D7), overlayed with the endogenous population (grey). Transferred cells were gated on live, $B220^+$, $CD45.1^+$, $CD45.2^-$ lymphocytes. (E) Enumeration of the HkiL B cells ($CD45.1^+$, $B220^+$) among recipient splenocytes on day 7. n=4. Number of experimental replicates (N) = 2(F) One million of purified HkiL B cells was adoptively transferred into animals infected with high dose rCl13 WE N119. Representative FACS plots show IgM/IgD expression profile of the HkiL cells ($B220^+$, $CD45.1^+$, $CD45.2^-$) on day 1 and 7 post transfer. n=2, N=2

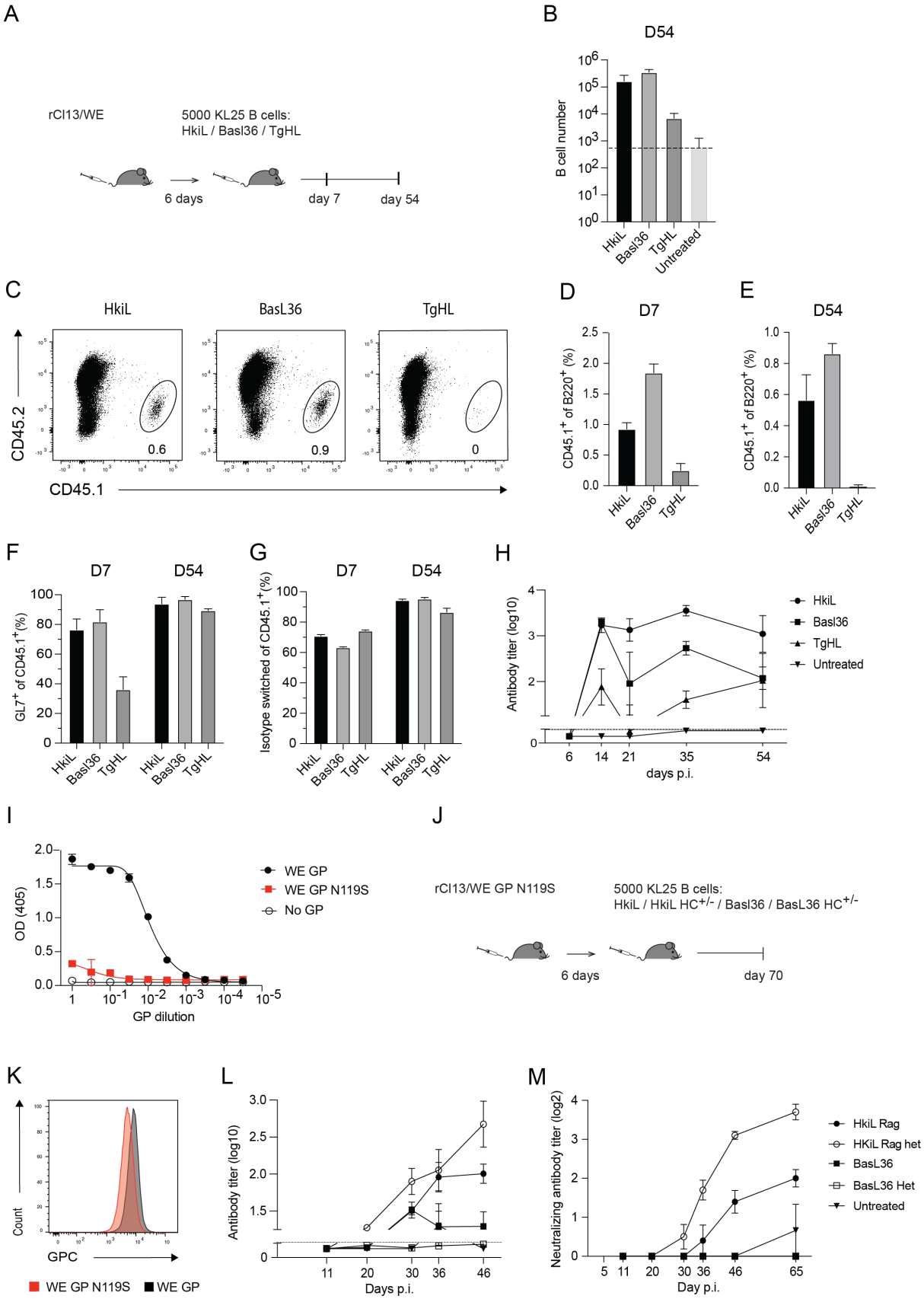
A
rCI13/WE
5000 KL25 B cells:
HkiL / Basl36 / TgHL
6 days
day 7
day 54
B
D54
B cell number
HkiL
Basl36
TgHL
Untreated
C
HkiL
BasL36
TgHL
CD45.2
CD45.1
0.6
0.9
0
D
D7
CD45.1+ of B220+ (%)
E
D54
F
D7
D54
GL7+ of CD45.1+(%)
G
Isotype switched of CD45.1+(%)
H
Antibody titer (log10)
days p.i.
I
OD (405)
GP dilution
WE GP
WE GP N119S
No GP
J
rCI13/WE GP N119S
5000 KL25 B cells:
HkiL / HkiL HC+/- / Basl36 / BasL36 HC+/-
6 days
day 70
K
Count
GPC
WE GP N119S
WE GP
L
Antibody titer (log10)
Days p.i.
M
Neutralizing antibody titer (log2)
Day p.i.
HkiL Rag
HKiL Rag het
BasL36
BasL36 Het
Untreated

Figure 2. 5: KL25-expressing IgM^{low} B cells enter germinal centers and produce antibody in chronic viral infection

(A) Schematic representation of the experiment: TgL mice (CD45.2$^+$) were intravenously infected with high dose rCl13 WE virus. 6 days later mice were treated with 5000 adoptively transferred B cells purified from the spleens of HkiL, BasL36 or TgHL donors or left untreated. Splenic lymphocytes were analyzed on day 13 and 54 post infection (B-H).
(B) Graph showing the number of recovered transferred B cells (B220$^+$, CD45.1$^+$, CD45.2$^-$) on day 54 post infection. (C) Representative FACS plots of transferred B cells on day 54, pre-gated on live lymphocytes (Sup.fig. 2.2B). (D) Percentage of transferred B cells (CD45.1$^+$) among recipient splenocytes on day 13, when gated as in Sup. Fig. 2.2A. (E) Percentage of transferred B cells among recipient splenocytes on day 54, when gated as in Sup. Fig. 2.2B. (F) Percentage of germinal center B cells among transferred cells (CD45.1$^+$, CD45.2$^-$ GL7$^+$, CD38$^-$) on day 13 and 54 (G) Percentage of isotype switched B cells among transferred cells (CD45.1$^+$, CD45.2$^-$, IgM$^-$, IgD$^-$) on day 13 and 54. (H) Graph of serum LCMV GP1- binding IgG antibody titer. (D-H) Symbols represent means ± SEM of one experiment. n=3-4. N=2. (I) Binding of KL25 antibody to the WE GP or WE GP with N119S mutation as measured by ELISA. Symbols show the means of two technical replicates. N = 2. (J) Schematic representation of the experiment: TgL mice (CD45.2$^+$) were intravenously infected with high dose rCl13 WE N119S virus. 6 days later mice were treated with 5000 adoptively transferred B cells purified from the spleens of HkiL, BasL36, and HkiL het, BasL36 het cells or left untreated. (J) Histogram showing binding of the HkiL B cells to the WE GP (Black) or WE GP with N119S mutation (red) as measured by flow cytometry prior to cell transfer. (L-M) Graphs of LCMV GPC N119S- binding IgG antibody titer measured by ELISA (L) and neutralizing antibody titer (M) measured by immunofocus reduction assay from the serum on indicated dates. (M) Symbols represent means ± SEM of one experiment. n=3-5. N=2

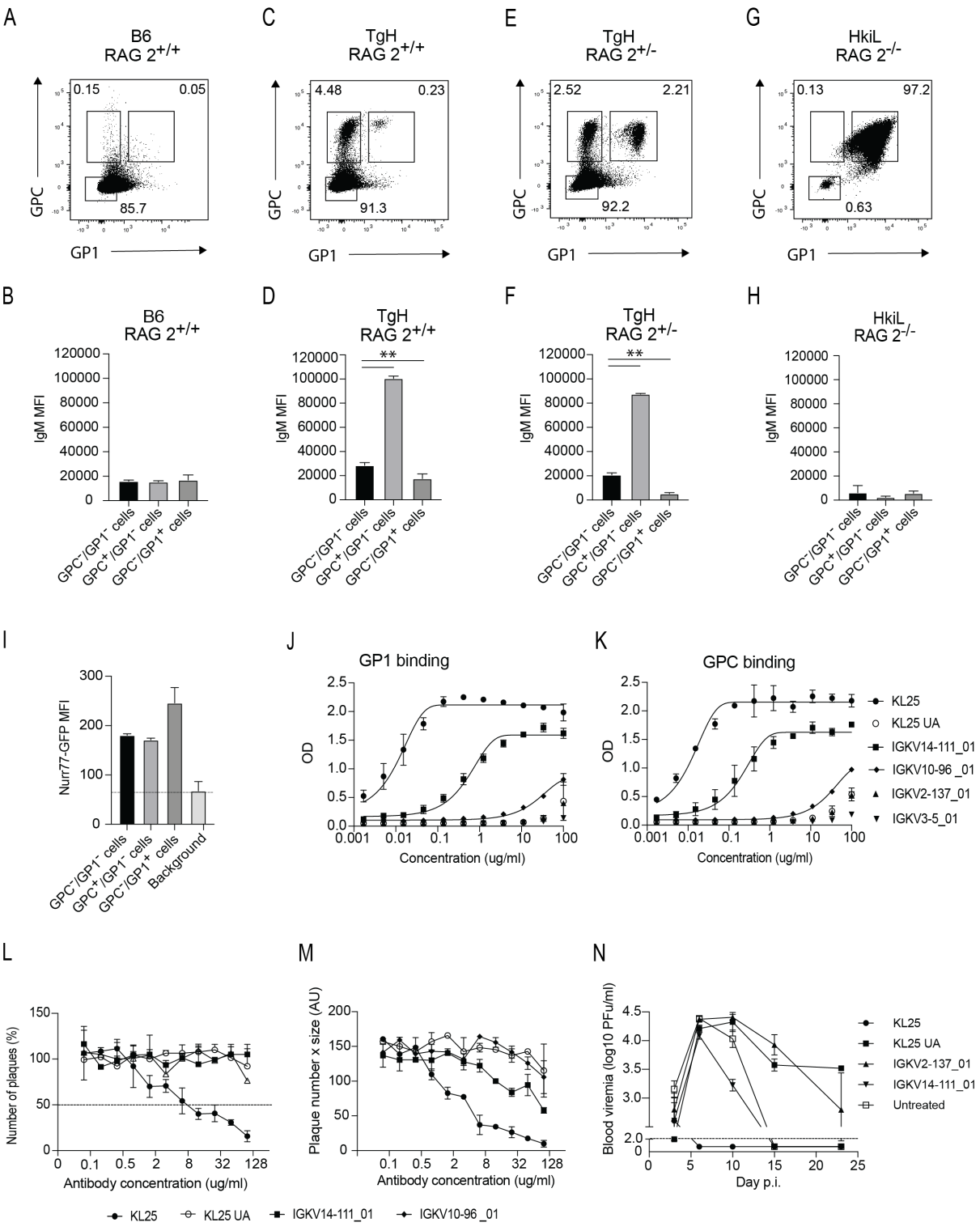
A
B6
RAG 2+/+
0.15
0.05
85.7
GPC
GP1
C
TgH
RAG 2+/+
4.48
0.23
91.3
E
TgH
RAG 2+/-
2.52
2.21
92.2
G
HkiL
RAG 2-/-
0.13
97.2
0.63
B
IgM MFI
120000
100000
80000
60000
40000
20000
0
GPC-/GP1- cells
GPC+/GP1- cells
GPC-/GP1+ cells
D
TgH
RAG 2+/+
**
F
TgH
RAG 2+/-
**
H
HkiL
RAG 2-/-
I
Nurr77-GFP MFI
300
200
100
0
GPC-/GP1- cells
GPC+/GP1- cells
GPC-/GP1+ cells
Background
J
GP1 binding
OD
2.5
2.0
1.5
1.0
0.5
0.0
0.001
0.01
0.1
1
10
100
Concentration (ug/ml)
K
GPC binding
KL25
KL25 UA
IGKV14-111_01
IGKV10-96 _01
IGKV2-137_01
IGKV3-5_01
L
Number of plaques (%)
150
100
50
0
0
0.1
0.5
2
8
32
128
Antibody concentration (ug/ml)
KL25
KL25 UA
IGKV14-111_01
IGKV10-96 _01
M
Plaque number x size (AU)
200
150
100
50
0
N
Blood viremia (log10 PFu/ml)
4.5
4.0
3.5
3.0
2.0
0
5
10
15
20
25
Day p.i.
KL25
KL25 UA
IGKV2-137_01
IGKV14-111_01
Untreated

Figure 2. 6: Rare GP1-binding B cells in oligoclonal and polyclonal repertoires downregulate IgM and report elevated levels of baseline BCR signaling

(A, C, E, G) Representative FACs plots of LCMV GPC and GP1 binding of B220+ B cells from the spleens of WT, TgH and HkiL mice with a different RAG 2 backgrounds as labeled. Numbers represent the percentage of gated cells as shown. (B, D, F, H) Graphs of IgM mean fluorescent intensity (MFI) of the IgM expressing GP binding cells of WT, TgH and HkiL mice when gated as in (A,C,E,G). Bars represent means ± SEM. Data were statistically analyzed using One-way ANOVA with Turkey's post-test for multiple comparisons. ** = $p > 0.0021$ n=2-5 (I) Graph of Nur77-GFP MFI (bars± SEM) of GP binding cells from the spleens of TgH mice when gated as in (C). n=5. (J-K) ELISAs showing LCMV GP1 and GPC binding of recombinant antibodies consisting of light chains sequenced from the $GP1^{+}/GPC^{+}$ binding TgH population as shown in (C) and a KL25 heavy chain. (L-M) Immunofocus reduction assay of LCMV Cl13 using binding recombinant antibodies binding to LCMV GP1 as in (J). (J-M) Symbols represent the mean ± SEM of 2 technical replicates. Dotted line indicates the detection limit of the assays. N=2 (N) We infected mice with rCl13 WE on day 0, followed by passive immunization with the indicated antibodies on day 3. Viremia was monitored. Symbols represent the means ± SEM of experimental group in one representative experiment. n=4

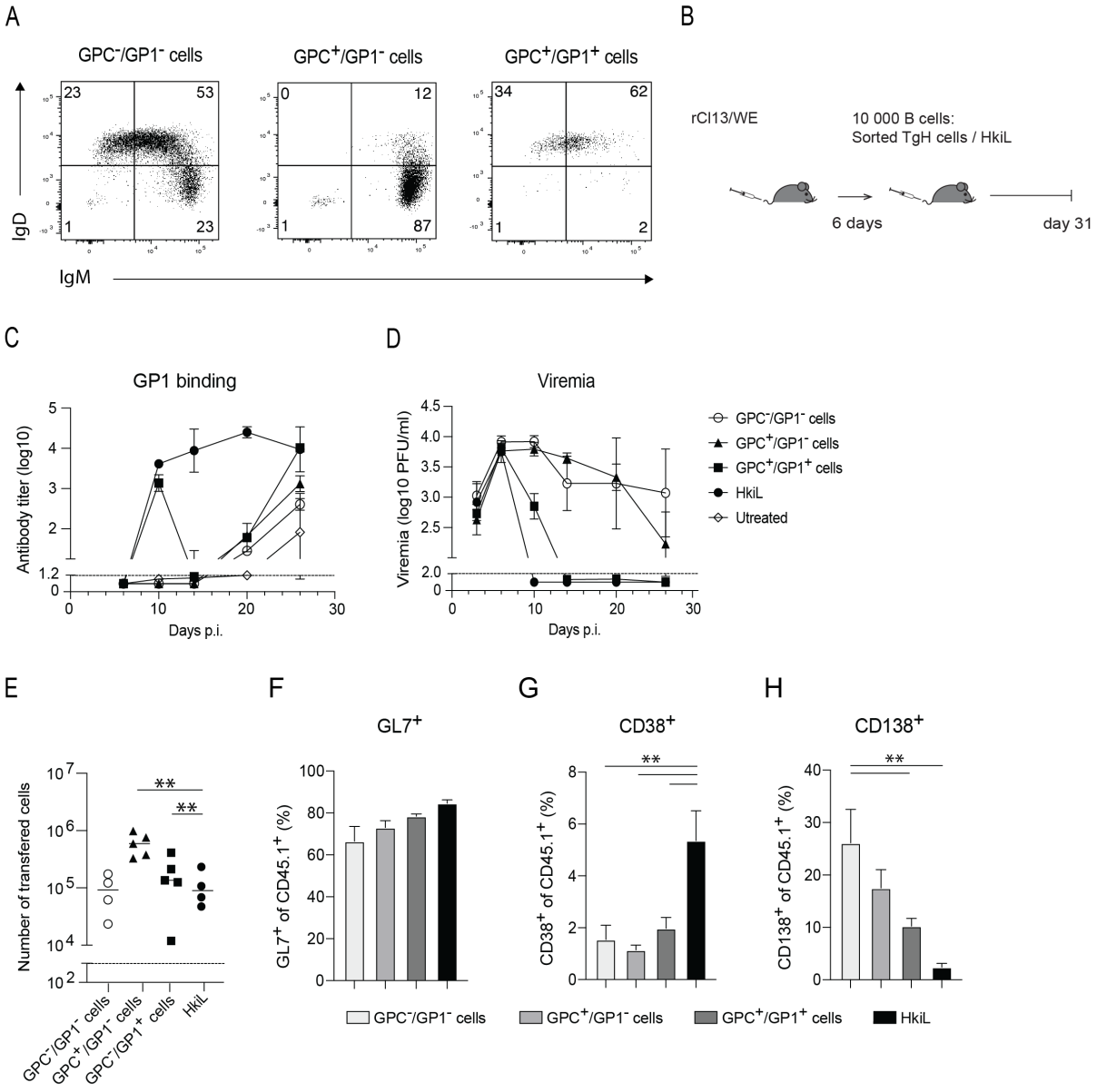

Figure 2. 7: GP1-binding IgMlow B cells but not GPC-only-binding IgMhigh B cells control chronic LCMV infection

(A) Representative FACS plots of the IgM/IgD profile of B220^{+}, GPC and GP1-binding B cells sorted from the spleens of TgH mice as in Fig. 2.6C. (B) Experimental schematic: TgL mice were infected with high dose rCL13 WE virus. Six days later 10 000 B cells with differential GP-binding properties sorted from the splenocytes of TgH mice (as shown in (A)) or the same number of HkiL B cells were adoptively transferred. The animals were sampled continuously

for serum and viremia for 25 days. (C) ELISA measurement of LCMV GP1 binding IgG serum antibodies throughout the course of the experiment. (D) Blood viremia measured by the immunofocus reduction assay (C-D) Symbols represent the mean ± SEM of the experimental groups. Dotted line indicates the detection limit of the assays.

(E) Enumeration of the transferred B cells ($CD45.1^+$, $CD45.2^-$, $B220^+$) in the recipients` spleens on d31 post infection. Symbols represent individual mice with a line indicating the mean of the experimental group. (F-H) Percentage of the germinal center ($CD38^-$, $GL7^+$) (F), memory cells ($CD38^+$, $GL7^-$) (G) and plasma cells ($CD138^+$) (H) among the transferred B cells from the spleen of recipient animals. The bars represent mean values per experimental group ± SEM. n=4-5 For gating strategy see Sup. Fig 2.3A.

Grouped data in E-H were statistically analyzed using One-way ANOVA with Turkey's post-test for multiple comparisons. ** = $p > 0.0021$, n = 4-5

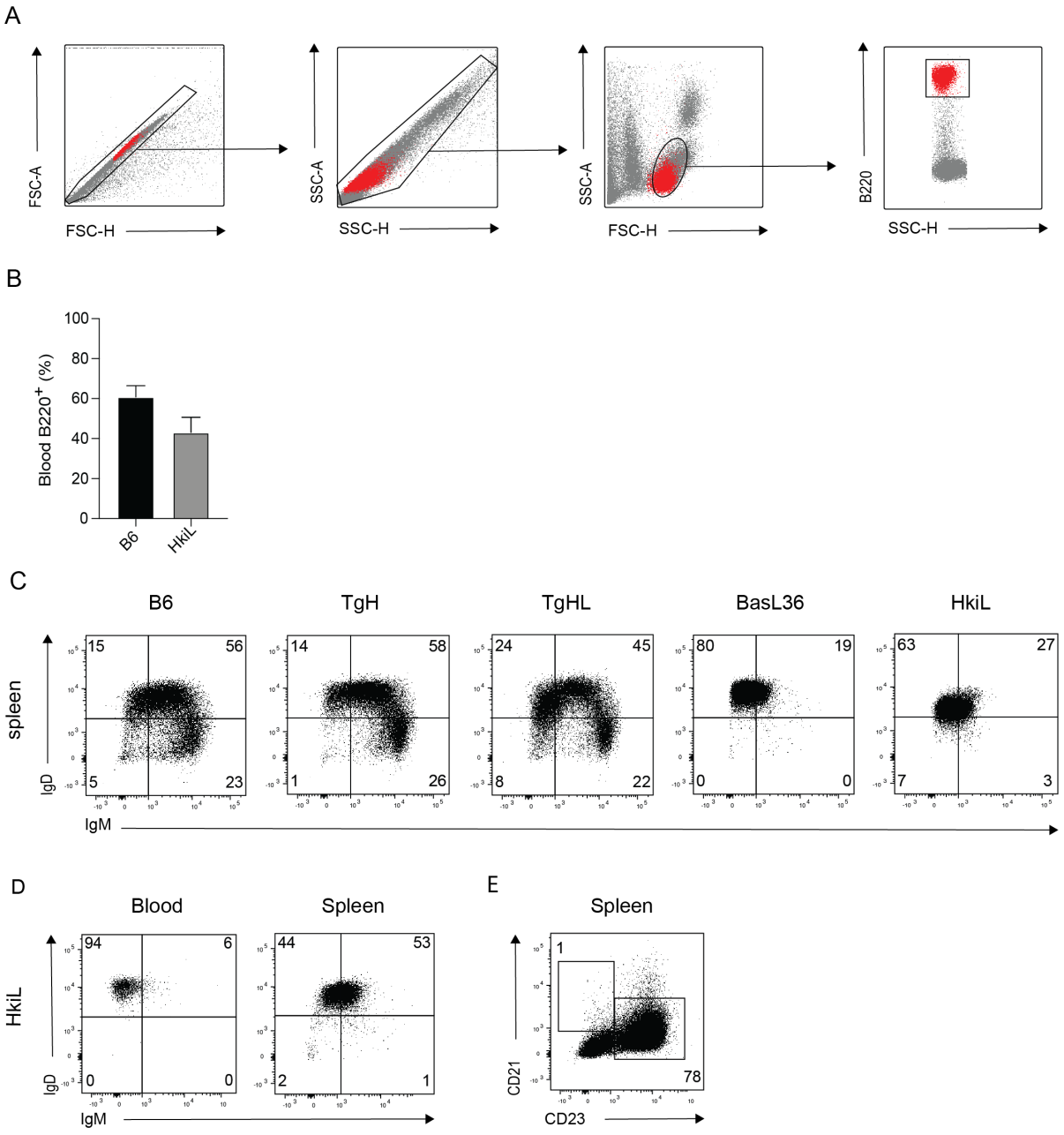

Supplementary figure 2. 1: IgM downregulation is characteristic of the phenotype of GP1 binding B cells in blood and lymphoid organs

(A) Gating strategy to identify $B220^+$ splenocytes in the experiments performed in Figure 2.2. (B) Graph of B cell percentage ($B220^+$) among splenocytes of KL25 transgenic animals as compared to B6. Bars show the means ± SD. (C) Flow cytometric analysis of $B220^+$ B cells

from the spleen of KL25 mouse models showing IgM/IgD profile. (D) Flow cytometric analysis of $B220^{+}$ B cells from the blood and spleen of HkiL mice showing IgM/IgD profile. (E) Flow cytometric analysis of $B220^{+}$ solenocytes with marginal zone B cells (MZ) gated as $CD23^{low}$ $CD21^{high}$ and follicular B cells (FO) as $CD23^{high}$, $CD21^{low}$. Numbers represent percentage of B cells in the gates. (B-E) n=2-5

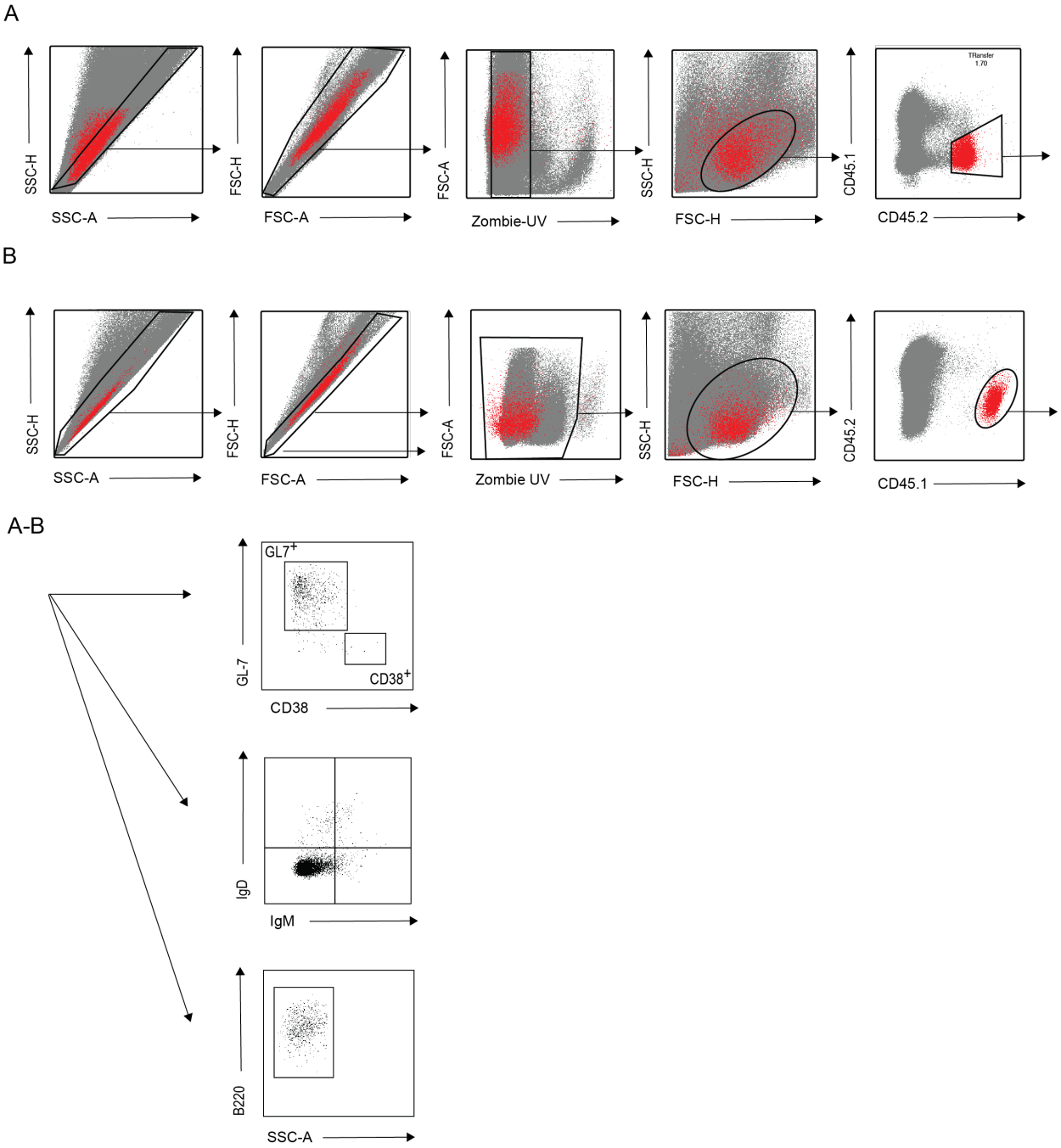

Supplementary figure 2. 2: KL25-expressing IgM^{low} B cells enter germinal centers and produce antibody in chronic viral infection

(A) Gating strategy for the experimental flow cytometry analysis of the day 7 for the figures 2.5D, F,G,H. (B) Gating strategy for the experimental flow cytometry analysis of the day 54 for the figures 2.5B,C,E,F,G,H.

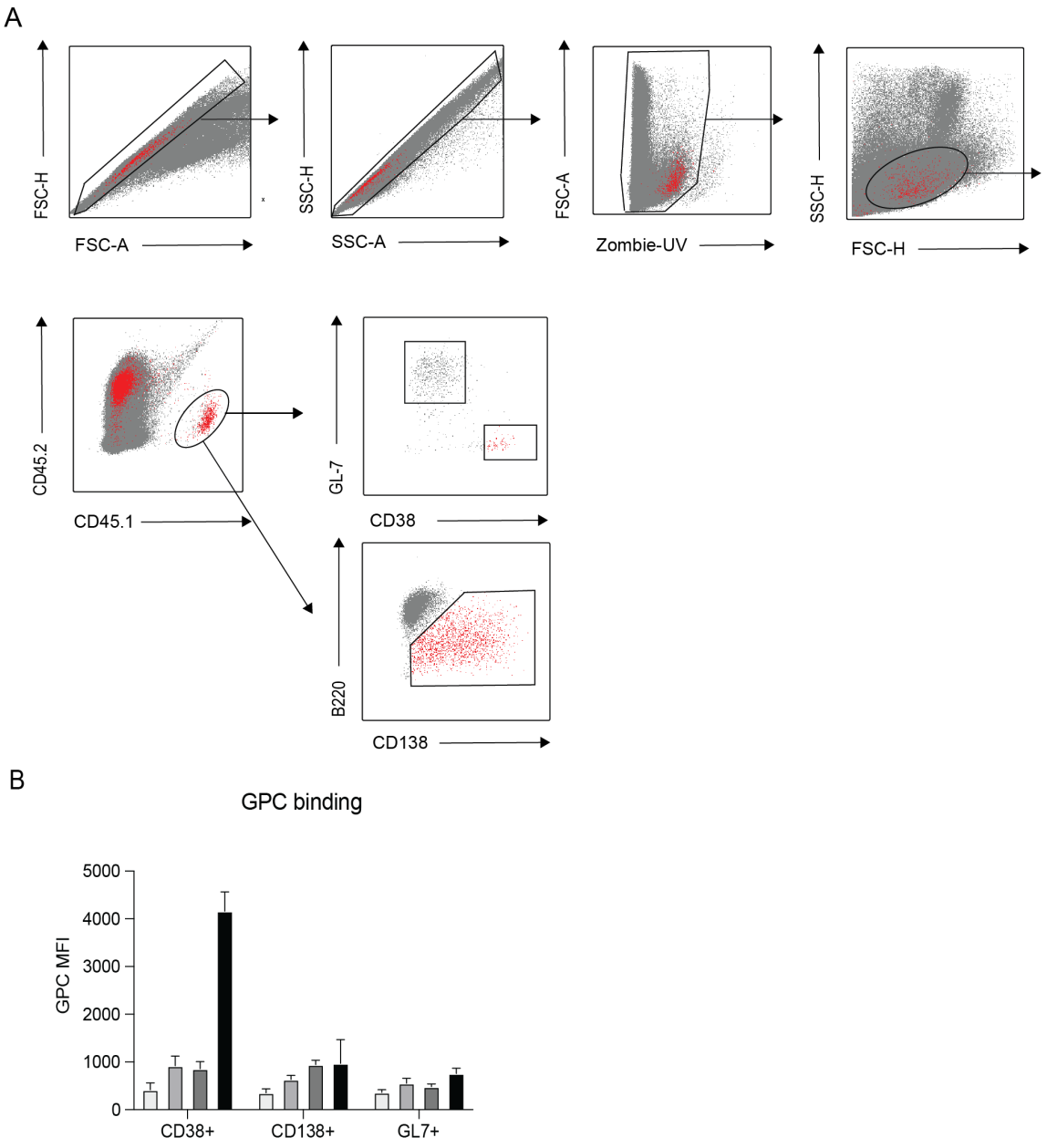

Supplementary figure 2. 3: GP1-binding IgMlow B cells but not GPC-only-binding IgMhigh B cells control chronic LCMV infection

(A) Gating strategy for the experimental flow cytometry analysis of the day 31 used for the figures 7E, F,G,H. (B) GPC-binding of the transferred ($CD45.1^+$, $B220^+$) B cells as measured by the mean fluorescent intensity (MFI) when gated as in (A).

Acknowledgements

We wish to thank Thorsten Buch and his team, Jane Biel-Wagner and Johannes vom Berg at the Laboratory animal services center at the Univeristy of Zurich of for their contribution in the intellectual and manual creation of the HkiL mouse. We thank Thomas A. Bowden and Quido Paesen at the Oxford university for providing LCMV GP recombinant protein, essential for the flow cytometric staining. We also thank Karsten Stauffer for his support in animal experimentation.

Author contributions

MF and DDP designed the experiments. MF, ASB, MS performed the experiments. MF and DDP analysed the data. MF wrote, DDP revised the manuscript.

3. CRISPR/Cas9-engineered B cells clear chronic viral infection and enter germinal centers in an affinity-dependent manner

Marianna Florova [1], Maysam Mansouri [1], Daniel D. Pinschewer [1]

Affilitiations

[1] Department of Biomedicine – Haus Petersplatz, Division of Experimental Virology, University of Basel, 4009 Basel, Switzerland.

[2] Molecular Cell Biology, Paul Scherrer Institute, 5232 Villigen, Switzerland

Corresponding author:

Daniel D. Pinschewer,

Department of Biomedicine – Haus Petersplatz, Division of Experimental Virology, University of Basel,

4009 Basel, Switzerland.

Daniel.Pinschewer@unibas.ch

One sentence summary

Primary B cells engineered to express an LCMV glycoprotein-specific, neutralizing antibody clear chronic viral infection upon adoptive transfer and have a distinct differentiation pathway in vivo.

Abstract

Effective vaccines preventing the viral mutational escape of chronic infections such as hepatitis C virus (HCV) or human immunodeficiency virus (HIV) remain a challenging, yet urgent medical need. A recently developed strategy proposes that primary B cells can be engineered with CRISPR/Cas9 to express broadly virus-neutralizing antibodies for prophylactic and therapeutic use against persisting viral pathogens.

Here we exploited the lymphocytic choriomeningitis virus (LCMV) infection model to assess the efficacy of CRISPR/Cas9-engineered primary B cells as a therapy for persistent infection and compared it to germline-edited B cells expressing the equivalent receptor. Somatically gene-edited B cells, expressing a neutralizing antibody (KL25) as receptor, transiently produced neutralizing antibody and were efficient at clearing chronic infection upon adoptive transfer into viremic hosts. However, these gene-edited cells exhibited lower B cell receptor (BCR) expression than germline-targeted KL25 B cells. The expression of the KL25-engineered cells for the viral antigen decided over their germinal center homing capacity and memory formation. Taken together, these results underscore the promising character but also persisting limitations of B cell receptor engineering-based therapies for persisting viral diseases.

Introduction

Passive antibody therapy has proven to be effective in multiple infectious diseases, such as HIV, Epstein-Barr virus (EBV), Ebola, dengue, and Zika; however, it requires repeated administration over a possibly lifelong period [111]. New therapeutic approaches with continuous long-term antibody administration are based on the intramuscular expression of virus-neutralizing, antibody-encoded adenoviral vectors and have been shown to protect against a viral challenge in nonhuman primate models [103, 286-288]. Despite the potential of this method to be further translated, critical issues in vector immunogenicity or its potential selective pressure for the viral escape variants will have to be addressed. Protective vaccines modulate multiple aspects of the immune response, including B cell affinity maturation towards the immunogen, the result of which, the antibody production, is the best surrogate of protection and vaccine efficacy to date (WHO). It is of concern that, for specific pathogens, such as HIV and HCV, developing a successful vaccine remains a challenge. Investigating the underlying reasons goes hand-in-hand with understanding how these viruses manage to persist within the host and establish chronicity. A limited starting B cell repertoire of precursor specificities binding viral epitopes [289], as well as rarely successful, epitope-dependent, antibody maturation [290], are challenges that need to be overcome for a successful humoral response. While our knowledge of viral immunopathology grows constantly, genome-editing techniques have brought new possibilities of immune response modulation [291]. Clinical outcomes from treatments using ex-vivo genome-edited chimeric antigen receptor (CAR) or T cell receptor (TCR) engineered T cells show promising efficacy [292-294]. At the same time, their safety lays the ground for the development of other therapies with lymphocytes possessing engineered functions. We and others have attempted proof of concept for B cell receptor (BCR) genome editing of B lymphocytes in mice. Indeed, it has been shown that genetically engineered B cells enter germinal centers, produce antibodies and respond to immunization [156-158, 295].

Given their ability to produce neutralizing antibodies and the possibility of adaptation to viral escape variants, engineered B cells could serve not only as a prophylactic therapy, creating a new B cell pool upon autologous adoptive transfer, it also holds the potential of curing chronic viral infections altogether.

We used the lymphocytic choriomeningitis virus (LCMV) model of chronic viral infection and introduced the neutralizing monoclonal antibody KL25 B cells to assess both the potential and limitations of this technology.

Results

CRISPR/Cas9 B cell editing optimization using a GFP reporter insert

In the initial set of experiments, we evaluated optimal conditions for the culture, activation, and permissibility of primary naïve B cells to the targeted genomic insertion of a foreign DNA introduced via transfection or transduction. Before editing, primary mouse B cells need to be activated. For this, we cultured splenic B cells on a CD40LB feeder layer supplemented with IL-4 [159]. B cells activated this way exhibit a germinal center-like phenotype ($GL7^+$, Fas^+) but do not isotype switch. Green fluorescent protein (Neon) expression from the template vectors three days after the intracellular delivery served as an efficiency readout. Initially, our vectors consisted of Neon and Puromycin resistance genes, but not a promoter, to ensure the expression from the targeted locus. As a template delivery vector, baculovirus has a large cargo capacity of 100kb and can be efficiently used for primary cells' editing [296, 297]. Indeed, we observed that activated primary mouse B cells were permissive to the infection with a yellow-fluorescent protein (EYFP)-expressing baculovirus with a transduction efficiency of up to 60%. Also, difficult-to-transduce non-activated primary B cells were permissible to the infection, albeit to a lower extent (Sup. Fig. 3.1A, B). Upon transduction, however, B cells downregulated the B220 surface marker (Fig. 3.1C). When using the same transduction protocol for AAV-GFP vectors of different serotypes, we could not reach comparable efficiencies (Fig 3.1D). Due to its versatility, we eventually resorted to double-stranded DNA templates (dsDNA) as a template gene delivery method. However, further investigation of baculoviral vectors as templates for homology-directed repair (HDR) remains to be undertaken.

Cas9 enzyme was delivered intracellularly as a ribonucleoprotein (RNP) preassembled with guide RNAs (gRNAs). When designing the targeting strategy for immunoglobulin knock-in, we foresaw the importance of maintaining the BCR-engineered B cells' capacity to isotype switch, as different isotypes confer different effector functions during chronic viral infection.

The strategies used for the germline antibody knock-ins, replacing the joining region (J_H1-J_H4) gene segments in the immunoglobulin heavy chain locus (IgH), are not feasible in the primary B cells, as one or both alleles are rearranged. Furthermore, targeting to replace a hybridoma's rearranged variable, diversity, and joining region (VDJ) gene with a green fluorescent protein (Neon) reporter template led to a significant culture lethality (Sup. Fig. 3.1E, F, G). In the alternative, non-lethal strategy, we introduced a single double-stranded break (DSB) in the intronic region downstream of the J_H4. Although J_H-segment replacement was not feasible as a targeting strategy, the hybridoma's lethality is a readout of gRNA's high cutting efficiency. Additionally, we induced two DSBs, removing only the last J_H4 element and a part of the downstream intron (Sup. Fig. 3.1G). Homology-directed repair (HDR) with a Neon template was less efficient in the J_H4 targeting strategy than in the targeting strategy using intron-specific gRNA only (Sup. Fig. 3.1H, I). Since the single-cut intron targeting, 374 base pairs (bp) downstream of J_H4 element, was the most efficient and allowed for a relatively long conserved 5-prime homology arm (HA) in a DNA template, we used it as a standard strategy for our experiments.

As a further step in optimization, we intended to investigate whether 20 bp microhomology arms, rather than a few hundred bp, would be sufficient for homology-directed repair (HDR) [160, 162]. Such an approach could reduce the template size and hence ease the intracellular delivery. We designed Neon-expressing double-stranded (ds) templates without a promoter (2A_Neon) with different length homology arms (Fig. 3.1A) and electroporated them together with Cas9 RNP into activated primary B cells (C57BL/6J). Three days later, the efficiency of integration was measured by the Neon expression. Transfections using the long HAs cassette favoring HDR yielded higher IgH editing efficiencies in primary B cells (Fig. 3.1B, C). To evaluate the possibility of an aberrant Neon expression, for example, from an off-target active

gene, we performed a set of control transfections. We targeted the HPRT gene as a control locus to which the cassette could potentially recombine via non-homologous end-joining. We observed that the expression of Neon cassette is dependent on a correct IgH integration via HDR (Fig. 3.1D).

In the case of the promoter-less cassette, 2A_Neon, the Neon gene expression depends on the strength of the endogenous VDJ promoter. Some studies elucidated the possibility of an allelic inclusion and bi-specific BCR expression [298]. Therefore, we hypothesized that adding a promoter into the Neon cassette (Fig. 3.1E) may increase the knock-in efficiency, as the number of alleles available for a repair-gene integration is doubled. Indeed, we could measure higher knock-in efficiencies and expression levels with a promoter-containing (prom_Neon) HDR cassette. Additionally, the second-in-tandem gene expression, tomato-fluorescent protein, was higher in the promoter-containing cassette. More specifically, only the Neon-high expressing B cells also expressed the tomato (Fig. 3.1F). Although the risk of off-target expression from the promoter-containing cassette was higher, we found an advantage in its increased expression of both template genes in tandem and, therefore, used it for our antibody studies.

KL25 antibody expression from the IgH locus of CRISPR/Cas9-edited mouse B cells

For an antibody expression from the IgH locus, we maintained the intron targeting strategy (Fig. 3.2A) and designed an LCMV glycoprotein (GP)-binding, neutralizing antibody, KL25, expression cassette, where the light chain (LC) gene, consisting of the variable, joining, and constant regions, precedes the heavy chain (HC) VDJ. A P2A self-cleaving peptide sequence between the LC and HC ensured the individual protein expression (Fig 3.2B). Both antibody cassettes with a promoter (prom_KL25) and without it (2A_KL25) were tested on primary B cells from various mouse strains differing in the number of in-germline recombined alleles available for somatic targeting.

To investigate the possibility of a dual-BCR expression and allelic inclusion in genetically modified B cells, we crossed the BasL36 mouse, transgenic for KL25 antibody binding LCMV GP, and the VI10 mouse, transgenic for VI10 antibody, binding GP of vesicular stomatitis virus (VSV). B cells of the progeny mice had both LCMV and VSV-specific BCRs expressed on their surface in a co-dominant fashion, as measured by flow cytometry (Sup. Fig 3.2B, C).

When targeting the activated primary B cells of WT mice, with one productively rearranged allele, we observed higher KL25 expression with the promoter-containing KL25 cassette (Fig. 3.2C, D). The higher expression of the prom_KL25, as opposed to the 2A_KL25 cassette, was further accentuated when another non-functionally rearranged allele was added to the pool of potential targets. This was demonstrated by the higher BCR- expression in the edited MD4 B cells (Fig 3.2E, F). Next, we utilized primary B cells of KL25HC mice, in which the KL25 VDJ gene is rearranged and knocked-in in the germline of both IgH alleles (Fig. 3.2G). These mice also express an LC transgene of the VI10 antibody to reduce the germline pool of LCMV GP-binding cells. When both targeted alleles are functionally rearranged and we further edit them with the prom_KL25 or the 2A_KL25 cassette, we obtain comparable knock-in efficiencies (Fig. 3.2H). Hence, using the promoter-containing dsDNA construct for primary B cell editing yields higher BCR knock-in efficiencies and allows for immunoglobulin expression from the allelically excluded locus.

Lower LCMV glycoprotein binding of KL25 engineered B cells is independent of the targeting construct

The overall engineered BCR expression, as measured by the percentage of LCMV GP-binding B cells three days after editing, was more than 3x higher in the KL25HC than in the WT mice for both prom_KL25 and 2A_KL25 constructs (Fig. 3.3A). The number of the IgH alleles available for targeting alone cannot, therefore, account for the difference. Additionally,

compared to the KL25 germline knocked-in B cells - HkiL (KL25tg), the primary engineered KL25 B cells (KL25eng) have a lower binding capacity for the LCMV GP, and this is independent of the targeting cassette construct (Fig. 3B).

Given the low KL25 expression of the KL25eng B cells and the decreased expression of the second-in-tandem fluorescent protein (Fig. 3.1F), we devised an experiment where engineered BCR expression is dependent solely on the second-in-tandem KL25 VDJ gene element. We used KL25 LC transgene expressing primary B cells of BasL36 mice to knock in the prom_KL25 cassette or a cassette without the LC gene (prom_KL25HC), thus making the KL25 VDJ gene the only knocked-in element (Fig. 3.3C). We observed slightly higher knock-in efficiency with the non-tandemic template; however, there was no enhanced expression of the engineered BCR for the LCMV GP (Fig. 3.3D). Hence, the in-tandem joining of the LC and HC engineered into the IgH locus does not negatively impact the antibody expression.

To circumvent the necessity of the P2A linker between the KL25 LC and HC genes, which could potentially interfere with the correct folding and expression of the immunoglobulin molecule, we designed a cassette with two different HC promoters in an ambi-sense orientation - one driving the expression of the HC, the other, reversed, that of the LC (ambi_KL25) (Fig. 3.3E). We saw no KL25 BCR-engineered B cells using this cassette in the primary B cells of WT mice (Fig. 3.3F, G). The engineering of the ambi_KL25 cassette into the KL25HC primary B cells rescued the KL25 antibody expression; however, the percentage of KL25 expressing B cells decreased slightly compared to the prom_KL25 cassette (Fig 3H). Therefore, using the ambi_KL25 cassette, as suggested here, does not improve the expression of the engineered-BCR. Our findings indicate that with the expression driven by neighboring ambi-sense promoters, the forward-reading is silenced, as opposed to a functional reverse transcription of the promoter, here LC, in the IgH targeting locus.

KL25 engineered cells clear chronic viral infection and enter germinal centers

It has been demonstrated that KL25 transgenic B cells can clear chronic LCMV infection [226]. To compare the efficacy of the KL25 germline-knocked-in HkiL B cells (KL25tg) to the primary KL25-engineered cells (KL25eng), we transferred one million of the KL25eng cells into chronically infected animals on day six after infection (Fig. 3.4A). Taking into account our mean BCR-editing efficiencies, this number corresponds to approximately 5000 edited B-cells. Therefore 5000 KL25tg B cells were transferred in parallel. As a control, mock-engineered (NEONeng) cells were transferred. The chronic LCMV infection was cleared on day eight post-transfer in both KL25eng and KL25tg groups but not in the controls (Fig. 3.4B). The IgG titer of LCMV GP1-binding antibodies peaks on day 14 post-transfer in the KL25eng group, after which the antibody production ceases. In the KL25tg group, however, the antibody production remains constant (Fig. 3.4C). Both KL25eng and KL25tg B cells expanded in the infectious environment, while nonspecific NEONeng, B cells failed to proliferate and were not present on day 29 post-transfer (Fig. 4D, E).

We observed different differentiation patterns of KL25eng and KL25tg B cells. While KL25tg cells were exclusively germinal center ($B220^{+}GL7^{+}$) phenotype on day 35 of analysis, only 40% of the KL25eng cells expressed the GL7 marker at this time point (Fig. 3.4E, F). The majority of the KL25eng transferred cells were of $CD38^{+}$, $GL7^{-}$ phenotype (Fig. 3.4E, G). While all the germinal center KL25eng B cells were isotype switched, only 50% of the $CD38^{+}GL7^{-}$ cells were, with the rest retaining an IgM^{+}/IgD^{+} phenotype (Fig. 3.4H, I). Such a differentiation pathway may be reflective of the germinal center independent stimulation and memory differentiation.

The B cells' entry to the germinal center during chronic viral infection has been shown to depend on the BCR affinity for the triggering antigen [6, 19]. Since the antigen-binding capacity of KL25eng cells for the LCMV GP is lower than that of KL25tg cells (Fig. 3.3B),

we investigated whether the difference also accounted for the participation rate of the KL25eng B cells in the germinal center reaction. We engineered C57BL/6, MD4, KL25HC primary B cells with KL25 specificity. Before an adoptive transfer into infected animals, we measured the binding capacity of the different KL25eng cells for LCMV GP. Only the KL25HC KL25eng cells contained a high-affinity B cell population comparable in BCR expression to the transgenic, HkiL cells (Fig. 3.4J). Upon transfer into the chronically infected animals, they preferentially homed to the germinal center, while only a lower percentage (20-40%) of the KL25eng low-affinity BCR-expressing cells of MD4 and WT mice did so (Fig. 3.4K).

In conclusion, KL25-engineered B cells were able to clear the chronic infection, despite their decreased ability to bind the LCMV GP when compared to germline knocked-in KL25 B cells and their binding ability decides the differentiation pathway.

Discussion

Genetically engineered primary B cells carrying a neutralizing antibody are the next anticipated step in the development of cell-based pharmaceuticals for the treatment of chronic viral infections. While this work has been ongoing, several comparable studies have been published, confirming that BCR-engineered B cells can expand, somatically hypermutate, and are functional when tested in the context of immunization and infection studies [156, 158]. To add to this knowledge, we confirm that B cells engineered with neutralizing specificity can suppress viremia and, therefore, functionally cure a chronic viral infection. To what extent this applies to other infections, such as HIV, remains to be elucidated. However, the cumulative knowledge of the protective capacity of the broadly neutralizing antibodies and the adaptability of the engineered cells encourages further research in the preventive, B cell pool-diversifying, and curative potential of the BCR-engineered B cells.

Off-target genome modification is of significant concern when using CRISPR/Cas9 technology. Combining the technological and immunological knowledge of highly specific sgRNAs and immunoglobulin locus regulation should guide the future investigation. A particular way to reduce the off-target expression that we and others show to be feasible is to use antibody templates without a promoter [157, 299]. However, we do observe a reduced protein expression of the second-in-tandem gene when the cassette is knocked in 376bp downstream of the last J_H4 element. Therefore, the expression of bi-cistonic antibody cassettes may depend on the distance and/or the strength of the endogenous promoter.

There is increasing evidence that engineered B cells participate in the immune response in viral infectious settings, transiently producing antibodies [157, 299]. Upon immunization, engineered B cells differentiate to form the memory compartment ($B220^+$, $CD38^+$, $GL7^-$) [158, 295]. Similarly, KL25-engineered B cells enter the germinal center, mature, and form an isotype-switched memory compartment. However, we observe “non-physiological”

differential pathways of the engineered B cells depending on the BCR antigen-binding capacity post-transfection. While germline transgenic neutralizing B cells with high affinity for the antigen primarily enter the germinal center and persist there, primary engineered B cells of the same specificity both enter the germinal center but mainly differentiate into $CD38^{+}$, $GL7^{-}$ sub-population, within which IgM^{+}/IgD^{+} B cells are present. Whether this population of cells is functional or an artifact remains to be investigated. Our comparison of the same specificity engineered and transgenic B cells suggests that for a physiologically predictable differentiation of BCR-engineered B cells, primary B cell editing techniques need to be improved towards higher BCR expression.

Methods

Cell lines, Primary B cell culture

CD40LB fibroblasts were obtained from and first described in Nojima et al., 2011. They were passaged in DMEM 10% FCS after the initial one-week passage in selection media containing 2.5ug/ml Puromycin and 0.5mg/ml G418. PnP-mRuby hybridoma, used for the targeting optimization was cultured as recommend and kindly provided by S. Reddy [150].

Primary naïve mouse B cells were isolated from spleens of C57BL/6, TgH, TgL, MD4 and TgHxVI10 mice and purified using negative selection, EasySep mouse B cell isolation kit (StemCell). Resting as well as activated B cells were cultured in B cell medium: DMEM (Sigma) supplied with 10% FCS (Life Biosciences), 2 mM l-glutamine, 2 mM sodium pyruvate, 2 mM Hepes (Gibco), 1× NAA (Gibco), β-mercaptoethanol (Sigma), and 10 μg/mL gentamicin (Lonza)

For B cell activation culture $1x10^5$ /cm^2 of CD40LB cells were seeded in T25 flasks (TPP) and their proliferation stopped with 80Gy Gamma irradiation. Subsequently, medium was replaced with 2.5ml fresh B cell medium and 12h later 2.5ml of freshly isolated B cells ($2x10^6$/ml) were added. The co-culture was supplemented with 1 ng/ml IL-4 (BioLegend) and incubated at 37°C for 48 hours.

B cells were post-transfection cultured analogously, however in 12-well plate (TTP), where $5x10^5$ of irradiated CD40LB cells in 500ul B cell medium were seeded a night prior to transfection. Post-transfection co-culture was supplied with 500ul of fresh B cell medium with IL-4 every day for 3 days. After this time, expansion to 6-well plate or T-25 flask is required.

B cell RNP transfection and post-transfection culture

To form an RNP complex for one transfection, equimolar ratios, 1ul (200 nmol) crRNA ((IDT) and 1ul (200 nmol) of tracrRNA (IDT) were incubated at 95°C and allowed to cool to RT. After hybridization, 2.4ul (150 pmol) of S. pyogenes Cas9 (IDT) was added and so-prepared Cas9 RNP complex was incubated for further 30 minutes at RT.

B cells in suspension were carefully aspirated without detaching the CD40LB feeder layer. 2x106 of B cells per sample were washed twice with 37°C warm PBS (Sigma). In between washings, the cells were span at 90g for 5 minutes each time.

The B cells were thereafter resuspended in transfection mixture consisting of 80ul freshly prepared transfection buffer (P4 Primary cell 4D Nucleofector X kit, Lonza), 15ul of DNA template in buffer (IDT), 4.4ul of Cas9 RNP complex (IDT) and 1ul Electroporation enhancer (IDT). Electroporation was executed immediately after, using Primary B cell program of AMAXA Nucleofector (Lonza). After nucleofection, the transfection cuvettes were filled with 500ul of B cell medium pre-warmed to 37°C, B cells aspirated and transferred onto a pre-prepared CD40LB feeder layer culture in 12-well plates (TTP) supplemented with IL-4. Based on the targeting strategy, different crRNAs were used for hybridization and RNP coupling; for intron targeting of Neon and KL25 crRNA_3HA (TTATACAGTATCCGATGCAT) was used. For J4 + intron targeting crRNA_3HA and crRNA_J4 (GGGGTTTTGTCGGGTATAG) were used. For hybridoma targeting crRNA_5HA-Ruby (GTCATGGAAGGTTCGGTCAACGG) and crRNA_3HA-Ruby (CATGCCGTTGATCACCGCC) were used.

dsDNA template production

The expression cassettes with florescent proteins, prom_Neon_Tom, 2A_Neon_tom, and KL25 antibody, prom_KL25 and 2A_KL25 flanked by the XhoI and NsiI restriction sides were

synthesized (Genescript) and subsequently subcloned into the vector containing Has, using the same restriction sides. (Complete maps upon request). These vectors were used as templates for PCR reaction, producing dsDNA templates. Per experiment, multiple PCR reactions were prepared. 5U of Phusion polymerase (NEB), 10uM of forward primer (dsTEMP_long_fwd - GCC TCT CCA GGT CTT TAT TTT TAA CCT TTG TTA TGG) (Microsynth), 10uM of reverse primer (dsTEMP_long_rev - TTT TCC CTT CCC CAA ATA GCC TTG CC) (Microsynth) and 10mM dNTP (NEB) and 50ng of plasmid template were completed with ddH20 to 40ul and cycled under following conditions: 98°C for 1 min; 35× (98°C for 10 s, 69.9°C for 25 s, and 72°C for 1 min 40 s); 72°C for 10 min. Sample PCR reaction was run on 1% agar gel to ensure a single DNA fragment amplification. DNA was purified and eluted in 2 steps (Qiagen PCR purification kit) from the remaining reactions. DNA content was measured using Nanodrop Spectrophotometer (ThermoFisher) and adjusted to 14ug in 560ul. Volume was subsequently reduced to 15ul using SpeedVac DNA Concentrator (Eppendorf).

Flow cytometry analysis

On day 3 and 7 post-transfection, the cell cultures were dislodged and 500ul of single cell suspension filtered for staining. In adoptive transfer experiments, splenocyte cell suspension was obtained by pressing the spleens of experimental animals through the grid and homogenizing by pipetting. Splenocytes were resuspended in B cell medium (see section Cell culture) and 1 ml of the suspension was used for staining. Dead cells in both cases were excluded from the analysis using Zombie UV Viability kit (BioLegend) and samples washed with PBS.

LCMV GP1 and/or GPC recombinant proteins were used to identify specific cells among cultured cells or splenocytes. Samples were incubated at 37C for 30 minutes while shaking in 200ul GPC-StreptagII supernatant, 5 ul of Fcγ blocking antibody (Jackson Immunoresearch)

and 1 ul (0.3 ug) of GP1-AF647. Subsequently, washed cells were resuspended in 50ul FACS buffer containing 0.2ul Streptactin-PE (IBA) and 0.5ul of B220-BV421(BioLegend) and incubated at RT for 15 minutes. Finally, samples were washed and resuspended in FACS buffer for acquisition.

Adoptively transferred cells were distinguished from those of recipients` using CD45.1 and CD45.2 markers. Following staining panel was used for phenotyping analysis: 0.5ul each of CD45.2-BV605 (BioLegend), CD45.1-BV421 (BioLegend), B220-AF700 (BioLegend), IgM-PerCP-eFluor710 (eBioscience, IgD- APC-Cy7 (BioLegend), GL-7-AF488 (BioLegend), CD38-APC (BioLegend), CD138-PE (BD). Incubation time of 15 minutes at room temperature preceded washing step and fixation with PBS 2% paraformaldehyde (Sigma). Samples were acquired with LSRFortessa flow cytometer (Becton Dickinson) and data analyzed using FlowJo software (Tree Star).

Viruses and transduction

A recombinant virus LCMV strain Clone 13 (rCl13) expressing the WE glycoprotein (WE-GP) was used for the high dose i.v. infection (2x106 PFU/ml) in all the adoptive transfer experiments. The virus stocks were propagated on BHK-21 cells (ATCC) via a cell infection at MOI 0.01 for 2 hours, after which the medium was replaced. The supernatant was collected 48 or 72 post infection and titrated on NIH 3T3 cells (ATCC) using a standard protocol.

A MultiBac baculovirus with integrated genes encoding eukaryotic yellow fluorescent protein (EYFP) and tubulin were a kindly provided by M. Mansouri and P. Berger [296]. AAV vectors of different serotypes with green fluorescent protein (GFP) under the transcriptional control of a cytomegalovirus (CMV) promoter were obtained from University of Pennsylvania Vector core facility.

Primary B cell transduction was performed at the MOI of ~100 for Baculovirus and ~1x10e5 for the AAV were used. Briefly, primary B cells were isolated from the spleens of C57BL/6 mice using and negative selection B cell isolation kit (Stemcell) and resuspended in the B cell medium at a density of 5x10e4 cells/ml. 2ml of B cells were then plated on the pre-prepared irradiated CD40LB feeder layer (5x10e4 cells/ml) and supplemented with 1 ng/ml of IL-4 in 6-well plate. 24h later, the supernatant with the B cells was collected, washed twice with PBS and resuspended in 0.5ul DMEM medium to an adjusted density of 1x10e5 cells/ml in a six well plate. Subsequently, 0.5ml of virus containing medium was added and the plates were incubated at 37°C for 1 hour while shaking. Finally, 3 ml of fresh pre-warmed medium was added, and the cultures were allowed to sit at 37°C for 3 hours before washing and plating on a new CD40LB feeder layer. For spin transduction on non-activated B cells, the protocol was performed analogously, except the B cells were not plated on a CD40LB feeder layer, but were cultured in B cells medium, prior to the infection, which was performed at RT, by centrifugation at 180g for 1h.

Mice

As donors, CD45.1-congenic C57BL/6J have been used and obtained from the Swiss Immunological Mouse Repository, (SwImMR). C57BL/6J wild-type mice (CD45.2) used as adoptive transfer recipientswere purchased from Charles River.

KL25L mice , which express the KL25 light chain were used as the recipients in the adoptive transfer experiments. KL25 heavy chain knock-in TgH [200] mice were crossed with the VI10 light chain transgenic VI10Ltg mice (unpublished) to generate KL25HC mice. B cells of this mouse strain, as opposed to TgH mice, do not bind to LCMV GP and hence the background in flow-cytometric staining was eliminated. MD4 mice, expressing anti-hen egg lysozyme

antibodies were obtained from C. Goodnow [105]. BasL36, expressing KL25 HC knock-in and LC transgene, were created in tour laboratory (Narr K., unpublished)

Adoptive transfers of engineered B cells

Engineered donor B cells ($CD45.1^+$) from C57BL/6, MD4 and KL25HC mice were transfected and cultured for three days prior to transfer. On day 6 of the infection, one million of the engineered B cells were transferred i.v. into recipients ($CD45.2^+$). B cells from the HkiL donors (CD45.1) were purified using a negative selection B-cell isolation kit (Stemcell) and 5000 of such cells were transferred i.v. into the infected recipients. As a control, one experimental group was left without a cell transfer.

GP1-binding enzyme-linked immunosorbent assay

GP1-binding antibodies in mouse serum were determined using recombinant HEK293 cell-derived GP1-Fc fusion protein as a substrate.[33]. The 96-well high-binding plates (Greiner Bio-One) were coated with goat anti-human IgG Fcγ antibody (Jackson) at a dilution 1:1000 i in coating buffer (Na_2CO_3 15mM, $NaHCO_3$ 35mM, pH9.6) at 4°C overnight. The plates were then blocked in a binding buffer (PBS / 0.05% Tween / 5% milk /0.2% BSA)
used for every subsequent step. GP1-Fc fusion protein supernatant was diluted in binding buffer and added to the plates to be incubated at the room temperature for one hour.
The plates were then washed with PBS/ 0.05% Tween (PBS-T) three times. 5 ul of the sera in binding buffer were serially diluted in the plate and incubated for 1 hour at room temperature. After the triple washing with PBS-T goat anti-mouse IgG-HRP conjugate antibody (Jackson) was diluted 1:750 and added for further 1 hour incubation. After washing, HRP activity was detected using ABTS as a chromogen (Pierce). OD_{405} was determined in an ELISA reader (Saphire II).

Figures

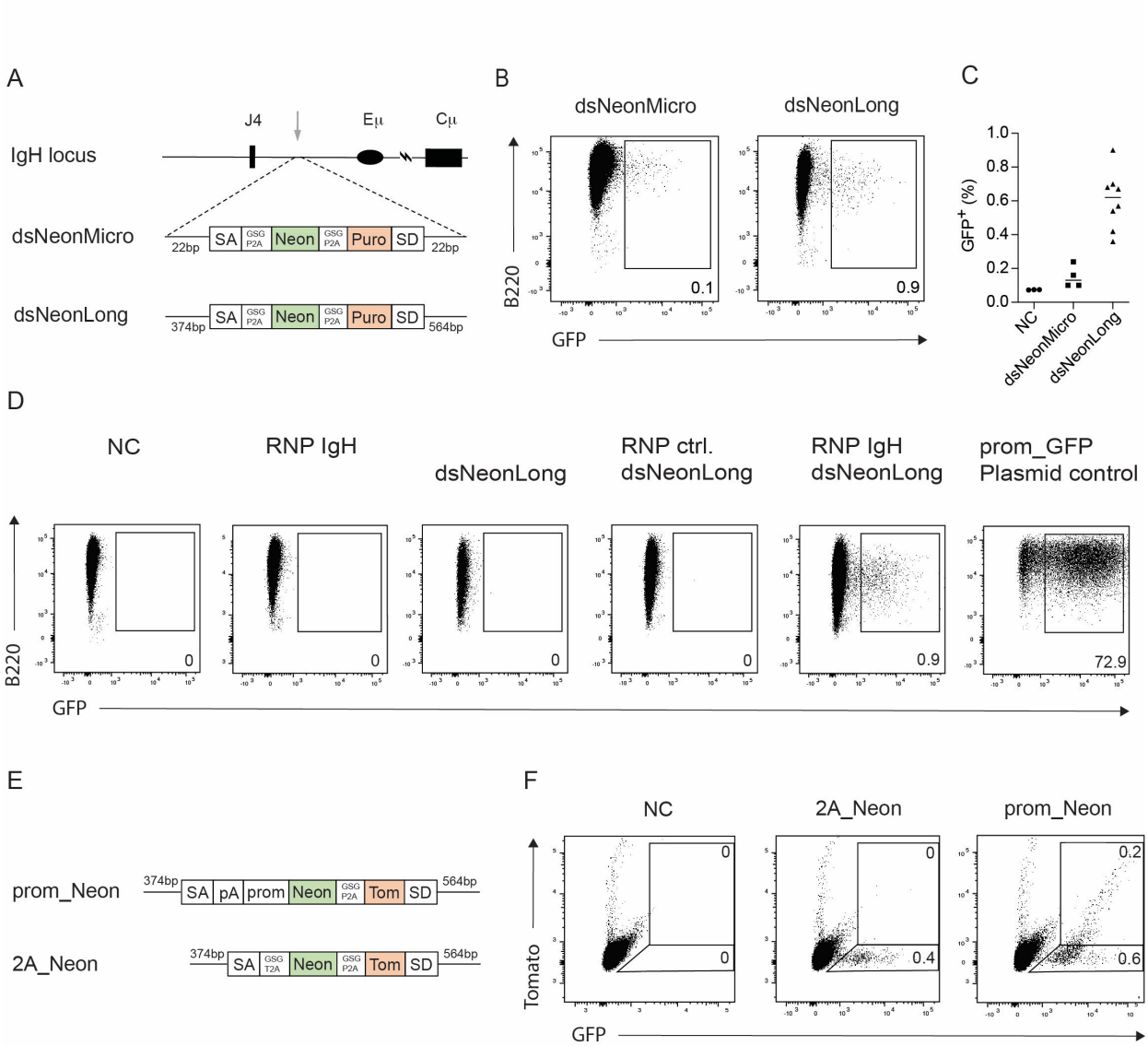

Figure 3. 1: CRISPR/Cas9 B cell editing optimization using a GFP reporter insert

(A) Schematic representation of the targeting strategy to insert a green fluorescent protein (Neon) expressing cassette into the intronic part of the IgH locus and the Neon and Puromycin expression dsDNA cassettes with the short (dsNeonMicro) and long (dsNeonLong) homology arms. Additional depicted cassette elements are: a splice acceptor site (SA), furin-cleaving side with a Gly-Ser-Gly linker and P2A self-cleaving peptide (GSG P2A) and a J_H3 splice donor site (SD). (B) FACS analysis of B cells targeted with either of the cassettes, using the targeting

strategy as in (A). Gates and numbers represent the percentage of GFP^+ B cells on day 3 when pre-gated on single, lymphocytes, live, $B220^+$ B cells. (C) A graph showing the percentage of recombined B cells after editing with either of the cassettes as in (A). Symbols represent mean and technical repeats from 2-3 experiments. (D) Activated primary mouse B cells were electroporated with Cas9 RNP with crRNA targeting IgH locus alone, dsNeonLong template alone, Cas9 RNP with crRNA targeting HPRT locus (RNP ctrl.) and dsNeonLong template, Cas9 RNP with crRNA targeting IgH locus and dsNeonLong template or a GFP plasmid with a promoter. Results are representative of two independent experiments.

(E) A schematic of the Neon and Tomato encoding dsDNA cassettes with (prom_Neon) and without (2A_Neon) a promoter. The additional cassette elements are: a splice acceptor site (SA), 2A linkers (GSG P2A) and a splice donor site (SD). (F) Activated B cells were electroporated with Cas9 RNP targeting IgH locus with either of the dsDNA templates as in (E) or left without the electroporation for a negative control (NC). Flow cytometry analysis was performed on day 3 post transfection. Gates and numbers represent the percentage of GFP^+ B cells on day 3 when pre-gated on single, lymphocytes, live, $B220^+$ B cells. Plots are representative of 2 independent experiments.

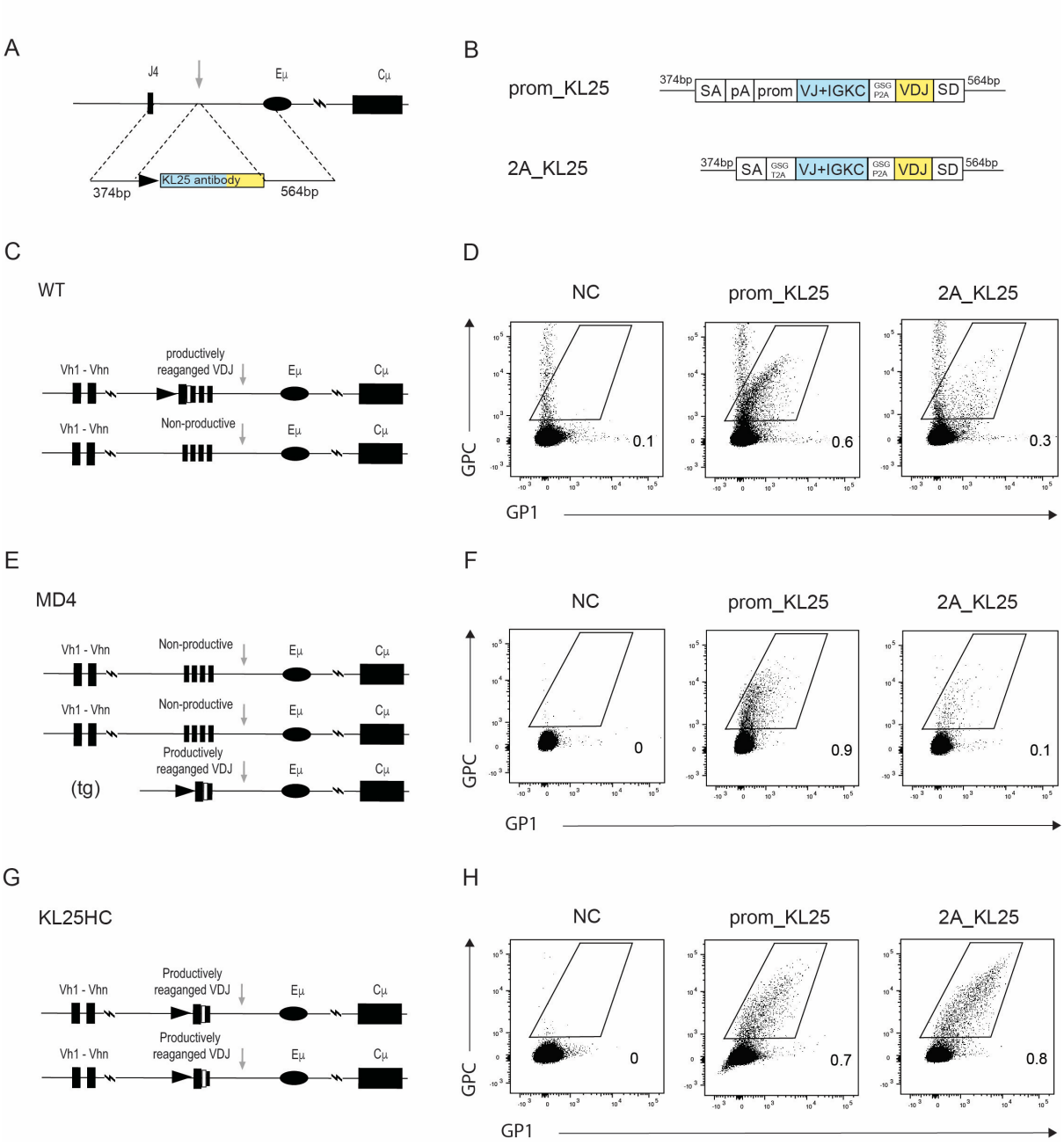

Figure 3. 2: KL25 antibody expression from the IgH locus of CRISPR/Cas9 edited mouse B cells

(A) Schematic representation of the targeting strategy to insert the KL25 antibody expressing cassette into the intronic part of the IgH locus on chromosome 12. (B) Schematic representation of the KL25 antibody dsDNA cassettes, where a splice acceptor site (SA) is followed by either

a SV40 polyadenylation signal (pA), the IGHV4-9 promoter (prom_KL25) or a furin-cleavage site, GSG linker, T2A self-cleaving peptide (2A_KL25) upstream of the leader and variable and joining regions (VJ) and the κ constant region (IGKC) of the KL25 light chain, followed by another furin-cleavage site, (GSG)–linker, and a P2A peptide sequence, the leader, VDJ of the KL25 antibody heavy chain (VDJ), and a short J_H3 donor site (SD). (C) Schematic representation of the IgH loci available for the bi-allelic targeting in C57BL/6J (WT) mice, showing the variable genes (Vh), non-productively or productively rearranged joining elements, the enhancer (Eμ) and a constant region (Cμ). (D) Activated primary B cells from C57BL/6J mice were transfected with Cas9 RNPs, including a crRNA targeting IgH loci as in (C) and either of the dsDNA templates as in (B) or left transfected (NC). 3 days after electroporation, KL25 antibody expression was analyzed by flow cytometry. Gates and numbers in the representative plots from the analysis show the percentage of LCMV GP binding cells, when pre-gated on single, lymphocyte, live $B220^+$ B cells. (E) A schematic of the IgH loci available for the bi-allelic targeting in MD4 mice. (F) Representative FACS plots of MD4 edited B cells in an experiment performed and analyzed analogously to (D) targeting alleles as in (E). (G) Schematic of the IgH loci available for the bi-allelic targeting in KL25HC mice. (H) Representative FACS plots of KL25HC edited B cells in an experiment performed and analyzed analogously to (D) targeting alleles as in (G). (D,F,H) Plots representative of 2 independent experiments

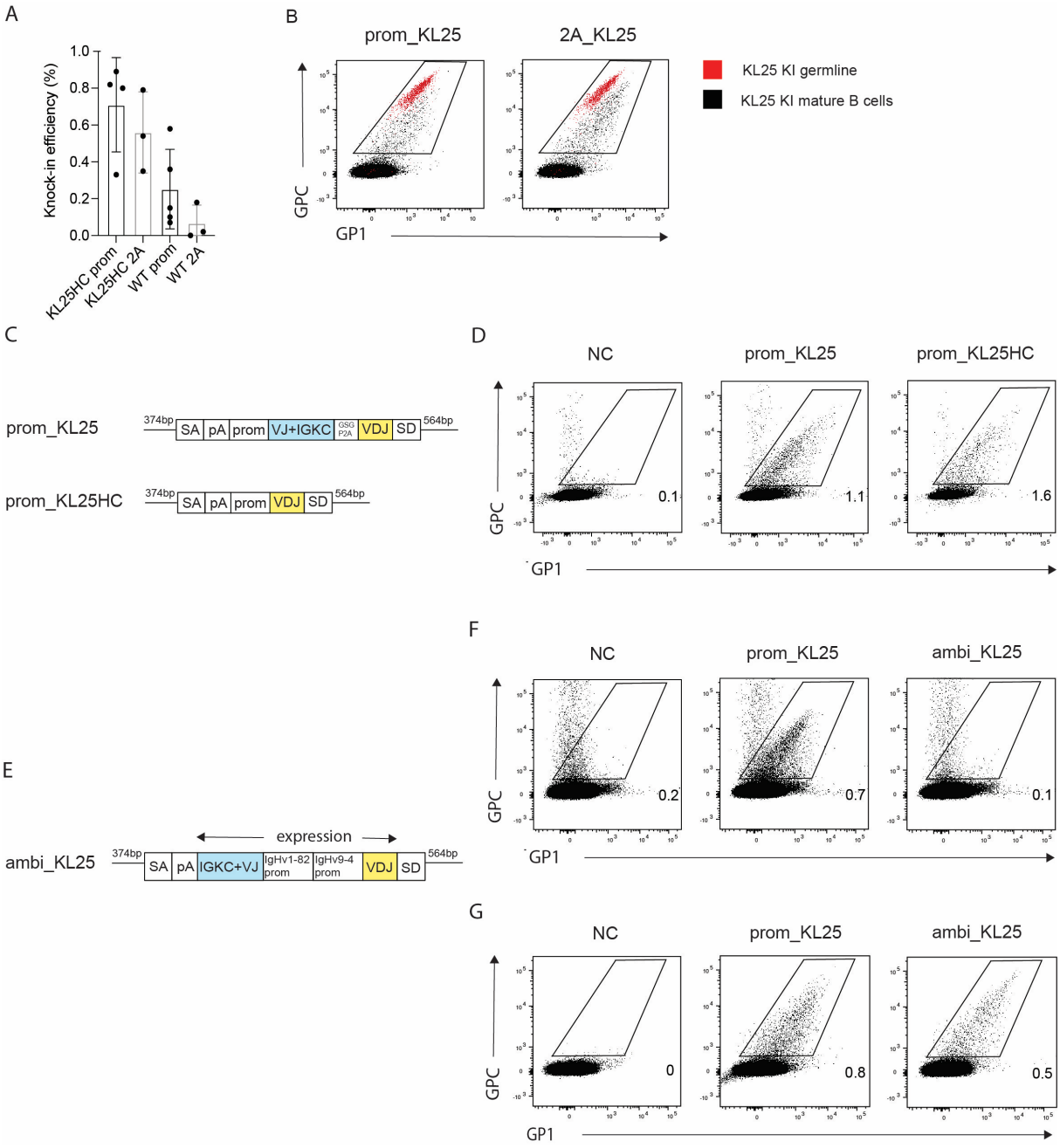

Figure 3. 3: Lower LCMV glycoprotein binding of KL25 engineered B cells is independent of the targeting construct

(A) A graph of recombination efficiencies using the KL25 cassette with a promoter (prom) or the cassette with a T2A linker (2A) (as in Fig. 3.2B) in KL25HC and WT mice. Symbols represent the technical replicates with the mean and SD of 2 independent pooled experiments. (B) Representative FACS plots for LCMV GP binding of primary mature $B220^{+}$ B cells

engineered to express KL25 antibody (black) and B220$^+$ HkiL B cells expressing KL25 from a germline antibody knock-in (red). Gates depict the LCMV GP binding cells. (C) Schematic representation of the KL25 antibody dsDNA cassettes with long homology arms coding for a complete KL25 antibody, including light chain leader, variable and constant region sequence (VJ+IGKC) and a heavy chain variable region (VDJ) joined via furin-cleavage site, GSG linker and a P2A peptide (prom_KL25). The second cassette (prom_KL25 HC) contains the KL25 leader and the heavy chain variable region (VDJ) only. Both cassettes include a splice acceptor site (SA) followed by a SV40 polyadenylation signal (pA), IGHV4-9 promoter on the 5-prime of the antibody sequence and a J_H3 splice donor site (SD) at the 3-prime end. (D) Primary B cells from the WT mice were edited using standard intron targeting strategy and dsDNA templates as in (C) or left transfected (NC). 3 days post transfection, the recombination efficiency was analyzed by flow cytometry. Gates and numbers in the representative plots from the analysis show the percentage of LCMV GP binding cells, when pre-gated on single, lymphocyte, live B220$^+$ B cells. (E) A schematic of the ambi_KL25 cassette where a splice acceptor site (SA) and a SV40 polyadenylation signal (pA) are followed by the reverse κ constant and KL25 variable region, with its leader and a IgHv1-82 promoter. Further IGHV4-9 promoter, the leader and the VDJ of the KL25 antibody heavy chain (VDJ), and short J_H3 donor site (SD) follow the chromosomal directionality. (F) Primary B cells from the WT mice were edited using the standard intron targeting strategy and dsDNA prom_KL25 targeting template as in (A) or the ambi_KL25 template as in (C) 3 days post transfection, recombination efficiency was analyzed by flow cytometry. Gates and numbers in the representative plots from the analysis show the percentage of LCMV GP binding cells, when pre-gated on single, lymphocyte, live B220$^+$ B cells. (G) The experiment was performed and analyzed analogously to (E) using activated KL25HC primary B cells. (C,E,F) Representative plots of 2 independent experiments.

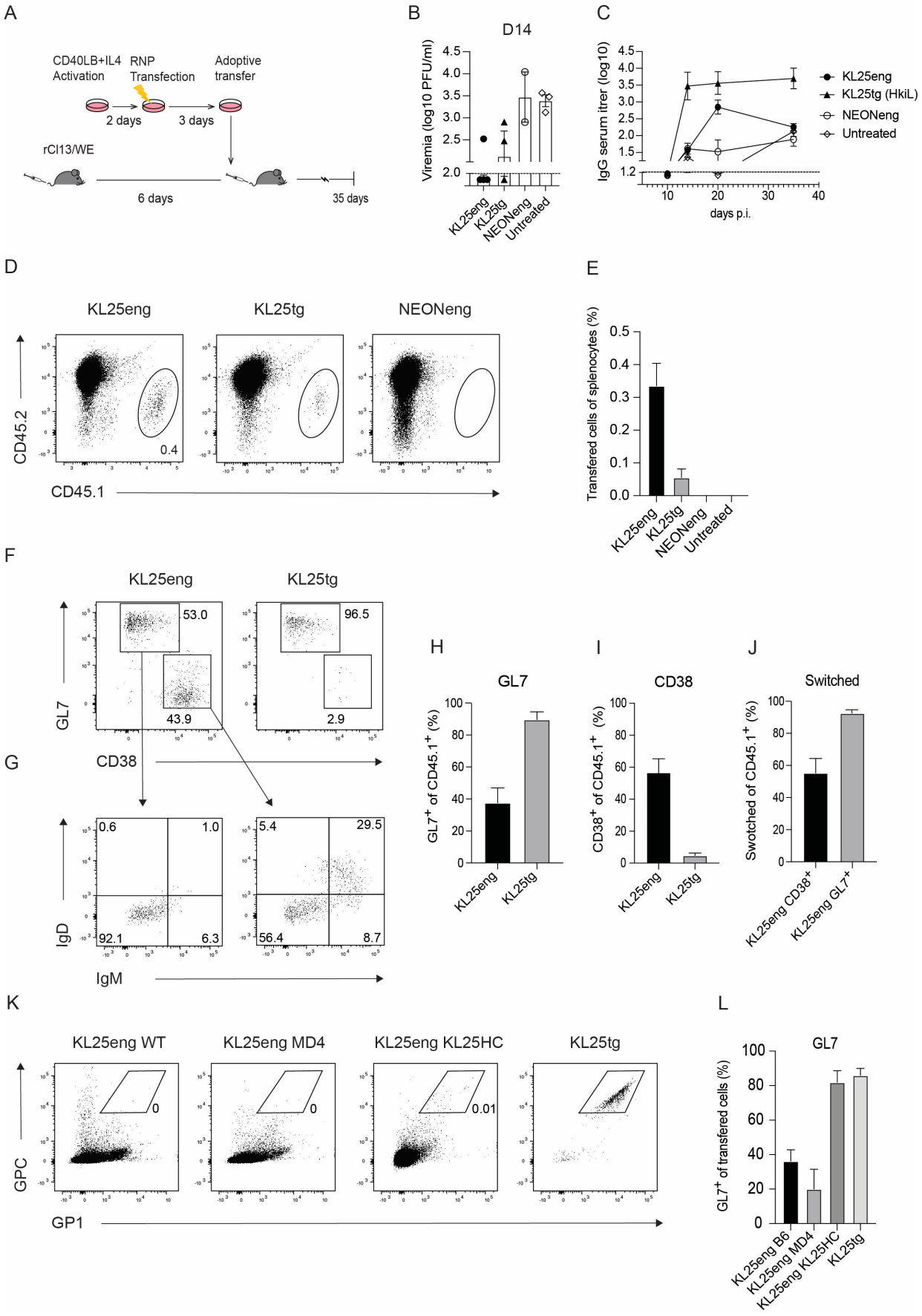
A
CD40LB+IL4 Activation
RNP Transfection
Adoptive transfer
2 days
3 days
rCl13/WE
6 days
35 days
B
D14
Viremia (log10 PFU/ml)
KL25eng
KL25tg
NEONeng
Untreated
C
IgG serum titrer (log10)
days p.i.
KL25eng
KL25tg (HkiL)
NEONeng
Untreated
D
KL25eng
KL25tg
NEONeng
CD45.2
CD45.1
0.4
E
Transfered cells of splenocytes (%)
KL25eng
KL25tg
NEONeng
Untreated
F
KL25eng
KL25tg
GL7
CD38
53.0
43.9
96.5
2.9
G
IgD
IgM
0.6
1.0
92.1
6.3
5.4
29.5
56.4
8.7
H
GL7
GL7+ of CD45.1+ (%)
KL25eng
KL25tg
I
CD38
CD38+ of CD45.1+ (%)
KL25eng
KL25tg
J
Switched
Swotched of CD45.1+ (%)
KL25eng CD38+
KL25eng GL7+
K
KL25eng WT
KL25eng MD4
KL25eng KL25HC
KL25tg
GPC
GP1
0
0
0.01
L
GL7
GL7+ of transfered cells (%)
KL25eng B6
KL25eng MD4
KL25eng KL25HC
KL25tg

Figure 3. 4: KL25 engineered cells cure chronic viral infection and enter germinal centers

(A) Experimental setup for the adoptive transfer of engineered B cells into animals chronically infected with high dose recombinant LCMV virus, strain Clone 13 expressing WE glycoprotein (rCl13/WE). Experimental groups of mouse recipients ($CD45.2^+$) were transferred with either 5000 HkiL B cells (KL25tg HkiL) or 1 million engineered B cells from the WT mice expected to contain 5000 KL25 (KL25eng) or Neon (KL25eng) expressing cells ($CD45.1^+$) 6 days post infection/ 3 days post transfection. Spleens of the experimental animals were analyzed by flow cytometry 35 days post infection. (B) Graph showing viremia as measured by focus forming assay on day 14 post infection. Symbols represent individual animals, bars group means ± SEM. Dotted horizontal line indicates assay`s detection limit. (C) Serum titers of LCMV GP1 binding IgG antibodies as measured by ELISA. Symbols represent means of the experimental groups ± SEM. Dotted horizontal line indicates assay`s detection limit. (D) Representative FACS plots of splenocytes on day 35 post infection for the experimental groups with transferred B cells. Gates and numbers represent percentage of donor $CD45.1^+$ B cells. (E) A graph of the mean percentage ± SEM of recovered adoptively transferred B cells per experimental group on day 35. (F) Flow cytometric analysis of transferred, $CD45.1^+$, cells when gated as in (D). (G) Flow cytometric analysis of transferred, $CD45.1^+$, B cells when gated as in (F). (H) Enumeration of the $GL7^+$, $CD38^-$, $CD45.1^+$ B cells in the spleen, when gated as in (F). (I) Enumeration of the $CD38^+$, $GL7^-$, $CD45.1^+$ B cells in the spleen, when gated as in (G). (J) Enumeration of the switched (IgM^-, IgD^-) $CD45.1^+$ donor B cells in the spleen of the KL25eng transferred animals, when gated as in (F). (H, I, J) The bars represent means ± SEM for given experimental group on day 35 post infection. (B- J) n = 2 (K-L) We transferred KL25eng B cells purified from WT, MD4 and KL25HC mice in parallel with KL25tg (HkiL) B cells into infected animals analogously to (A). (K) Representative FACS plots of relative KL25 expression of the B cells before transfer. Gates indicate KL25-high expressing B cells.

(L) Enumeration of live, $CD45.1^+$, $GL7^+$ B cells among splenocytes. Bars represent means ± SEM for given experimental group on day 35 post infection. Results are representative of one experiment.

A

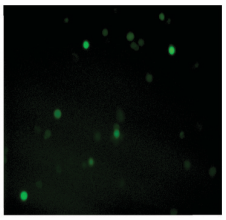

B

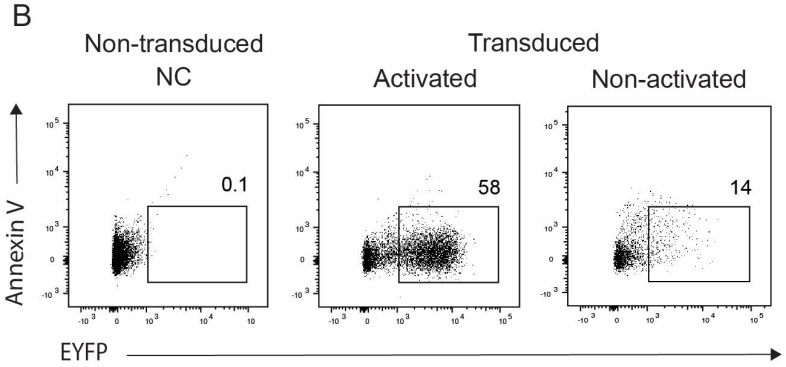

C

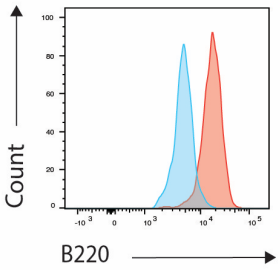

D

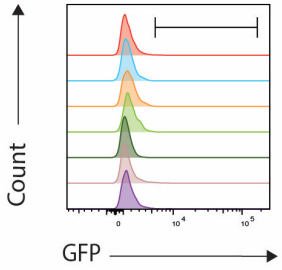

Virus serotype	GFP+ (%)
AAV1	1.19
AAV2	0
AAV5	0
AAV6	0
AAV7	0.15
AAV8	1.88
AAV9	1.09

E

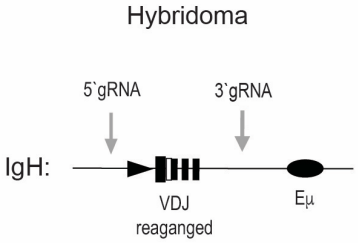

F

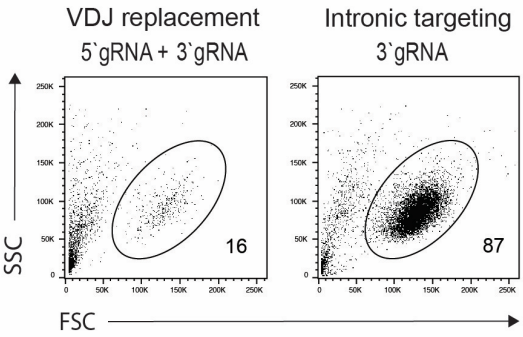

G

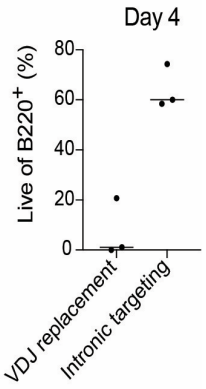

H

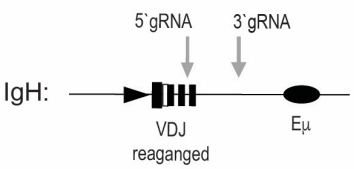

I

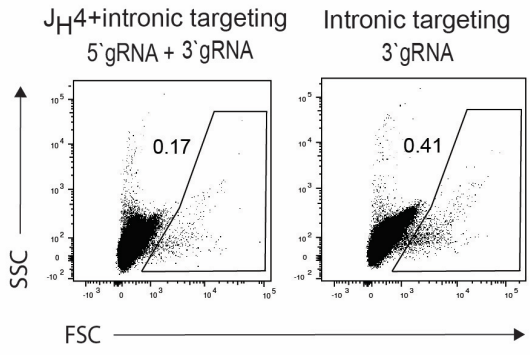

J

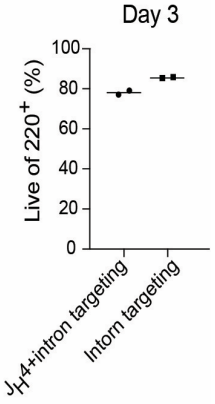

Supplementary figure 3. 1: CRISPR/Cas9 B cell editing optimization using GFP reporter insert

(A) Fluorescent microscopy of B cells in culture 3d post baculoviral transduction (B) FACS analysis of B cells transduced with EYFP-expressing baculoviral vectors 1d post transduction of B cells activated with CD40LB and IL-4, or non-activated B-cells. A spin-transduction protocol was used for non-activated cells. Gates show the percentages of $B220^{+}$, $EYFP^{+}$ cells. (C) B220 expression according to FACS analysis of the baculovirus transduced EYFP-expressing B cells (blue) and control non-transduced B cells in culture (red) (B-C) Plots are representative of three technical replicates (D) FACS analysis of GFP expression for B cells transduced with AAV-GFP vectors. Each color codes one serotype. Numbers represent percentages when gated as in the histogram. (E) Schematic of a targeting strategy for VDJ replacement in the rearranged IgH locus using 5`and 3`gRNAs, or intronic targeting with 3`gRNA. Eμ shows the position if IgH enhancer. (F) FACS analysis of the hybridoma survival when electroporated with a GFP double stranded template (prom_Neon) and Cas9 RNPs navigated with gRNAs for VDJ replacement or intronic targeting as in (E). Gates show the percentages of live cells on 3 days post transfection (G) A graph summarizing the survival of the hybridoma cultures on day 4 after the electroporation. Symbols represent technical replicates and their mean. (H) Schematic of a primary B cells editing strategy to target both, J_H4 and the intron with the 5`and 3`gRNAs or the intron alone with the 3`gRNA. RNP complexes and a dsDNA GFP template (prom_Neon) were electroporated and flow cytometry read-out performed on day 3 (I) FACS analysis showing percentages of prom_Neon cassette recombination as given by GFP expression for the targeting strategies as in (H). Gates represent the GFP^{+} cells pre-gated on single, live, $B220^{+}$ cells. (J) Survival of the B cells 3 days after electroporation when employing the targeting strategies as in (H). Symbols represent the technical replicates with their means.

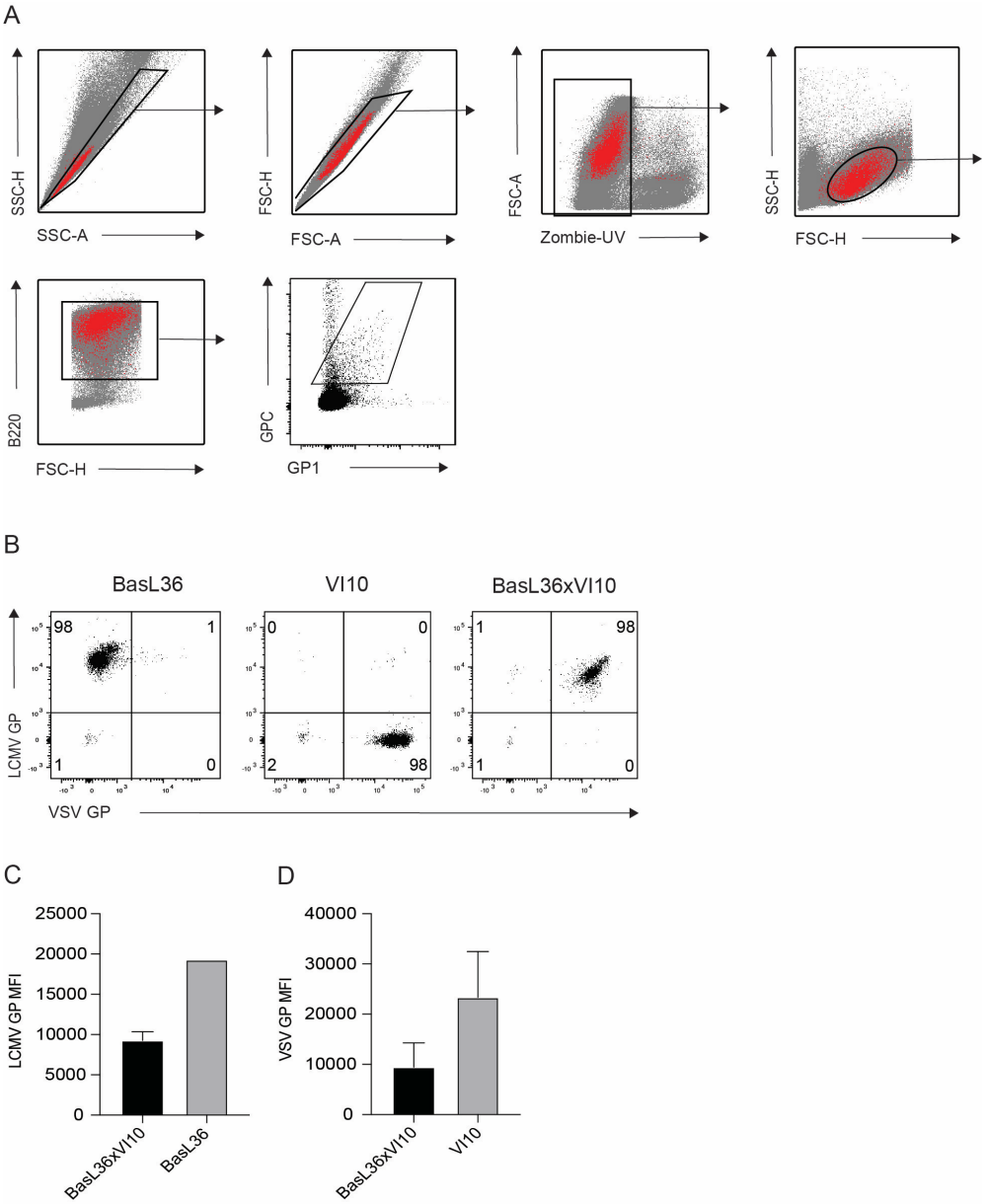

Supplementary figure 3. 2: KL25 antibody expression from the IgH locus of CRISPR/Cas9 edited mouse B cells

(A) A gating strategy for the flow cytometric analyses of LCMV GP blinding of KL25-engineered cells in this manuscript. (B) Representative FACS plots of KL25 antibody and VI10 antibody expressing B cells, originating form BasL36 and VI10 mice respectively and their intercross (BasL36xVI10) (C) Antigen, LCMV GP, binding MFI of $B220^{+}$ splenocytes (D) Antigen, VSV GP, binding MFI of $B220^{+}$ splenocytes (C-D) Bars represent mean ± SD. n=4

Acknowledgements

We wish to thank Lukas Jeker at the university of Basel and Justin Taylor at the Fred Hutchinson Cancer Research canter for helpful discussions and plasmid material. We also thank Sai T. Reddy at the ETH Zurich for the initial brain storming and his team, namely Cristina Parola for providing us with PnP-Ruby hybridoma and CD40LB cell line. We thank Thomas A. Bowden and Quido Paesen at the Oxford university for providing LCMV GP recombinant protein, essential for the flow cytometric staining. We also thank Philipp Berger and Maysam Mansouri at the Paul Scherrer institute for sharing their knowledge about Baculovirus production and viruses for the experiments. We also thank Karsten Stauffer for his support in animal experimentation.

Author contributions

MF and DDP designed the experiments. MF performed the experiments. MF and DDP analyzed the data. MF wrote the manuscript, DDP revised the content.

II. General discussion

Role of B cell affinity and adaptation in protecting against chronic LCMV infection

In our manuscripts, we show that somatic hypermutation of antibodies is essential for high-affinity binding of the viral glycoprotein. We and others also demonstrate that upon adoptive transfer, physiologically rare virus-specific cells are sustained and compete for antigen presentation in the germinal center, given they possess a high or intermediate affinity for the viral antigen [284, 300]. The above is also true for the KL25 BCR engineered B cells. The KL25 B cells in the chronic infection setting can adapt to a lower affinity virus escape variant, highlighting the main potential therapeutic advantage of the engineered B cells over passive monoclonal antibody administration.

Antibodies of KL25 unmutated antibody light chain coupled to KL25 HC, found in the rare repertoire of the GP1-binding cells within TgH mice, as well as completely germline reverted KL25, Wen 1, and Wen 3 antibodies have a marginal affinity for the LCMV glycoprotein. They are unable to protect against viral challenge. However, the KL25 neutralizing antibody is a result of affinity maturation during viral immunization challenge and is, therefore, a manifestation of the possibility to elicit high-affinity, strongly neutralizing antibody within the tolerance spectrum upon immunization, from a rare, low-affinity B cell repertoire.

The potential of the LCMV infection model in studies on B cell tolerance mechanisms

The concept of molecular mimicry between virus and host may have far-reaching consequences for the development of autoimmune diseases, if proven as suggested by the clinical, epidemiological, and experimental evidence from multiple infections [301]. The correlation between multiple sclerosis and EBV [302], postinfectious Guillain-Barre syndrome caused by influenza [303], HSV [304], EBV [305] as well as chronic infections of HIV, and HCV with

rheumatoid arthritis [306], calls for more experimental investigations of pathogen-induced autoimmune reaction. Using the HkiL mouse model, we have demonstrated the connection between the viral specificity and immune tolerance modulation in an infectious physiological context. Presumably, our infectious setting can be used to study immune dysregulation and self-tolerance loss during chronic viral infection. The treatment with immune checkpoint inhibitors in humans, monkeys, and mice enhances not only T cell mediated immune response, but also B cell mediated immunity and neutralizing antibody output, leading to a decreased viral load [307, 308], indicating a host benefit of tolerance breakdown for the immune response in chronic viral infection. However, as shown in the chronic LCMV infection, the success of the treatment with checkpoint inhibitors is dependent on the time of administration and can lead to a lethal immunopathology [309, 310]. In light of our findings, the mechanisms of tolerance breakdown and its effect on antibody formation can be investigated in the context of a monoclonal specificity. Assuming there is a self-antigen with which KL25 B cells interact, and it could be identified, dual virus and self- binding nature of these cells could favor new insights into how autoantibodies are formed in viral infection.

Viral host-mimicry as a caveat for an efficient B cell response in chronic viral infection

The delayed neutralizing antibody formation, completely absent at the onset of chronic viral infection and hardly inducible by vaccination, can be explained by the virus-host co-evolution and based on the hypothesis of molecular mimicry, where pathogen antigenic determinants resemble that of a host [311, 312]. The consequences are the decreased immunogenicity of the viral antigen and a very limited starting B cell precursor repertoire available for neutralizing antibody formation [270, 271]. In the model of LCMV, the glycan-shield decreases the immunogenicity of the viral glycoprotein and is deterministic for the KL25 antibody affinity [44]. Similarly, in HIV, the B12 antibody binds the N-glycosylated V-3 loop of glycoprotein

120 [313], and glycan-binding antibodies are correlated with the long-term non-progression of the viral disease [314]. Is there a link between the epitope glycan shield and the tolerant B cell state? Important implications for delayed neutralizing antibody formation can be drawn from a lower on-rate engagement with glycosylated epitopes [41, 44]. Can this be modified by differential BCR signaling or a B cell isotype? Is glycan host-mimicry, as implied by the LCMV model, the only kind that can lead to the formation of a potently neutralizing, mildly self-reactive B cell response? New infectious models with recombinant viruses with glycan-deficient glycoproteins [44] and adoptive transfers of either HkiL or KL25-engineered would be necessary for the answers.

Concluding remarks

B cell mediated viral clearance depends on the formation of neutralizing antibodies. It has been shown that neutralizing antibodies alone are sufficient for viral clearance, both in the macaque model of simian immunodeficiency virus [315] and mouse models of hepatitis C [316] and lymphocytic choriomeningitis virus [32], however, their delayed formation precludes viral control.

In our studies we demonstrated how neutralization capacity in LCMV chronic infection is achieved through an efficient process of affinity maturation in the germinal centers. (Manuscript 1) However, limited starting B cell repertoire and employment of the immune tolerance mechanisms contribute to, if not cause, a delayed neutralizing antibody formation (Manuscript 2). This can be potentially therapeutically circumvented by the infusion of engineered B cells with high affinity, neutralizing BCRs. (Manuscript 3).

III. References

1. Ciurea, A., et al., *CD4+ T-cell-epitope escape mutant virus selected in vivo.* Nat Med, 2001. **7**(7): p. 795-800.
2. Richman, D.D., et al., *Rapid evolution of the neutralizing antibody response to HIV type 1 infection.* Proc Natl Acad Sci U S A, 2003. **100**(7): p. 4144-9.
3. Borrow, P., et al., *Antiviral pressure exerted by HIV-1-specific cytotoxic T lymphocytes (CTLs) during primary infection demonstrated by rapid selection of CTL escape virus.* Nat Med, 1997. **3**(2): p. 205-11.
4. Wiertz, E.J.H.J., S. Mukherjee, and H.L. Ploegh, *Viruses use stealth technology to escape from the host immune system.* Molecular Medicine Today, 1997. **3**(3): p. 116-123.
5. Garber, D.A., P.A. Schaffer, and D.M. Knipe, *A LAT-associated function reduces productive-cycle gene expression during acute infection of murine sensory neurons with herpes simplex virus type 1.* Journal of Virology, 1997. **71**(8): p. 5885-5893.
6. Zack, J.A., et al., *HIV-1 entry into quiescent primary lymphocytes: molecular analysis reveals a labile, latent viral structure.* Cell, 1990. **61**(2): p. 213-22.
7. Weiss, R., et al., *Interleukin-24 inhibits influenza A virus replication in vitro through induction of toll-like receptor 3 dependent apoptosis.* Antiviral Res, 2015. **123**: p. 93-104.
8. Strumillo, S.T., et al., *HIV-1 infection modulates IL-24 expression which contributes to cell apoptosis in vitro.* Cell Biol Int, 2019. **43**(5): p. 574-579.
9. Bertin, J., et al., *Death effector domain-containing herpesvirus and poxvirus proteins inhibit both Fas- and TNFR1-induced apoptosis.* Proc Natl Acad Sci U S A, 1997. **94**(4): p. 1172-6.
10. Bukrinsky, M.I., et al., *Quiescent T lymphocytes as an inducible virus reservoir in HIV-1 infection.* Science, 1991. **254**(5030): p. 423-7.
11. Borza, C.M. and L.M. Hutt-Fletcher, *Alternate replication in B cells and epithelial cells switches tropism of Epstein-Barr virus.* Nat Med, 2002. **8**(6): p. 594-9.
12. Fadda, L., et al., *HLA-Cw*0102-restricted HIV-1 p24 epitope variants can modulate the binding of the inhibitory KIR2DL2 receptor and primary NK cell function.* PLoS Pathog, 2012. **8**(7): p. e1002805.
13. Burgert, H.G. and S. Kvist, *An adenovirus type 2 glycoprotein blocks cell surface expression of human histocompatibility class I antigens.* Cell, 1985. **41**(3): p. 987-97.
14. Zhang, M., et al., *Identification of a potential HIV-induced source of bystander-mediated apoptosis in T cells: upregulation of trail in primary human macrophages by HIV-1 tat.* J Biomed Sci, 2001. **8**(3): p. 290-6.
15. Wiertz, E.J., et al., *The human cytomegalovirus US11 gene product dislocates MHC class I heavy chains from the endoplasmic reticulum to the cytosol.* Cell, 1996. **84**(5): p. 769-79.
16. Kostavasili, I., et al., *Mechanism of complement inactivation by glycoprotein C of herpes simplex virus.* J Immunol, 1997. **158**(4): p. 1763-71.
17. Munson, L.G., et al., *Decreased levels of complement receptor 1 (CD35) on B lymphocytes in persons with HIV infection.* Clin Immunol Immunopathol, 1995. **75**(1): p. 20-5.
18. Loisel-Meyer, S., et al., *Glut1-mediated glucose transport regulates HIV infection.* Proc Natl Acad Sci U S A, 2012. **109**(7): p. 2549-54.

19. Spencer, J.V., et al., *Potent immunosuppressive activities of cytomegalovirus-encoded interleukin-10.* J Virol, 2002. **76**(3): p. 1285-92.
20. Habjan, M., et al., *Processing of genome 5' termini as a strategy of negative-strand RNA viruses to avoid RIG-I-dependent interferon induction.* PLoS One, 2008. **3**(4): p. e2032.
21. Virgin, H.W., E.J. Wherry, and R. Ahmed, *Redefining chronic viral infection.* Cell, 2009. **138**(1): p. 30-50.
22. Moskophidis, D., et al., *Role of virus and host variables in virus persistence or immunopathological disease caused by a non-cytolytic virus.* J Gen Virol, 1995. **76 (Pt 2)**: p. 381-91.
23. Bergthaler, A., et al., *Viral replicative capacity is the primary determinant of lymphocytic choriomeningitis virus persistence and immunosuppression.* Proc Natl Acad Sci U S A, 2010. **107**(50): p. 21641-6.
24. Wherry, E.J., et al., *Viral persistence alters CD8 T-cell immunodominance and tissue distribution and results in distinct stages of functional impairment.* J Virol, 2003. **77**(8): p. 4911-27.
25. Moskophidis, D., et al., *Virus persistence in acutely infected immunocompetent mice by exhaustion of antiviral cytotoxic effector T cells.* Nature, 1993. **362**(6422): p. 758-61.
26. Zajac, A.J., et al., *Viral immune evasion due to persistence of activated T cells without effector function.* J Exp Med, 1998. **188**(12): p. 2205-13.
27. Bergthaler, A., et al., *Impaired antibody response causes persistence of prototypic T cell-contained virus.* PLoS Biol, 2009. **7**(4): p. e1000080.
28. Hangartner, L., et al., *Nonneutralizing antibodies binding to the surface glycoprotein of lymphocytic choriomeningitis virus reduce early virus spread.* J Exp Med, 2006. **203**(8): p. 2033-42.
29. Seiler, P., et al., *Enhanced virus clearance by early inducible lymphocytic choriomeningitis virus-neutralizing antibodies in immunoglobulin-transgenic mice.* J Virol, 1998. **72**(3): p. 2253-8.
30. Fallet, B., et al., *Interferon-driven deletion of antiviral B cells at the onset of chronic infection.* Sci Immunol, 2016. **1**(4).
31. Bruns, M., et al., *Lymphocytic choriomeningitis virus. VI. Isolation of a glycoprotein mediating neutralization.* Virology, 1983. **130**(1): p. 247-251.
32. Seiler, P., et al., *Induction of protective cytotoxic T cell responses in the presence of high titers of virus-neutralizing antibodies: implications for passive and active immunization.* J Exp Med, 1998. **187**(4): p. 649-54.
33. Eschli, B., et al., *Early antibodies specific for the neutralizing epitope on the receptor binding subunit of the lymphocytic choriomeningitis virus glycoprotein fail to neutralize the virus.* J Virol, 2007. **81**(21): p. 11650-7.
34. Pinschewer, D.D., et al., *Kinetics of protective antibodies are determined by the viral surface antigen.* J Clin Invest, 2004. **114**(7): p. 988-93.
35. Battegay, M., et al., *Impairment and delay of neutralizing antiviral antibody responses by virus-specific cytotoxic T cells.* J Immunol, 1993. **151**(10): p. 5408-15.
36. Gray, E.S., et al., *Neutralizing antibody responses in acute human immunodeficiency virus type 1 subtype C infection.* J Virol, 2007. **81**(12): p. 6187-96.
37. Bar, K.J., et al., *Early low-titer neutralizing antibodies impede HIV-1 replication and select for virus escape.* PLoS Pathog, 2012. **8**(5): p. e1002721.
38. Plotkin, S.A., *Complex correlates of protection after vaccination.* Clin Infect Dis, 2013. **56**(10): p. 1458-65.

39. Stefanati, A., et al., *Long-term persistency of hepatitis B immunity: an observational cross-sectional study on medical students and resident doctors.* J Prev Med Hyg, 2019. **60**(3): p. E184-e190.
40. Ciurea, A., et al., *Viral persistence in vivo through selection of neutralizing antibody-escape variants.* Proc Natl Acad Sci U S A, 2000. **97**(6): p. 2749-54.
41. Wei, X., et al., *Antibody neutralization and escape by HIV-1.* Nature, 2003. **422**(6929): p. 307-12.
42. Kwong, P.D., et al., *HIV-1 evades antibody-mediated neutralization through conformational masking of receptor-binding sites.* Nature, 2002. **420**(6916): p. 678-82.
43. Frey, G., et al., *A fusion-intermediate state of HIV-1 gp41 targeted by broadly neutralizing antibodies.* Proc Natl Acad Sci U S A, 2008. **105**(10): p. 3739-44.
44. Sommerstein, R., et al., *Arenavirus Glycan Shield Promotes Neutralizing Antibody Evasion and Protracted Infection.* PLoS Pathog, 2015. **11**(11): p. e1005276.
45. Hastie, K.M., et al., *Structural basis for antibody-mediated neutralization of Lassa virus.* Science, 2017. **356**(6341): p. 923-928.
46. Pape, K.A., et al., *The humoral immune response is initiated in lymph nodes by B cells that acquire soluble antigen directly in the follicles.* Immunity, 2007. **26**(4): p. 491-502.
47. Carrasco, Y.R. and F.D. Batista, *B cells acquire particulate antigen in a macrophage-rich area at the boundary between the follicle and the subcapsular sinus of the lymph node.* Immunity, 2007. **27**(1): p. 160-71.
48. Jaiswal, A.I. and M. Croft, *CD40 ligand induction on T cell subsets by peptide-presenting B cells: implications for development of the primary T and B cell response.* J Immunol, 1997. **159**(5): p. 2282-91.
49. Song, W. and J. Craft, *T follicular helper cell heterogeneity: Time, space, and function.* Immunol Rev, 2019. **288**(1): p. 85-96.
50. Garside, P., et al., *Visualization of specific B and T lymphocyte interactions in the lymph node.* Science, 1998. **281**(5373): p. 96-9.
51. Okada, T., et al., *Antigen-engaged B cells undergo chemotaxis toward the T zone and form motile conjugates with helper T cells.* PLoS Biol, 2005. **3**(6): p. e150.
52. Tas, J.M., et al., *Visualizing antibody affinity maturation in germinal centers.* Science, 2016. **351**(6277): p. 1048-54.
53. Lingwood, D., et al., *Structural and genetic basis for development of broadly neutralizing influenza antibodies.* Nature, 2012. **489**(7417): p. 566-70.
54. Chen, X., et al., *Vaccination induces maturation in a mouse model of diverse unmutated VRC01-class precursors to HIV-neutralizing antibodies with >50% breadth.* Immunity, 2021. **54**(2): p. 324-339.e8.
55. Eisen, H.N., *Affinity enhancement of antibodies: how low-affinity antibodies produced early in immune responses are followed by high-affinity antibodies later and in memory B-cell responses.* Cancer Immunol Res, 2014. **2**(5): p. 381-92.
56. Abbott, R.K., et al., *Precursor Frequency and Affinity Determine B Cell Competitive Fitness in Germinal Centers, Tested with Germline-Targeting HIV Vaccine Immunogens.* Immunity, 2018. **48**(1): p. 133-146 e6.
57. Berek, C. and C. Milstein, *Mutation drift and repertoire shift in the maturation of the immune response.* Immunol Rev, 1987. **96**: p. 23-41.
58. Muramatsu, M., et al., *Pillars Article: Class Switch Recombination and Hypermutation Require Activation-Induced Cytidine Deaminase (AID), a Potential RNA Editing Enzyme. Cell. 2000. 102: 553-563.* J Immunol, 2018. **201**(9): p. 2530-2540.

59. Viant, C., et al., *Antibody Affinity Shapes the Choice between Memory and Germinal Center B Cell Fates.* Cell, 2020. **183**(5): p. 1298-1311 e11.
60. Shlomchik, M.J., et al., *The role of clonal selection and somatic mutation in autoimmunity.* Nature, 1987. **328**(6133): p. 805-11.
61. Tiller, T., et al., *Autoreactivity in human IgG+ memory B cells.* Immunity, 2007. **26**(2): p. 205-13.
62. Chan, T.D., et al., *Elimination of germinal-center-derived self-reactive B cells is governed by the location and concentration of self-antigen.* Immunity, 2012. **37**(5): p. 893-904.
63. Koncz, G. and A.O. Hueber, *The Fas/CD95 Receptor Regulates the Death of Autoreactive B Cells and the Selection of Antigen-Specific B Cells.* Front Immunol, 2012. **3**: p. 207.
64. Butt, D., et al., *FAS Inactivation Releases Unconventional Germinal Center B Cells that Escape Antigen Control and Drive IgE and Autoantibody Production.* Immunity, 2015. **42**(5): p. 890-902.
65. Burnett, D.L., et al., *Germinal center antibody mutation trajectories are determined by rapid self/foreign discrimination.* Science, 2018. **360**(6385): p. 223-226.
66. Reed, J.H., et al., *Clonal redemption of autoantibodies by somatic hypermutation away from self-reactivity during human immunization.* J Exp Med, 2016. **213**(7): p. 1255-65.
67. Mouquet, H., et al., *Polyreactivity increases the apparent affinity of anti-HIV antibodies by heteroligation.* Nature, 2010. **467**(7315): p. 591-5.
68. Pieper, K., et al., *Public antibodies to malaria antigens generated by two LAIR1 insertion modalities.* Nature, 2017. **548**(7669): p. 597-601.
69. Liu, M., et al., *Polyreactivity and autoreactivity among HIV-1 antibodies.* J Virol, 2015. **89**(1): p. 784-98.
70. Haynes, B.F., et al., *Cardiolipin polyspecific autoreactivity in two broadly neutralizing HIV-1 antibodies.* Science, 2005. **308**(5730): p. 1906-8.
71. Khurana, S., et al., *Autoreactivity of Broadly Neutralizing Influenza Human Antibodies to Human Tissues and Human Proteins.* Viruses, 2020. **12**(10).
72. Yang, G., et al., *Identification of autoantigens recognized by the 2F5 and 4E10 broadly neutralizing HIV-1 antibodies.* J Exp Med, 2013. **210**(2): p. 241-56.
73. Gitlin, A.D., et al., *Independent Roles of Switching and Hypermutation in the Development and Persistence of B Lymphocyte Memory.* Immunity, 2016. **44**(4): p. 769-81.
74. Erazo, A., et al., *Unique maturation program of the IgE response in vivo.* Immunity, 2007. **26**(2): p. 191-203.
75. Duchez, S., et al., *Premature replacement of mu with alpha immunoglobulin chains impairs lymphopoiesis and mucosal homing but promotes plasma cell maturation.* Proc Natl Acad Sci U S A, 2010. **107**(7): p. 3064-9.
76. Weisel, F.J., et al., *A Temporal Switch in the Germinal Center Determines Differential Output of Memory B and Plasma Cells.* Immunity, 2016. **44**(1): p. 116-130.
77. Halliley, J.L., et al., *Long-Lived Plasma Cells Are Contained within the CD19(-)CD38(hi)CD138(+) Subset in Human Bone Marrow.* Immunity, 2015. **43**(1): p. 132-45.
78. Tangye, S.G., D.T. Avery, and P.D. Hodgkin, *A division-linked mechanism for the rapid generation of Ig-secreting cells from human memory B cells.* J Immunol, 2003. **170**(1): p. 261-9.

79. Bernasconi, N.L., E. Traggiai, and A. Lanzavecchia, *Maintenance of serological memory by polyclonal activation of human memory B cells.* Science, 2002. **298**(5601): p. 2199-202.
80. Taylor, J.J., K.A. Pape, and M.K. Jenkins, *A germinal center-independent pathway generates unswitched memory B cells early in the primary response.* J Exp Med, 2012. **209**(3): p. 597-606.
81. Bohannon, C., et al., *Long-lived antigen-induced IgM plasma cells demonstrate somatic mutations and contribute to long-term protection.* Nat Commun, 2016. **7**: p. 11826.
82. Mesin, L., et al., *Restricted Clonality and Limited Germinal Center Reentry Characterize Memory B Cell Reactivation by Boosting.* Cell, 2020. **180**(1): p. 92-106.e11.
83. Seifert, M., et al., *Functional capacities of human IgM memory B cells in early inflammatory responses and secondary germinal center reactions.* Proc Natl Acad Sci U S A, 2015. **112**(6): p. E546-55.
84. Jardine, J.G., et al., *HIV-1 broadly neutralizing antibody precursor B cells revealed by germline-targeting immunogen.* Science, 2016. **351**(6280): p. 1458-63.
85. Havenar-Daughton, C., et al., *The human naive B cell repertoire contains distinct subclasses for a germline-targeting HIV-1 vaccine immunogen.* Science translational medicine, 2018. **10**(448): p. eaat0381.
86. Kuraoka, M., et al., *Complex Antigens Drive Permissive Clonal Selection in Germinal Centers.* Immunity, 2016. **44**(3): p. 542-552.
87. Angeletti, D., et al., *Defining B cell immunodominance to viruses.* Nat Immunol, 2017. **18**(4): p. 456-463.
88. Abbott, R.K., et al., *Precursor Frequency and Affinity Determine B Cell Competitive Fitness in Germinal Centers, Tested with Germline-Targeting HIV Vaccine Immunogens.* Immunity, 2018. **48**(1): p. 133-146.e6.
89. Havenar-Daughton, C., J.H. Lee, and S. Crotty, *Tfh cells and HIV bnAbs, an immunodominance model of the HIV neutralizing antibody generation problem.* Immunol Rev, 2017. **275**(1): p. 49-61.
90. Angeletti, D. and J.W. Yewdell, *Is It Possible to Develop a "Universal" Influenza Virus Vaccine? Outflanking Antibody Immunodominance on the Road to Universal Influenza Vaccination.* Cold Spring Harb Perspect Biol, 2018. **10**(7).
91. Tonegawa, S., *Somatic generation of antibody diversity.* Nature, 1983. **302**(5909): p. 575-81.
92. Pieper, K., B. Grimbacher, and H. Eibel, *B-cell biology and development.* J Allergy Clin Immunol, 2013. **131**(4): p. 959-71.
93. Lieber, M.R., *The Mechanism of Double-Strand DNA Break Repair by the Nonhomologous DNA End-Joining Pathway.* Annual Review of Biochemistry, 2010. **79**(1): p. 181-211.
94. Yu, L. and Y. Guan, *Immunologic Basis for Long HCDR3s in Broadly Neutralizing Antibodies Against HIV-1.* Front Immunol, 2014. **5**: p. 250.
95. Pinto, D., et al., *Structural Basis for Broad HIV-1 Neutralization by the MPER-Specific Human Broadly Neutralizing Antibody LN01.* Cell Host Microbe, 2019. **26**(5): p. 623-637.e8.
96. Nemazee, D., *Mechanisms of central tolerance for B cells.* Nat Rev Immunol, 2017. **17**(5): p. 281-294.
97. Noviski, M., et al., *IgM and IgD B cell receptors differentially respond to endogenous antigens and control B cell fate.* Elife, 2018. **7**.

98. Nemazee, D.A. and K. Bürki, *Clonal deletion of B lymphocytes in a transgenic mouse bearing anti-MHC class I antibody genes.* Nature, 1989. **337**(6207): p. 562-6.
99. Gay, D., et al., *Receptor editing: an approach by autoreactive B cells to escape tolerance.* J Exp Med, 1993. **177**(4): p. 999-1008.
100. Tiegs, S.L., D.M. Russell, and D. Nemazee, *Receptor editing in self-reactive bone marrow B cells.* J Exp Med, 1993. **177**(4): p. 1009-20.
101. *<334676a0(1).pdf>*.
102. Pillai, S., H. Mattoo, and A. Cariappa, *B cells and autoimmunity.* Curr Opin Immunol, 2011. **23**(6): p. 721-31.
103. Brady, J.M., D. Baltimore, and A.B. Balazs, *Antibody gene transfer with adeno-associated viral vectors as a method for HIV prevention.* Immunol Rev, 2017. **275**(1): p. 324-333.
104. Halverson, R., R.M. Torres, and R. Pelanda, *Receptor editing is the main mechanism of B cell tolerance toward membrane antigens.* Nat Immunol, 2004. **5**(6): p. 645-50.
105. Goodnow, C.C., et al., *Altered immunoglobulin expression and functional silencing of self-reactive B lymphocytes in transgenic mice.* Nature, 1988. **334**(6184): p. 676-82.
106. Goodnow, C.C., et al., *Clonal silencing of self-reactive B lymphocytes in a transgenic mouse model.* Cold Spring Harb Symp Quant Biol, 1989. **54 Pt 2**: p. 907-20.
107. Brombacher, F., G. Köhler, and H. Eibel, *B cell tolerance in mice transgenic for anti-CD8 immunoglobulin mu chain.* J Exp Med, 1991. **174**(6): p. 1335-46.
108. Schroeder, K.M., A. Agazio, and R.M. Torres, *Immunological tolerance as a barrier to protective HIV humoral immunity.* Curr Opin Immunol, 2017. **47**: p. 26-34.
109. Zikherman, J., R. Parameswaran, and A. Weiss, *Endogenous antigen tunes the responsiveness of naive B cells but not T cells.* Nature, 2012. **489**(7414): p. 160-4.
110. Steach, H.R., et al., *Cross-Reactivity with Self-Antigen Tunes the Functional Potential of Naive B Cells Specific for Foreign Antigens.* J Immunol, 2020. **204**(3): p. 498-509.
111. Walker, L.M. and D.R. Burton, *Passive immunotherapy of viral infections: 'super-antibodies' enter the fray.* Nat Rev Immunol, 2018. **18**(5): p. 297-308.
112. Misasi, J. and N.J. Sullivan, *Immunotherapeutic strategies to target vulnerabilities in the Ebolavirus glycoprotein.* Immunity, 2021. **54**(3): p. 412-436.
113. Ali, M.G., et al., *Recent advances in therapeutic applications of neutralizing antibodies for virus infections: an overview.* Immunol Res, 2020. **68**(6): p. 325-339.
114. Casadevall, A., L.A. Pirofski, and M.J. Joyner, *The Principles of Antibody Therapy for Infectious Diseases with Relevance for COVID-19.* mBio, 2021. **12**(2).
115. Bonsignori, M., et al., *Analysis of a Clonal Lineage of HIV-1 Envelope V2/V3 Conformational Epitope-Specific Broadly Neutralizing Antibodies and Their Inferred Unmutated Common Ancestors.* Journal of Virology, 2011. **85**(19): p. 9998-10009.
116. Bonsignori, M., et al., *Inference of the HIV-1 VRC01 Antibody Lineage Unmutated Common Ancestor Reveals Alternative Pathways to Overcome a Key Glycan Barrier.* Immunity, 2018. **49**(6): p. 1162-1174.e8.
117. Alam, S.M., et al., *Recognition of synthetic glycopeptides by HIV-1 broadly neutralizing antibodies and their unmutated ancestors.* Proceedings of the National Academy of Sciences, 2013. **110**(45): p. 18214-18219.
118. Coutelier, J.P., et al., *IgG2a restriction of murine antibodies elicited by viral infections.* J Exp Med, 1987. **165**(1): p. 64-9.
119. Vidarsson, G., G. Dekkers, and T. Rispens, *IgG subclasses and allotypes: from structure to effector functions.* Front Immunol, 2014. **5**: p. 520.
120. Jaenisch, R. and B. Mintz, *Simian virus 40 DNA sequences in DNA of healthy adult mice derived from preimplantation blastocysts injected with viral DNA.* Proceedings

of the National Academy of Sciences of the United States of America, 1974. **71**(4): p. 1250-1254.
121. Pelanda, R., et al., *A prematurely expressed Ig?? transgene, but not a V??J?? gene segment targeted into the Ig?? locus, can rescue B cell development in ??5-deficient mice.* Immunity, 1996.
122. Sonoda, E., et al., *B cell development under the condition of allelic inclusion.* Immunity, 1997. **6**(3): p. 225-33.
123. Hartley, S.B., et al., *Elimination from peripheral lymphoid tissues of self-reactive B lymphocytes recognizing membrane-bound antigens.* Nature, 1991. **353**(6346): p. 765-9.
124. Erikson, J., et al., *Expression of anti-DNA immunoglobulin transgenes in non-autoimmune mice.* Nature, 1991. **349**(6307): p. 331-4.
125. Okamoto, M., et al., *A transgenic model of autoimmune hemolytic anemia.* J Exp Med, 1992. **175**(1): p. 71-9.
126. Chen, C., et al., *Immunoglobulin heavy chain gene replacement: a mechanism of receptor editing.* Immunity, 1995. **3**(6): p. 747-55.
127. Goodnow, C.C., et al., *Induction of self-tolerance in mature peripheral B lymphocytes.* Nature, 1989. **342**(6248): p. 385-91.
128. Cyster, J.G., S.B. Hartley, and C.C. Goodnow, *Competition for follicular niches excludes self-reactive cells from the recirculating B-cell repertoire.* Nature, 1994. **371**(6496): p. 389-95.
129. Li, Y., H. Li, and M. Weigert, *Autoreactive B cells in the marginal zone that express dual receptors.* J Exp Med, 2002. **195**(2): p. 181-8.
130. Doyle-Cooper, C., et al., *Immune tolerance negatively regulates B cells in knock-in mice expressing broadly neutralizing HIV antibody 4E10.* J Immunol, 2013. **191**(6): p. 3186-3191.
131. Verkoczy, L., et al., *Autoreactivity in an HIV-1 broadly reactive neutralizing antibody variable region heavy chain induces immunologic tolerance.* Proc Natl Acad Sci U S A, 2010. **107**(1): p. 181-6.
132. Verkoczy, L., et al., *Rescue of HIV-1 broad neutralizing antibody-expressing B cells in 2F5 VH x VL knockin mice reveals multiple tolerance controls.* J Immunol, 2011. **187**(7): p. 3785-97.
133. Chen, Y., et al., *Common tolerance mechanisms, but distinct cross-reactivities associated with gp41 and lipids, limit production of HIV-1 broad neutralizing antibodies 2F5 and 4E10.* J Immunol, 2013. **191**(3): p. 1260-75.
134. Ota, T., et al., *B cells from knock-in mice expressing broadly neutralizing HIV antibody b12 carry an innocuous B cell receptor responsive to HIV vaccine candidates.* J Immunol, 2013. **191**(6): p. 3179-85.
135. Zhang, R., et al., *Initiation of immune tolerance-controlled HIV gp41 neutralizing B cell lineages.* Sci Transl Med, 2016. **8**(336): p. 336ra62.
136. McGuire, A.T., et al., *Engineering HIV envelope protein to activate germline B cell receptors of broadly neutralizing anti-CD4 binding site antibodies.* J Exp Med, 2013. **210**(4): p. 655-63.
137. Dosenovic, P., et al., *Immunization for HIV-1 Broadly Neutralizing Antibodies in Human Ig Knockin Mice.* Cell, 2015. **161**(7): p. 1505-15.
138. Escolano, A., et al., *Sequential Immunization Elicits Broadly Neutralizing Anti-HIV-1 Antibodies in Ig Knockin Mice.* Cell, 2016. **166**(6): p. 1445-1458 e12.
139. Jinek, M., et al., *A programmable dual-RNA-guided DNA endonuclease in adaptive bacterial immunity.* Science, 2012. **337**(6096): p. 816-21.

140. Jinek, M., et al., *Structures of Cas9 endonucleases reveal RNA-mediated conformational activation.* Science, 2014. **343**(6176): p. 1247997.
141. Knott, G.J. and J.A. Doudna, *CRISPR-Cas guides the future of genetic engineering.* Science, 2018. **361**(6405): p. 866-869.
142. Lin, Y.C., et al., *One-step CRISPR/Cas9 method for the rapid generation of human antibody heavy chain knock-in mice.* EMBO J, 2018. **37**(18).
143. Wang, X., et al., *Multiplexed CRISPR/CAS9-mediated engineering of pre-clinical mouse models bearing native human B cell receptors.* Embo j, 2021. **40**(2): p. e105926.
144. Jacobsen, J.T., et al., *One-step generation of monoclonal B cell receptor mice capable of isotype switching and somatic hypermutation.* J Exp Med, 2018. **215**(10): p. 2686-2695.
145. Bailey, S.R. and M.V. Maus, *Gene editing for immune cell therapies.* Nat Biotechnol, 2019. **37**(12): p. 1425-1434.
146. Maganti, H.B., et al., *Persistence of CRISPR/Cas9 gene edited hematopoietic stem cells following transplantation: A systematic review and meta-analysis of preclinical studies.* Stem Cells Transl Med, 2021.
147. Salisbury-Ruf, C.T. and A. Larochelle, *Advances and Obstacles in Homology-Mediated Gene Editing of Hematopoietic Stem Cells.* J Clin Med, 2021. **10**(3).
148. Eyquem, J., et al., *Targeting a CAR to the TRAC locus with CRISPR/Cas9 enhances tumour rejection.* Nature, 2017. **543**(7643): p. 113-117.
149. Voss, J.E., et al., *Reprogramming the antigen specificity of B cells using genome-editing technologies.* Elife, 2019. **8**.
150. Pogson, M., et al., *Immunogenomic engineering of a plug-and-(dis)play hybridoma platform.* Nat Commun, 2016. **7**: p. 12535.
151. Chu, V.T., et al., *Efficient CRISPR-mediated mutagenesis in primary immune cells using CrispRGold and a C57BL/6 Cas9 transgenic mouse line.* Proc Natl Acad Sci U S A, 2016. **113**(44): p. 12514-12519.
152. Cheong, T.C., M. Compagno, and R. Chiarle, *Editing of mouse and human immunoglobulin genes by CRISPR-Cas9 system.* Nat Commun, 2016. **7**: p. 10934.
153. Wu, C.M., et al., *Genetic engineering in primary human B cells with CRISPR-Cas9 ribonucleoproteins.* J Immunol Methods, 2018. **457**: p. 33-40.
154. Hung, K.L., et al., *Engineering Protein-Secreting Plasma Cells by Homology-Directed Repair in Primary Human B Cells.* Mol Ther, 2018. **26**(2): p. 456-467.
155. Johnson, M.J., et al., *Engineering of Primary Human B cells with CRISPR/Cas9 Targeted Nuclease.* Sci Rep, 2018. **8**(1): p. 12144.
156. Moffett, H.F., et al., *B cells engineered to express pathogen-specific antibodies protect against infection.* Sci Immunol, 2019. **4**(35).
157. Hartweger, H., et al., *HIV-specific humoral immune responses by CRISPR/Cas9-edited B cells.* J Exp Med, 2019. **216**(6): p. 1301-1310.
158. Nahmad, A.D., et al., *Engineered B cells expressing an anti-HIV antibody enable memory retention, isotype switching and clonal expansion.* Nat Commun, 2020. **11**(1): p. 5851.
159. Nojima, T., et al., *In-vitro derived germinal centre B cells differentially generate memory B or plasma cells in vivo.* Nat Commun, 2011. **2**: p. 465.
160. Nakade, S., et al., *Microhomology-mediated end-joining-dependent integration of donor DNA in cells and animals using TALENs and CRISPR/Cas9.* Nat Commun, 2014. **5**: p. 5560.
161. Sakuma, T., et al., *MMEJ-assisted gene knock-in using TALENs and CRISPR-Cas9 with the PITCh systems.* Nat Protoc, 2016. **11**(1): p. 118-33.

162. Yao, X., et al., *CRISPR/Cas9 - Mediated Precise Targeted Integration In Vivo Using a Double Cut Donor with Short Homology Arms.* EBioMedicine, 2017. **20**: p. 19-26.
163. Aida, T., et al., *Gene cassette knock-in in mammalian cells and zygotes by enhanced MMEJ.* BMC Genomics, 2016. **17**(1): p. 979.
164. Suzuki, K., et al., *In vivo genome editing via CRISPR/Cas9 mediated homology-independent targeted integration.* Nature, 2016. **540**(7631): p. 144-149.
165. Radoshitzky, S.R., et al., *ICTV Virus Taxonomy Profile: Arenaviridae.* Journal of General Virology, 2019. **100**(8): p. 1200-1201.
166. Charrel, R.N., X. de Lamballerie, and S. Emonet, *Phylogeny of the genus Arenavirus.* Current Opinion in Microbiology, 2008. **11**(4): p. 362-368.
167. Briese, T., et al., *Genetic Detection and Characterization of Lujo Virus, a New Hemorrhagic Fever–Associated Arenavirus from Southern Africa.* PLOS Pathogens, 2009. **5**(5): p. e1000455.
168. Siddle, K.J., et al., *Genomic Analysis of Lassa Virus during an Increase in Cases in Nigeria in 2018.* New England Journal of Medicine, 2018. **379**(18): p. 1745-1753.
169. Iapalucci, S., et al., *Tacaribe virus L gene encodes a protein of 2210 amino acid residues.* Virology, 1989. **170**(1): p. 40-47.
170. Zhang, L., et al., *Reassortant Analysis of Guinea Pig Virulence of Pichinde Virus Variants.* Virology, 2001. **290**(1): p. 30-38.
171. Charrel, R.N., et al., *New insights into the evolutionary relationships between arenaviruses provided by comparative analysis of small and large segment sequences.* Virology, 2003. **317**(2): p. 191-196.
172. Blasdell, K.R., et al., *Host range and genetic diversity of arenaviruses in rodents, United Kingdom.* Emerging infectious diseases, 2008. **14**(9): p. 1455-1458.
173. Yama, I.N., et al., *Isolation and characterization of a new strain of lymphocytic choriomeningitis virus from rodents in southwestern France.* Vector Borne Zoonotic Dis, 2012. **12**(10): p. 893-903.
174. Ushijima, Y., et al., *Identification of potential novel hosts and the risk of infection with lymphocytic choriomeningitis virus in humans in Gabon, Central Africa.* Int J Infect Dis, 2021. **105**: p. 452-459.
175. Vilibic-Cavlek, T., et al., *Emerging and Neglected Viruses of Zoonotic Importance in Croatia.* Pathogens, 2021. **10**(1).
176. Van Cuong, N., et al., *Rodents and risk in the Mekong Delta of Vietnam: seroprevalence of selected zoonotic viruses in rodents and humans.* Vector Borne Zoonotic Dis, 2015. **15**(1): p. 65-72.
177. Kallio-Kokko, H., et al., *Hantavirus and arenavirus antibody prevalence in rodents and humans in Trentino, Northern Italy.* Epidemiol Infect, 2006. **134**(4): p. 830-6.
178. Stephensen, C.B., et al., *Prevalence of serum antibodies against lymphocytic choriomeningitis virus in selected populations from two U.S. cities.* J Med Virol, 1992. **38**(1): p. 27-31.
179. Drager, S., et al., *Lymphocytic choriomeningitis virus meningitis after needlestick injury: a case report.* Antimicrob Resist Infect Control, 2019. **8**: p. 77.
180. Fevola, C., et al., *Seroprevalence of lymphocytic choriomeningitis virus and Ljungan virus in Finnish patients with suspected neurological infections.* J Med Virol, 2018. **90**(3): p. 429-435.
181. Alburkat, H., et al., *Lymphocytic Choriomeningitis Virus Infections and Seroprevalence, Southern Iraq.* Emerg Infect Dis, 2020. **26**(12): p. 3002-3006.
182. Stone, G.S., et al., *Case 40-2019: A 26-Year-Old Returning Traveler with Headache.* N Engl J Med, 2019. **381**(26): p. 2553-2560.

183. Delaine, M., et al., *Microcephaly Caused by Lymphocytic Choriomeningitis Virus.* Emerg Infect Dis, 2017. **23**(9): p. 1548-1550.
184. Meritet, J.F., et al., *A case of congenital lymphocytic choriomeningitis virus (LCMV) infection revealed by hydrops fetalis.* Prenat Diagn, 2009. **29**(6): p. 626-7.
185. Kinori, M., et al., *Congenital lymphocytic choriomeningitis virus-an underdiagnosed fetal teratogen.* J aapos, 2018. **22**(1): p. 79-81.e1.
186. Moraz, M.L. and S. Kunz, *Pathogenesis of arenavirus hemorrhagic fevers.* Expert Rev Anti Infect Ther, 2011. **9**(1): p. 49-59.
187. Oldstone, M.B., *Biology and pathogenesis of lymphocytic choriomeningitis virus infection.* Curr Top Microbiol Immunol, 2002. **263**: p. 83-117.
188. Traub, E., *A FILTERABLE VIRUS RECOVERED FROM WHITE MICE.* Science, 1935. **81**(2099): p. 298-9.
189. Salvato, M., et al., *Virus-lymphocyte interactions. IV. Molecular characterization of LCMV Armstrong (CTL+) small genomic segment and that of its variant, Clone 13 (CTL-).* Virology, 1988. **164**(2): p. 517-22.
190. Salvato, M., E. Shimomaye, and M.B. Oldstone, *The primary structure of the lymphocytic choriomeningitis virus L gene encodes a putative RNA polymerase.* Virology, 1989. **169**(2): p. 377-84.
191. Salvato, M.S. and E.M. Shimomaye, *The completed sequence of lymphocytic choriomeningitis virus reveals a unique RNA structure and a gene for a zinc finger protein.* Virology, 1989. **173**(1): p. 1-10.
192. Neuman, B.W., et al., *Complementarity in the supramolecular design of arenaviruses and retroviruses revealed by electron cryomicroscopy and image analysis.* J Virol, 2005. **79**(6): p. 3822-30.
193. Lee, K.J., et al., *NP and L proteins of lymphocytic choriomeningitis virus (LCMV) are sufficient for efficient transcription and replication of LCMV genomic RNA analogs.* J Virol, 2000. **74**(8): p. 3470-7.
194. Perez, M., R.C. Craven, and J.C. de la Torre, *The small RING finger protein Z drives arenavirus budding: implications for antiviral strategies.* Proc Natl Acad Sci U S A, 2003. **100**(22): p. 12978-83.
195. Buchmeier, M.J. and M.B. Oldstone, *Protein structure of lymphocytic choriomeningitis virus: evidence for a cell-associated precursor of the virion glycopeptides.* Virology, 1979. **99**(1): p. 111-20.
196. Hastie, K.M., et al., *Crystal structure of the prefusion surface glycoprotein of the prototypic arenavirus LCMV.* Nat Struct Mol Biol, 2016. **23**(6): p. 513-521.
197. Cao, W., et al., *Identification of alpha-dystroglycan as a receptor for lymphocytic choriomeningitis virus and Lassa fever virus.* Science, 1998. **282**(5396): p. 2079-81.
198. Flatz, L., et al., *Recovery of an arenavirus entirely from RNA polymerase I/II-driven cDNA.* Proc Natl Acad Sci U S A, 2006. **103**(12): p. 4663-8.
199. Sanchez, A.B. and J.C. de la Torre, *Rescue of the prototypic Arenavirus LCMV entirely from plasmid.* Virology, 2006. **350**(2): p. 370-80.
200. Hangartner, L., et al., *Antiviral immune responses in gene-targeted mice expressing the immunoglobulin heavy chain of virus-neutralizing antibodies.* Proc Natl Acad Sci U S A, 2003. **100**(22): p. 12883-8.
201. Parekh, B.S. and M.J. Buchmeier, *Proteins of lymphocytic choriomeningitis virus: antigenic topography of the viral glycoproteins.* Virology, 1986. **153**(2): p. 168-78.
202. Parekh, B.S. and M.J. Buchmeier, *Proteins of lymphocytic choriomeningitis virus: Antigenic topography of the viral glycoproteins.* Virology, 1986. **153**(2): p. 168-178.
203. Seiler, P., et al., *In vivo selection of neutralization-resistant virus variants but no evidence of B cell tolerance in lymphocytic choriomeningitis virus carrier mice*

expressing a transgenic virus-neutralizing antibody. J Immunol, 1999. **162**(8): p. 4536-41.
204. WHO, *Hepatitis B Key Facts.* http://www.who.int/news-room/fact-sheets/detail/hepatitis-b, 2018.
205. WHO, *Hepatitis C Key Facts.* http://www.who.int/news-room/fact-sheets/detail/hepatitis-c, 2018.
206. WHO, *HIV Key Facts.* http://www.who.int/news-room/fact-sheets/detail/hiv-aids, 2018.
207. Moskophidis, D., E. Laine, and R.M. Zinkernagel, *Peripheral clonal deletion of antiviral memory CD8+ T cells.* Eur J Immunol, 1993. **23**(12): p. 3306-11.
208. Gallimore, A., et al., *Induction and exhaustion of lymphocytic choriomeningitis virus-specific cytotoxic T lymphocytes visualized using soluble tetrameric major histocompatibility complex class I-peptide complexes.* J Exp Med, 1998. **187**(9): p. 1383-93.
209. Moir, S. and A.S. Fauci, *B-cell exhaustion in HIV infection: the role of immune activation.* Curr Opin HIV AIDS, 2014. **9**(5): p. 472-7.
210. Burton, A.R., et al., *Circulating and intrahepatic antiviral B cells are defective in hepatitis B.* J Clin Invest, 2018. **128**(10): p. 4588-4603.
211. Moir, S., et al., *Evidence for HIV-associated B cell exhaustion in a dysfunctional memory B cell compartment in HIV-infected viremic individuals.* J Exp Med, 2008. **205**(8): p. 1797-805.
212. Salimzadeh, L., et al., *PD-1 blockade partially recovers dysfunctional virus-specific B cells in chronic hepatitis B infection.* J Clin Invest, 2018. **128**(10): p. 4573-4587.
213. Malaspina, A., et al., *Compromised B cell responses to influenza vaccination in HIV-infected individuals.* J Infect Dis, 2005. **191**(9): p. 1442-50.
214. Wheatley, A.K., et al., *HIV-dependent depletion of influenza-specific memory B cells impacts B cell responsiveness to seasonal influenza immunisation.* Sci Rep, 2016. **6**: p. 26478.
215. Leist, T.P., E. Ruedi, and R.M. Zinkernagel, *Virus-triggered immune suppression in mice caused by virus-specific cytotoxic T cells.* J Exp Med, 1988. **167**(5): p. 1749-54.
216. Rusert, P., et al., *Determinants of HIV-1 broadly neutralizing antibody induction.* Nat Med, 2016. **22**(11): p. 1260-1267.
217. Guidotti, L.G., M. Isogawa, and F.V. Chisari, *Host-virus interactions in hepatitis B virus infection.* Curr Opin Immunol, 2015. **36**: p. 61-6.
218. Kinchen, V.J., et al., *Broadly Neutralizing Antibody Mediated Clearance of Human Hepatitis C Virus Infection.* Cell Host Microbe, 2018. **24**(5): p. 717-730 e5.
219. Osburn, W.O., et al., *Clearance of hepatitis C infection is associated with the early appearance of broad neutralizing antibody responses.* Hepatology, 2014. **59**(6): p. 2140-51.
220. Raghuraman, S., et al., *Spontaneous clearance of chronic hepatitis C virus infection is associated with appearance of neutralizing antibodies and reversal of T-cell exhaustion.* J Infect Dis, 2012. **205**(5): p. 763-71.
221. Pestka, J.M., et al., *Rapid induction of virus-neutralizing antibodies and viral clearance in a single-source outbreak of hepatitis C.* Proc Natl Acad Sci U S A, 2007. **104**(14): p. 6025-30.
222. Helle, F., et al., *Role of N-linked glycans in the functions of hepatitis C virus envelope proteins incorporated into infectious virions.* J Virol, 2010. **84**(22): p. 11905-15.
223. Pinschewer, D.D., et al., *Kinetics of protective antibodies are determined by the viral surface antigen.* J. Clin. Invest., 2004. **114**: p. 988-993.

224. Law, J.L., et al., *A hepatitis C virus (HCV) vaccine comprising envelope glycoproteins gpE1/gpE2 derived from a single isolate elicits broad cross-genotype neutralizing antibodies in humans.* PLoS One, 2013. **8**(3): p. e59776.
225. Rose, N.F., et al., *Glycoprotein exchange vectors based on vesicular stomatitis virus allow effective boosting and generation of neutralizing antibodies to a primary isolate of human immunodeficiency virus type 1.* J Virol, 2000. **74**(23): p. 10903-10.
226. Fallet, B., et al., *Interferon-driven deletion of antiviral B cells at the onset of chronic infection* Sci Immunol, 2016. **1**(4): p. eaah6817.
227. Sammicheli, S., et al., *Inflammatory monocytes hinder antiviral B cell responses.* Sci Immunol, 2016. **1**(4).
228. Moseman, E.A., et al., *Type I interferon suppresses virus-specific B cell responses by modulating CD8(+) T cell differentiation.* Sci Immunol, 2016. **1**(4).
229. Doria-Rose, N.A., et al., *Developmental pathway for potent V1V2-directed HIV-neutralizing antibodies.* Nature, 2014. **509**(7498): p. 55-62.
230. Schweier, O., et al., *Residual LCMV antigen in transiently CD4(+) T cell-depleted mice induces high levels of virus-specific antibodies but only limited B-cell memory.* Eur J Immunol, 2019.
231. Zellweger, R.M., et al., *Parameters governing exhaustion of rare T cell-independent neutralizing IgM-producing B cells after LCMV infection.* Eur J Immunol, 2006. **36**(12): p. 3175-85.
232. Di Niro, R., et al., *Salmonella Infection Drives Promiscuous B Cell Activation Followed by Extrafollicular Affinity Maturation.* Immunity, 2015. **43**(1): p. 120-31.
233. Krishnamurty, A.T., et al., *Somatically Hypermutated Plasmodium-Specific IgM(+) Memory B Cells Are Rapid, Plastic, Early Responders upon Malaria Rechallenge.* Immunity, 2016. **45**(2): p. 402-14.
234. Xiao, X., et al., *Germline-like predecessors of broadly neutralizing antibodies lack measurable binding to HIV-1 envelope glycoproteins: implications for evasion of immune responses and design of vaccine immunogens.* Biochem Biophys Res Commun, 2009. **390**(3): p. 404-9.
235. Wiehe, K., et al., *Functional Relevance of Improbable Antibody Mutations for HIV Broadly Neutralizing Antibody Development.* Cell Host Microbe, 2018. **23**(6): p. 759-765 e6.
236. Georgiev, I.S., et al., *Antibodies VRC01 and 10E8 neutralize HIV-1 with high breadth and potency even with Ig-framework regions substantially reverted to germline.* J Immunol, 2014. **192**(3): p. 1100-1106.
237. Jardine, J.G., et al., *Minimally Mutated HIV-1 Broadly Neutralizing Antibodies to Guide Reductionist Vaccine Design.* PLoS Pathog, 2016. **12**(8): p. e1005815.
238. Simonich, C.A., et al., *HIV-1 Neutralizing Antibodies with Limited Hypermutation from an Infant.* Cell, 2016. **166**(1): p. 77-87.
239. Bailey, J.R., et al., *Broadly neutralizing antibodies with few somatic mutations and hepatitis C virus clearance.* JCI Insight, 2017. **2**(9).
240. Bergthaler, A., et al., *Contributions of the LCMV glycoprotein and polymerase to strain-specific differences in murine liver pathogenicity.* J Gen Virol, 2007. **88**(2): p. 592-603.
241. Kalinke, U., et al., *The role of somatic mutation in the generation of the protective humoral immune response against vesicular stomatitis virus.* Immunity, 1996. **5**(6): p. 639-52.
242. Harada, Y., et al., *Unmutated immunoglobulin M can protect mice from death by influenza virus infection.* J Exp Med, 2003. **197**(12): p. 1779-85.

243. Chen, M., et al., *Limited humoral immunity in hepatitis C virus infection.* Gastroenterology, 1999. **116**(1): p. 135-43.
244. Kwong, P.D. and J.R. Mascola, *Human antibodies that neutralize HIV-1: identification, structures, and B cell ontogenies.* Immunity, 2012. **37**(3): p. 412-25.
245. Dogan, I., et al., *Multiple layers of B cell memory with different effector functions.* Nat Immunol, 2009. **10**(12): p. 1292-9.
246. Thai, L.H., et al., *BAFF and CD4(+) T cells are major survival factors for long-lived splenic plasma cells in a B-cell-depletion context.* Blood, 2018. **131**(14): p. 1545-1555.
247. Le Gallou, S., et al., *A splenic IgM memory subset with antibacterial specificities is sustained from persistent mucosal responses.* J Exp Med, 2018. **215**(8): p. 2035-2053.
248. Wei, M., et al., *Mice carrying a knock-in mutation of Aicda resulting in a defect in somatic hypermutation have impaired gut homeostasis and compromised mucosal defense.* Nat Immunol, 2011. **12**(3): p. 264-70.
249. Frebel, H., et al., *Programmed death 1 protects from fatal circulatory failure during systemic virus infection of mice.* J Exp Med, 2012. **209**(13): p. 2485-99.
250. Gupta, A. and R.J. Quigg, *Glomerular Diseases Associated With Hepatitis B and C.* Adv Chronic Kidney Dis, 2015. **22**(5): p. 343-51.
251. Kaufmann, D.E., et al., *Upregulation of CTLA-4 by HIV-specific CD4+ T cells correlates with disease progression and defines a reversible immune dysfunction.* Nat Immunol, 2007. **8**(11): p. 1246-54.
252. Oxenius, A., R.M. Zinkernagel, and H. Hengartner, *Comparison of activation versus induction of unresponsiveness of virus-specific CD4+ and CD8+ T cells upon acute versus persistent viral infection.* Immunity, 1998. **9**(4): p. 449-57.
253. Brooks, D.G., et al., *Intrinsic functional dysregulation of CD4 T cells occurs rapidly following persistent viral infection.* J Virol, 2005. **79**(16): p. 10514-27.
254. Fahey, L.M., et al., *Viral persistence redirects CD4 T cell differentiation toward T follicular helper cells.* J Exp Med, 2011. **208**(5): p. 987-99.
255. Lindqvist, M., et al., *Expansion of HIV-specific T follicular helper cells in chronic HIV infection.* J Clin Invest, 2012. **122**(9): p. 3271-80.
256. Feng, J., et al., *Patients with chronic hepatitis C express a high percentage of CD4(+)CXCR5(+) T follicular helper cells.* J Gastroenterol, 2012. **47**(9): p. 1048-56.
257. Xin, G., et al., *Single-cell RNA sequencing unveils an IL-10-producing helper subset that sustains humoral immunity during persistent infection.* Nat Commun, 2018. **9**(1): p. 5037.
258. Greczmiel, U., et al., *Sustained T follicular helper cell response is essential for control of chronic viral infection.* Sci Immunol, 2017. **2**(18).
259. Harker, J.A., et al., *Late interleukin-6 escalates T follicular helper cell responses and controls a chronic viral infection.* Science, 2011. **334**(6057): p. 825-9.
260. Burton, D.R. and L. Hangartner, *Broadly Neutralizing Antibodies to HIV and Their Role in Vaccine Design.* Annu Rev Immunol, 2016. **34**: p. 635-59.
261. Gage, E., et al., *Memory CD4(+) T cells enhance B-cell responses to drifting influenza immunization.* Eur J Immunol, 2019. **49**(2): p. 266-276.
262. Mankowski, M.C., et al., *Synergistic anti-HCV broadly neutralizing human monoclonal antibodies with independent mechanisms.* Proc Natl Acad Sci U S A, 2018. **115**(1): p. E82-E91.
263. Zwick, M.B., et al., *Neutralization synergy of human immunodeficiency virus type 1 primary isolates by cocktails of broadly neutralizing antibodies.* J Virol, 2001. **75**(24): p. 12198-208.

264. Nowakowski, A., et al., *Potent neutralization of botulinum neurotoxin by recombinant oligoclonal antibody.* Proc Natl Acad Sci U S A, 2002. **99**(17): p. 11346-50.
265. Pinschewer, D.D., et al., *A Btk transgene restores the antiviral TI-2 antibody responses of xid mice in a dose-dependent fashion.* Eur J Immunol, 1999. **29**(9): p. 2981-7.
266. Frey, S., et al., *Mismatch repair deficiency interferes with the accumulation of mutations in chronically stimulated B cells and not with the hypermutation process.* Immunity, 1998. **9**(1): p. 127-34.
267. Battegay, M., et al., *Quantification of lymphocytic choriomeningitis virus with an immunological focus assay in 24- or 96-well plates.* J Virol Methods, 1991. **33**(1-2): p. 191-8.
268. Menzel, U., et al., *Comprehensive evaluation and optimization of amplicon library preparation methods for high-throughput antibody sequencing.* PLoS One, 2014. **9**(5): p. e96727.
269. Cohen, M.S., et al., *Acute HIV-1 Infection.* N Engl J Med, 2011. **364**(20): p. 1943-54.
270. Havenar-Daughton, C., et al., *When designing vaccines, consider the starting material: the human B cell repertoire.* Curr Opin Immunol, 2018. **53**: p. 209-216.
271. Watanabe, A., et al., *Self-tolerance curtails the B cell repertoire to microbial epitopes.* JCI Insight, 2019. **4**(10).
272. Wyatt, R., et al., *The antigenic structure of the HIV gp120 envelope glycoprotein.* Nature, 1998. **393**(6686): p. 705-11.
273. Ota, T., et al., *B cells from knock-in mouse expressing broadly neutralizing HIV antibody b12 carry an innocuous BCR responsive to HIV vaccine candidates.* JOurnal of immunology, 2013.
274. Allman, D. and S. Pillai, *Peripheral B cell subsets.* Curr Opin Immunol, 2008. **20**(2): p. 149-57.
275. Hertz, M. and D. Nemazee, *BCR ligation induces receptor editing in IgM+IgD- bone marrow B cells in vitro.* Immunity, 1997. **6**(4): p. 429-36.
276. Hardy, R.R., et al., *Resolution and characterization of pro-B and pre-pro-B cell stages in normal mouse bone marrow.* J Exp Med, 1991. **173**(5): p. 1213-25.
277. Moran, A.E., et al., *T cell receptor signal strength in Treg and iNKT cell development demonstrated by a novel fluorescent reporter mouse.* J Exp Med, 2011. **208**(6): p. 1279-89.
278. Luning Prak, E.T., M. Monestier, and R.A. Eisenberg, *B cell receptor editing in tolerance and autoimmunity.* Ann N Y Acad Sci, 2011. **1217**: p. 96-121.
279. Goodnow, C.C., et al., *Altered immunoglobulin expression and functional silencing of self-reactive B lymphocytes in transgenic mice.* Nature, 1988. **334**(6184): p. 676-682.
280. Goodnow, C.C., et al., *Induction of self-tolerance in mature peripheral B lymphocytes.* Nature, 1989. **342**(6248): p. 385-391.
281. Verkoczy, L., F.W. Alt, and M. Tian, *Human Ig knockin mice to study the development and regulation of HIV-1 broadly neutralizing antibodies.* Immunol Rev, 2017. **275**(1): p. 89-107.
282. Verkoczy, L., et al., *Induction of HIV-1 broad neutralizing antibodies in 2F5 knock-in mice: selection against membrane proximal external region-associated autoreactivity limits T-dependent responses.* J Immunol, 2013. **191**(5): p. 2538-50.
283. Burnett, D.L., et al., *Clonal redemption and clonal anergy as mechanisms to balance B cell tolerance and immunity.* Immunol Rev, 2019. **292**(1): p. 61-75.
284. Fallet, B., et al., *Chronic Viral Infection Promotes Efficient Germinal Center B Cell Responses.* Cell Rep, 2020. **30**(4): p. 1013-1026.e7.

285. Battegay, M., et al., *Quantification of lymphocytic choriomeningitis virus with an immunological focus assay in 24- or 96-well plates.* J Virol Methods, 1991. **33**(1-2): p. 191-8.
286. Johnson, P.R., et al., *Vector-mediated gene transfer engenders long-lived neutralizing activity and protection against SIV infection in monkeys.* Nat Med, 2009. **15**(8): p. 901-6.
287. Saunders, K.O., et al., *Broadly Neutralizing Human Immunodeficiency Virus Type 1 Antibody Gene Transfer Protects Nonhuman Primates from Mucosal Simian-Human Immunodeficiency Virus Infection.* Journal of Virology, 2015. **89**(16): p. 8334-8345.
288. Fuchs, S.P., et al., *AAV-Delivered Antibody Mediates Significant Protective Effects against SIVmac239 Challenge in the Absence of Neutralizing Activity.* PLOS Pathogens, 2015. **11**(8): p. e1005090.
289. Dosenovic, P., et al., *Anti-HIV-1 B cell responses are dependent on B cell precursor frequency and antigen-binding affinity.* Proc Natl Acad Sci U S A, 2018. **115**(18): p. 4743-4748.
290. Tian, M., et al., *Induction of HIV Neutralizing Antibody Lineages in Mice with Diverse Precursor Repertoires.* Cell, 2016. **166**(6): p. 1471-1484 e18.
291. Zych, A.O., M. Bajor, and R. Zagozdzon, *Application of Genome Editing Techniques in Immunology.* Arch Immunol Ther Exp (Warsz), 2018. **66**(4): p. 289-298.
292. Zhang, J. and L. Wang, *The Emerging World of TCR-T Cell Trials Against Cancer: A Systematic Review.* Technol Cancer Res Treat, 2019. **18**: p. 1533033819831068.
293. Yang, Q., et al., *Efficacy and Safety of CAR-T Therapy for Relapse or Refractory Multiple Myeloma: A systematic review and meta-analysis.* Int J Med Sci, 2021. **18**(8): p. 1786-1797.
294. Hao, L., et al., *Adoptive Immunotherapy for B-cell Malignancies Using CD19-Targeted Chimeric Antigen Receptor T-Cells: A Systematic Review of Efficacy and Safety.* Curr Med Chem, 2019. **26**(17): p. 3068-3079.
295. Huang, D., et al., *Vaccine elicitation of HIV broadly neutralizing antibodies from engineered B cells.* Nat Commun, 2020. **11**(1): p. 5850.
296. Mansouri, M., et al., *Highly efficient baculovirus-mediated multigene delivery in primary cells.* Nat Commun, 2016. **7**: p. 11529.
297. Mansouri, M., et al., *Baculovirus-based genome editing in primary cells.* Plasmid, 2017. **90**: p. 5-9.
298. Casellas, R., et al., *Igkappa allelic inclusion is a consequence of receptor editing.* J Exp Med, 2007. **204**(1): p. 153-60.
299. Barzel, A., et al., *Promoterless gene targeting without nucleases ameliorates haemophilia B in mice.* Nature, 2015. **517**(7534): p. 360-364.
300. Huang, D., et al., *B cells expressing authentic naive human VRC01-class BCRs can be recruited to germinal centers and affinity mature in multiple independent mouse models.* Proc Natl Acad Sci U S A, 2020. **117**(37): p. 22920-22931.
301. Rojas, M., et al., *Molecular mimicry and autoimmunity.* J Autoimmun, 2018. **95**: p. 100-123.
302. Xiao, D., et al., *A meta-analysis of interaction between Epstein-Barr virus and HLA-DRB1*1501 on risk of multiple sclerosis.* Sci Rep, 2015. **5**: p. 18083.
303. Mori, M., et al., *Haemophilus influenzae infection and Guillain-Barré syndrome.* Brain, 2000. **123 (Pt 10)**: p. 2171-8.
304. Gerken, G., et al., *Rare association of herpes simplex virus IgM-specific antibodies and Guillain-Barré syndrome successfully treated with plasma exchange and immunosuppression.* Klin Wochenschr, 1985. **63**(10): p. 468-74.

305. Jacobs, B.C., et al., *The spectrum of antecedent infections in Guillain-Barré syndrome: a case-control study.* Neurology, 1998. **51**(4): p. 1110-5.
306. Becker, J. and K.L. Winthrop, *Update on rheumatic manifestations of infectious diseases.* Current Opinion in Rheumatology, 2010. **22**(1): p. 72-77.
307. Velu, V., et al., *Enhancing SIV-specific immunity in vivo by PD-1 blockade.* Nature, 2009. **458**(7235): p. 206-10.
308. Bradley, T., et al., *Immune checkpoint modulation enhances HIV-1 antibody induction.* Nat Commun, 2020. **11**(1): p. 948.
309. Raju, S., D.J. Verbaro, and T. Egawa, *PD-1 Signaling Promotes Control of Chronic Viral Infection by Restricting Type-I-Interferon-Mediated Tissue Damage.* Cell Rep, 2019. **29**(9): p. 2556-2564.e3.
310. Barber, D.L., et al., *Restoring function in exhausted CD8 T cells during chronic viral infection.* Nature, 2006. **439**(7077): p. 682-7.
311. Oldstone MB. Molecular mimicry as a mechanism for the cause and a probe uncovering etiologic agent(s) of autoimmune disease. Curr Top Microbiol Immunol. 1989
312. Damian, R.T., *Molecular mimicry revisited.* Parasitol Today, 1987. **3**(9): p. 263-6.
313. Zhou, T., et al., *Structural definition of a conserved neutralization epitope on HIV-1 gp120.* Nature, 2007. **445**(7129): p. 732-7.
314. González, N., et al., *Characterization of broadly neutralizing antibody responses to HIV-1 in a cohort of long term non-progressors.* PLoS One, 2018. **13**(3): p. e0193773.
315. Hessell, A.J., et al., *Broadly neutralizing monoclonal antibodies 2F5 and 4E10 directed against the human immunodeficiency virus type 1 gp41 membrane-proximal external region protect against mucosal challenge by simian-human immunodeficiency virus SHIVBa-L.* J Virol, 2010. **84**(3): p. 1302-13.
316. Law, M., et al., *Broadly neutralizing antibodies protect against hepatitis C virus quasispecies challenge.* Nat Med, 2008. **14**(1): p. 25-7.

IV. Appendix

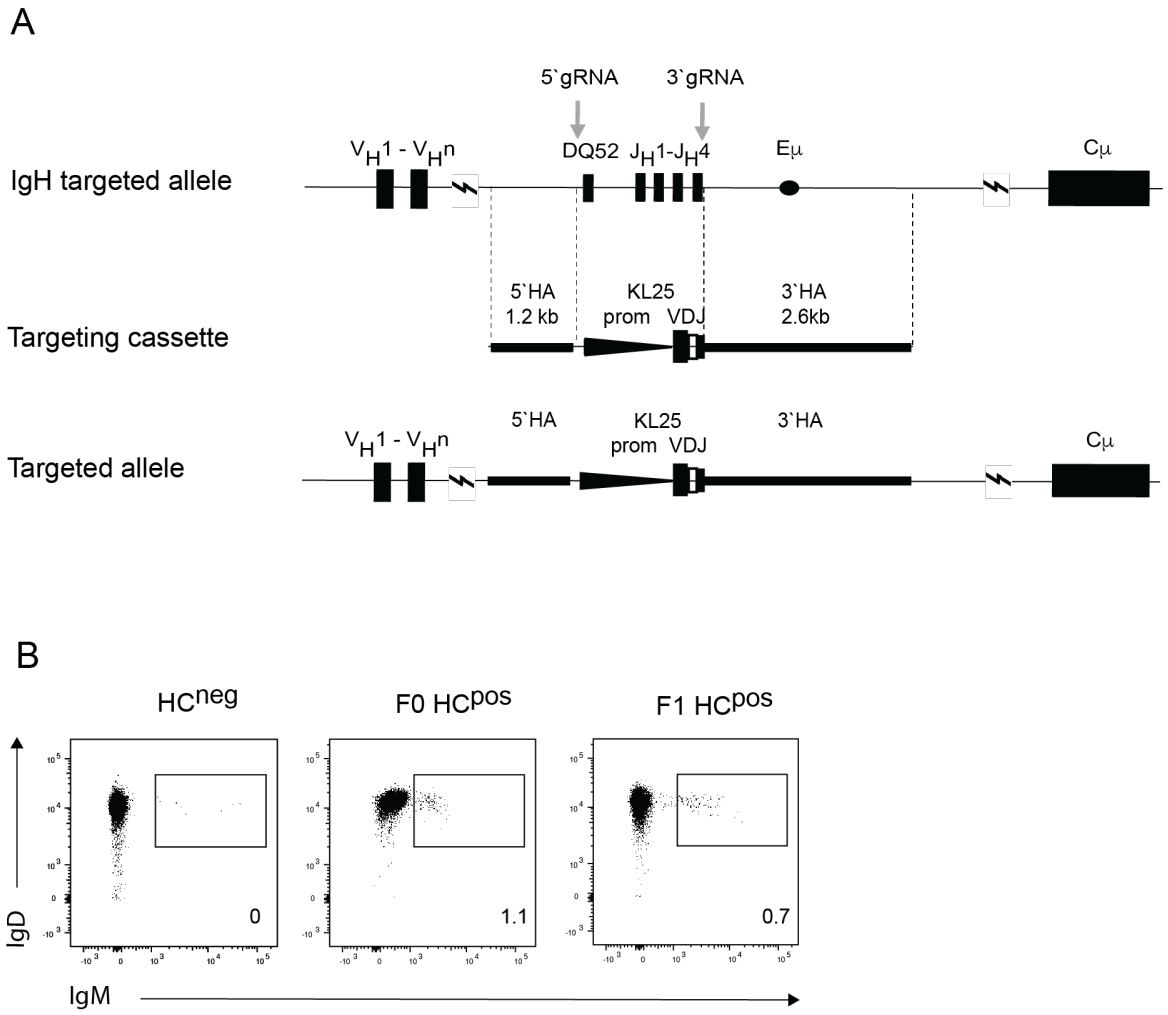

Appendix 1 Figure 1: Heavy chain knock-in, KL25H-Cki mice

(A) Targeting strategy for the generation of KL25H-Cki mice. The IgH locus of C57BL/6 mice was targeted with a 5`gRNA (CGCTAAAGTTCTCGAGCCTG) and 3`gRNA (GGAGAGGCCATTCTTACCTG) (grey arrows) deleting the DQ52 element and joining regions (J_H1-J_H5). IgH variable regions (V_H1-V_HN). Prior to mouse generation, gRNAs, targeting the IgH locus in the closest proximity to the cassette`s homology arms (HA) were chosen (http://crispor.tefor.net/, https://crisprgold.mdc-berlin.de/) and tested on mouse

embryos for their cutting efficiency. The most efficient gRNA pair, deleting the DQ52-J_H5 segment in 2/20 pups, as confirmed by PCR was chosen. The targeting cassette was generated via DNA synthesis in pUC57 vector (Genescrit) and consists of 1.2kb 5 prime homology arm (5`HA) 173bp downstream of the IgH DQ52 element, 1558bp IgHV1-74 promoter (prom), KL25 variable-diversity-joining region (VDJ) and a 2.6kb 3 prime homology arm (3`HA). Both homology arms are identical to C57BL/6 genome (IMGT). The pronuclear injections of 234 fertilized oocytes delivered both Cas9 RNPs, including depicted gRNAs (IDT) and an enzymatically linearized plasmid targeting cassette. Zygotes were then transferred to pseudopregnatnt foster mothers, which delivered 14 pups, including 2 founders. The pronuclear injections and PCR genotyping was performed at the Centre for transgenic model (CTM) at the University of Basel. (B) Representative FACS plots of LCMV GPC binding B cells ($B220^+$) of the founder animal (F0) and subsequent generation (F1).

Contributions to the work

The vast majority of the experiments and analyses presented here were performed by myself. Manuscript 1 is a collaborative work of three main autors, including me, where I contributed with the neutralizing antibody and revision studies shown in the Fig. 1D, E, F; Fig. 6D, E; Sup. Fig. 1; Sup. Fig. 2A, B; Sup. Fig. 5C, D, E, F. Manuscripts 2 and 3 show only my work. Pro-nuclear injections leading to the generation of HkiL and KL25H-Cki mice were performed by the experts at the core facilities for animal transgenic models at University of Zurich or University of Basel respectively.

Acknowledgements

This work would not be possible without the input, help, and support of many people, who I would like to mention here.

First, I thank my PhD committee members for accompanying me in this journey, namely professor Jean Pieters and professor Doron Merkler. Thank you for your patience, helpful comments, and kind encouragement. Also, many thanks to professor Hanspeter Pircher for stepping in as my external supervisor.

My utmost gratitude goes to my supervisor, professor Daniel D. Pinschewer.
Daniel, thank you for giving me the opportunity to join your lab and allowing me to experiment in the truest sense of the meaning, while learning about infectious immunology. I must say, your broad knowledge and complexity of thinking still amazes me, but I think I grew, and my interest in the topic is even bigger thanks to our discussions. Your support in whatever I found important and optimistic patience when things did not go well are extraordinary. I think only a great teacher can ask, “Is there something I can help you with?” on Friday evenings. I hope the significance of our work and other projects currently running in the lab will be well recognized.

I would like to thank all the lab members, especially the early-morning faces Min, and Karen and the late-night one, Mehmet. You are more than colleagues to me by now.
The work would not be such a pleasant experience without the positively charged people working in the lab. Thank you, Kerstin, Katrin, Peter, Weldy, Mirela, Anna, Tiago, for all the

well-intentioned advice that helped my work. Thank you, padawans, Lena and Matias, for guarding my place.

I thank my all-accepting, all-supporting parents. I know it was not easy to let your child leave for the world at such early age, but you recognized my passion and allowed me to always follow my dreams. For that, I am infinitely thankful, and I hope you can be proud.

I would also like to thank my friends Satomi, Julie, Fabio, and Dany for filling my work-free time with climbing and joy.

Many thanks to a special man, Christopher, whose thumbs must be hurting by now from all the pressing.

Lastly, I dedicate this work to the memory of the dearest people that I lost during my PhD.
My beloved grandparents who showed me the meaning of unconditional love and kindness.
My best friend and a brilliant scientist, Katarina, whose curiosity and need for objective inquiry was almost infectious. Without them, I probably wouldn't be here, and I hope to carry their greatness with me until my last day.

Curriculum Vitae

Marianna Florova, MUDr., Dr. Med.

Affiliation: Experimental Virology, Department of Biomedicine, University of Basel
Address: Johanniterstrasse 13, Basel, 4056 Switzerland
Date of Birth: 17. December 1990, Banovce nad Bebravou
Nationality Slovak
Contact: marianna.florova@gmail.ch ,+41 78 628 1370

Education:

09/2016 – 06/2021.	University of Basel, Biomedicine; Dr. med (17.4.2020)
09/2009 – 06/2015	Charles university in Prague, General medicine; MUDr. (16.6.2015)
09/2007 – 06/2009	The Regent's international school Bangkok, British A-levels, Chemistry, Mathematics, Physics, Biology

Work experience:

10/2016 – present	Research fellow, Experimental virology; *University of Basel;*
08/2015 –09/2016	Assistant physician, Department of Tropical medicine *St. Elizabeth University of health and social sciences Bratislava*;
09/2012 – 07/2015	Translator and coordinator; *People in Need;* Prague
03/2013 – 03/2014	Personal assistant for a disabled child; Prague
06/2011 –09/2011	Assistant for a medical subdivision; *Mondial assistance*; Prague

Research placements:

10/2016 – present Experimental virology; *University of Basel*
- Crispr/Cas9-mediated immunoglobulin engineering to control persistent viral infection

9/2015 – 9/2016 Department of tropical medicine*; St. Elizabeth University of health and social sciences Bratislava*
- Susceptibility to co-morbidities in H. pylori-colonized, HIV-positive children

12/2012 – 1/2013 Department of Neuroscience; *Institute of experimental medicine*, *Czech academy of sciences*
- Introduction to research in medicine and clinical trial protocols

9/2011 - 4/2012 Department of Physiology; *Second faculty of medicine in coop. with University of New York Prague*
- Florova M., Humby B., Nerad L.; Perception of temporal order of sounds is not restricted to neural signals representing stimuli onset

Scientific service:

9/2016 – present	Resource coordinator for European virus archive, *EVAg and University of Basel*
9/2019 – 9/2020.	Supervision of a medical master thesis, *University of Basel* *Specific antibodies for LCMV glycoprotein complex binding to virus escape variants*
4/2020	Lecturer at an immunology block course, *University of Basel*

Internships:

6/2014 – 7/2014	Cameroon partnership for development; International volunteer placement in Cameroon
7/2012 – 9/2012	Ifmsa/UN Recap project; International volunteer placement in Palestine
06/2009	Volunteer at Burmese refugee camp for children; *Children of the forest,* Thailand

Clinical placements:

4/2015 University of Innsbruck, Zams general hospital: Paediatrics
5/2014 University of Gdansk: Infectious diseases
4/2014 University of Gdansk: Emergency medicine and medicine of catastrophes

Scholarships and recognitions:

2016 University of Basel interfaculty biomedical research MD-PhD Program
2014 Erasmus scholarship at the Medical university in Gdansk
2009 Outstanding performance in GCE Biology (human): Top ten worldwide international students
2007 Full Global connect scholarship to study AS and A levels at Regent`s international school

Memberships:

Swiss Society for Immunology und Allergology (SGAI/SSAI)
Swiss MD-PhD association (SMPA)

Languages:

- Slovak	mother tongue
- Czech	State exams C2
- English language	TOEFL 107, IELTS certificate 7.5
- German	Goethe certificate C1
- Russian	basic
- French	basic